الجمهورية الجزائرية الديمقراطية الشعبية
People's Democratic republic of Algeria
وزارة التعليم العالي و البحث العلمي
Ministry of Higher Education and Scientific Research
جامعة عبد الحميد بن باديس – مستغانم
Abdel Hamid Ibn Badis University – Mostaganem
كلية العلوم و التكنولوجيا
Faculty of Sciences and Technology
قسم هندسة الطرائق
Department of Process Engineering

Order N°:D ...../GP/2022

In partial fulfillment of the requirements for the academic degree of

DOCTORATE IN SCIENCES

In

PROCESS ENGINEERING

Submitted by

HAFANI Mustapha

Contribution to the Development of a New Membrane Technology for Methane Gas Dehydration

Defence date: 02/03/2022 at Abdel Hamid Ibn Badis University – Mostaganem

Dissertation committee:

Chairman	BENDERDOUCHE Nouredine	Prof.	Mostaganem University
Examiner	MOUFFOK Benali	Prof.	University of Sidi Bel Abbes
Examiner	BELBACHIR Mohammed	Prof.	Oran 1 University
Thesis Director	DJENNAD M'hamed	Prof.	Mostaganem University
Invited	BENACHOUR Djafer	Prof.	Setif University

Academic Year 2021/2022

Publication

Part of this thesis has been published online on 22 Jun 2021, in the POLYMER-PLASTICS TECHNOLOGY AND MATERIALS journal.

To link to this article: https://doi.org/10.1080/25740881.2021.1912091

Keywords

Asymmetric membrane, methane, permeability, separation, water vapour

Abstract

Poly (ethylene terephthalate) (PET)-based membranes were prepared in the laboratory, where the dehydration performance of pure PET membranes is improved by incorporating different amounts of Poly (ethylene glycol) (PEG) average Mn 6000 as polymeric additive, flat sheet membranes are formed using the phase inversion method, the thickness of the obtained films was in the range between 60 and 130 μm. The produced membranes were evaluated in two experimental setups, where the permeabilities of water vapor and methane gas were measured, allowing the examination of membranes performance for the dehydration of methane gas.

The results showed that the prepared films have an asymmetric structure, and as the PEG amount increased, large macro-voids formed, the sub-layer pores size diameter, skin layer thickness and water vapour permeabilities WVP's increased also. It was significantly found that the polyethylene glycol (PEG) content in polyethylene terephthalate (PET) membranes has a great role in improving the dehydration of methane gas, whereby if the polyethylene glycol (PEG) content is higher than 20%, overall, the methane gas permeabilities decrease significantly. The results obtained showed that the polyethylene terephthalate films are able to dehydrate methane gas and their performance for methane dehydration were improved by the addition of polyethylene glycol (PEG).

Résumé

Des membranes à base de poly (éthylène téréphtalate) (PET) ont été préparées au laboratoire, où la performance de déshydratation des membranes en PET pur est améliorée par l'incorporation de différentes quantités de poly (éthylène glycol) (PEG) comme additif polymère de masse molaire moyenne de 6000 (Mn 6000). Des membranes de films plats ont été formées en utilisant la méthode d'inversion de phase, à partir de laquelle l'épaisseur des films a été obtenue dans la gamme entre 60 et 130 μm. Les membranes produites ont été évaluées dans deux montages expérimentaux, où les perméabilités de la vapeur d'eau et du gaz de méthane ont été mesurées, permettant l'examination de performance des membranes pour la déshydratation du gaz méthane.

Les résultats ont montré que les films préparés ont une structure asymétrique, et que lorsque la quantité de PEG augmente, de grands macro-vides se forment, le diamètre de la taille des pores de la sous-couche, l'épaisseur de la couche de peau et les perméabilités à la vapeur d'eau (PVE) augmentent également. Il a été constaté que la teneur en polyéthylène glycol (PEG) des membranes en polyéthylène téréphtalate (PET) joue un rôle important dans l'amélioration de la déshydratation du gaz de méthane. Si la teneur en polyéthylène glycol (PEG) est supérieure à 20%, les perméabilités du gaz (PGM) diminuent de manière significative. Les résultats obtenus ont montré que les films de polyéthylène téréphtalate sont capables de déshydrater le gaz de méthane et que leurs performances ont été améliorées par l'ajout de polyéthylène glycol (PEG).

ملخص

تم تحضير أغشية البولي إيثيلين تيريفثاليت (PET) في المختبر، حيث تم تحسين أداء الترشيح وذلك بإدماج كميات مختلفة كبوليمر مضاف من بولي إيثيلين جلايكول (PEG) ذات متوسط الكتلة المولية 6000، فقد تم تشكيل اغشية مستوية باستعمال طريقة تقليب الحالة والتي تم من خلالها الحصول على سماكة الأغشية في نطاق يتراوح بين 60 و130 مايكرومتر. تم تقييم الاغشية المتشكلة في إعدادين تجريبيين، فهذا سمح بقياس نفاذية بخار الماء وغاز الميثان، والحصول على أداء الأغشية لترشيح غاز الميثان.

أظهرت النتائج أن الأغشية المحضرة لديها بنية غير متماثلة، وأنه مع زيادة كمية بولي إيثيلين جلايكول (PEG)، تكونت فراغات كبيرة على الطبقة السفلية عليها مع زيادة قطر حجمها، كما هو الحال فقد زاد سمك طبقة الجلدية ونفاذية الماء أيضًا. ما لوحظ حقا، كما كان له دور كبير في تحسين ترشيح غاز الميثان هو محتوى بولي إيثيلين جلايكول (PEG) في أغشية البولي إيثيلين تيريفثاليت (PET)، بحيث إذا كان المحتوى أكثر من 20٪، فان نفاذية الغاز تنخفض بشكل ملحوظ على العموم، فقد أظهرت النتائج التي تم الحصول عليها، ان أداء أغشية البولي إيثيلين تيريفثاليت قادرة على تجفيف غاز الميثان وأنه تم تحسين أدائها بإضافة البولي إيثيلين جلايكول (PEG).

Table of contents

Keywords ii
Abstract iii
Résumé iv
ملخص v
Tables des matières vi
List of Figures viii
List of Tables x
List of Abbreviations xi
Statement of Original Authorship xiii
Acknowledgements xiv
INTRODUCTION 1
1.1 Background & Research objectives 1
1.2 Framework of the thesis study 3
Chapter 1: Literature review 4
1.1 Importance of methane gas 4
1.2 Methane purification for effective dtilization 5
1.3 conventional Separation for methane gas dehydration 6
1.3.1 Absorption-based dehydration 6
1.3.2 Adsorption-based dehydration 7
1.3.3 Dehydration by refrigeration 7
1.4 Dehydration of methane gas using membranes 8
1.5 Principle of membrane separation 9
1.6 Materials used for membrane Fabrication 9
1.6.1 Organic membrane materials: Polymers 9
1.6.2 Inorganic membrane materials 10
1.7 Membrane modules 10
1.8 Membrane morphology 11
1.8.1 Isotropic membranes 12
1.8.2 Anisotropic membranes 12
1.9 Phase Separation process for membranes preparation 12
1.10 Solution casting film applicator: 13
1.11 gas separation mechanism in polymeric membrnes 14
Chapter 2: Materials and methods for PET membranes preparation 16
2.1 MATERIALS 16

2.1.1 Polymers 16
2.1.2 Pure methane gas 18
2.1.3 PET membrane solvents 19
2.1.4 PET Membrane solvent mixture TCA/DCM 21
2.1.5 Non-solvent solution 23
2.1.6 Instruments 23
2.2 METHODS 38
2.2.1 Blended PET/PEG flat membranes fabrication 38
2.2.2 Membrane's characterization 40
2.2.3 Performance of the membranes 48
Chapter 3: Characterization of prepared PET-based membranes 55
3.1 Formation of flat sheet membrane 55
3.2 Sectional and top surface morphology of membranes 56
3.3 Surface characterization 60
3.3.1 Membranes M1 62
3.3.2 Membranes M2 62
3.3.3 Membranes M3 63
3.3.4 Membranes M4 64
3.3.5 Membranes mean pore diameter 65
3.4 Energy dispersive X-ray spectrometry 66
Chapter 4: Methane gas dehydration by PET-based membranes 69
4.1 Water vapor Permeability measurement (WVP) 69
4.1.1 Membrane's thickness 69
4.1.2 Water vapor transmission rate (WVTR) 70
4.1.3 Water vapor permeance (P) 77
4.1.4 Water vapor permeability (WVP) 77
4.2 Effect of the PEG on the WVP 78
4.3 Methane gas permeability measurement (MGP) 79
4.3.1 Methane gas volume-flow rate (Vr) 79
4.3.2 Average Methane gas volume-flow rate (Vr) of membranes 83
4.4 Effect of the PEG on the methane gas permeability 86
CONCLUSIONS AND FUTURE PERSPECTIVE 88
Bibliography 90

List of Figures

Figure 0-1. Thesis graphical abstract 3
Figure 1-1. Relevant sources for renewable methane gas production 5
Figure 1-2. Absorption dehydration process 6
Figure 1-3. Adsorption dehydration process 7
Figure 1-4. Water vapor permeability (extrapolated to zero activity) and H_2O/CH_4 selectivity at about 30 ◦C in various polymers 8
Figure 1-5. Membrane principal separation process 9
Figure 1-6. Membrane configuration types 11
Figure 1-7. Isotropic and anisotropic membranes morphology 11
Figure 1-8. Typical film applicators widely used 13
Figure 1-9. Gas transport mechanisms through membranes 15
Figure 2-1. Polyethylene terephthalate (PET) polymer with chemical structure 17
Figure 2-2. Polyethylene glycol (PEG) additive polymer with chemical structure 18
Figure 2-3. Chemical structure of Dichloromethane (DCM) 19
Figure 2-4. Trichloroacetic acid (TCA) with chemical structure 20
Figure 2-5. Polymers-solvents mixing glass bottle 24
Figure 2-6. Mixing process with magnetic stirrer- stir bar 26
Figure 2-7. Flat glass plate for dope solution application 27
Figure 2-8. Coagulation bath filled with distilled water 28
Figure 2-9. 2D layout structure of the water cup 29
Figure 2-10. Water cup with main integrated elements 30
Figure 2-11. Cutting flat sheet membranes steps 31
Figure 2-12. Schematic of bubble flowmeter 32
Figure 2-13. Home glass and four-sided film applicators design 33
Figure 2-14. Oven structure with temperature controller 34
Figure 2-15. Measurement with digital micrometer 35
Figure 2-16. ImageJ program overview 36
Figure 2-17. FEI Quanta 650 FEG SEM equipped with an EDS analyzer (Bruker QUNATX EDS XFlash® 6|10) 38
Figure 2-18. Coating of PET dope solution 40
Figure 2-19. EDS analyzer (Bruker QUNATX EDS XFlash® 6|10) 41
Figure 2-20. SEM image calibration 43
Figure 2-21. SEM image pre-treatment steps 44
Figure 2-22. SEM image pre-treatment steps 45
Figure 2-23. Pores size analysis steps 46
Figure 2-24. Excel model for calculation of pores diameter 47
Figure 2-25. Experimental setup for MGP measurement cross PET membranes 51
Figure 2-26. Practical experimental setup for MGP measurement 52
Figure 3-1. Holes build-up in distilled water coagulation bath for M5 membrane (60%/40%) 55
Figure 3-2. Build-up of PET/PEG membranes: M1 (100%/0%), M2 (90%/10%), M3 (80%/20%), M4 (70%/30%), M5 (60%/40%) 56

Figure 3-3. Scanning electron microscopy images of the porous sub-layer surface of PET membranes. (M1, no added PEG; M2=10% PEG; M3=20% PEG, M4=30% PEG) 58
Figure 3-4. Scanning electron microscopy images of membrane cross sections. (M1, no added PEG, M2=10% PEG, M3=20% PEG, M4=30% PEG) 59
Figure 3-5. SEM suface analysis of membranes : A- Pores size distribution of membranes, B- Detected pores in binary SEM images: black = Pores, white = membrane matrix 61
Figure 3-6. M3 SEM image of sub-layer surface 62
Figure 3-7. M2 SEM image of sub-layer surface 63
Figure 3-8. M3 SEM image of sub-layer surface 64
Figure 3-9. Zoom out inside the macro voids of M4 membrane sub-surface 65
Figure 3-10. Sub-layer mean pore diameter of PET/PEG membranes 66
Figure 3-11. Energy dispersive X-ray spectrometry images of the sub-layer surface of PET membranes. Series = characteristic X-ray lines, C [wt. %] = the concentration in weight percent of the element 68
Figure 4-1. Membrane thickness loose after water vapor permeability test 70
Figure 4-2. Weight loss slope of M1 membrane 72
Figure 4-3. Weight loss slope of M2 membrane 73
Figure 4-4. Weight loss slope of M3 membrane 74
Figure 4-5. Weight loss slope of M4 membrane 75
Figure 4-6. Water vapour permeability of PET/PEG membranes: M1 (100%/0%), M2 (90%/10%), M3 (80%/20%), M4 (70%/30%). *(R square =0.9497)* 79
Figure 4-7. M1 Membrane escaped methane volume regression line with slopes 80
Figure 4-8. M2 Membrane escaped methane volume regression line with slopes 81
Figure 4-9. M3 Membrane escaped methane volume regression line with slopes 82
Figure 4-10. M4 Membrane escaped methane volume regression line with slopes 83
Figure 4-11. Effect of PEG additive on gas transport properties of methane gas, (*R square=0.9323)* 87

List of Tables

Table 2-1. Polyethylene terephthalate (PET) specification 17
Table 2-2. Polyethylene glycol (PEG) specification (Specification Sheet: sigmaaldrich.com) 18
Table 2-3. Dichloromethane (DCM) specification 20
Table 2-4. Trichloroacetic acid (TCA) specification 21
Table 2-5. Ratios of solvent solution TCA/DCM for dissolving of PET membranes 23
Table 2-6. Mixing glass bottle properties 25
Table 2-7. Compositions of dope casting solutions of PET membranes 39
Table 4-1. Average thickness of membranes 70
Table 4-2. Weight loss vs time data of M1 membrane 71
Table 4-3. Weight loss vs time data of M2 membrane 73
Table 4-4. Water weight loss of M3 membrane 74
Table 4-5. Water weight loss of M4 membrane 75
Table 4-6. Average slopes of membranes 76
Table 4-7. Water vapour transmission rate (WVTR) 76
Table 4-8. Water vapor permeance (P) 77
Table 4-9. Water vapor permeability (WVP) 77
Table 4-10. Water weight loss of M1 membrane 80
Table 4-11. Water weight loss of M2 membrane 81
Table 4-12. Water weight loss of M3 membrane 82
Table 4-13. Water weight loss of M4 membrane 83
Table 4-14. Average Slope=(Vr) of membranes 84
Table 4-15. Methane gas transmission rate (GTR) 85
Table 4-16. Methane gas permeance (P) 85
Table 4-17. Methane gas permeability (MGP) 86

List of Abbreviations

ASTM	American Society for Testing and Materials
BM	biomethane
CBT	coagulation bath temperature
CA	cellulose acetate
DCM	dichloromethane
DMPC	dynamic moisture permeation cell
EC	ethyl cellulose
EDS	energy-dispersive X-ray spectroscopy
GHG	greenhouse gas
HNTs	halloysite nanotubes
HPC	hydroxypropyl cellulose
ImageJ	image processing and analysis in java
MGP	methane gas permeability
NG	natural gas
NR	natural rubber
PE	polyethylene
PES	poly(ether-Sulfone)
PA	polyamide
PAN	polyacrylonitrile
Pebax	polyether block amide
PEG	poly(ethylene glycol)
PEI	polyetherimide
PEO-PBT	poly(ethylene oxide)-poly(butylene terephthalate)
PET	poly(ethylene terephthalate)
PC	polycarbonate
PDMS	poly(dimethyl siloxane)
PI	polyimide
PLA	poly(lactic acid)
PP	polypropylene
PPO	poly(phenylene oxide)

PSF	polysulfone
PTFE	polytetrafluoroethylene
PU	polyurethane
PVDF	poly(vinylidene fluoride)
PVP	poly(vinylpyrrolidone)
SEM	scanning electron microscopy
SPAI	sulfonated polyamide-imide
TCA	trichloroacetic
WVP	water vapour permeability
WVTR	water vapour transmission rate

Statement of Original Authorship

The work contained in this thesis has not been previously submitted to meet requirements for an award at this or any other higher education institution. To the best of my knowledge and belief, the thesis contains no material previously published or written by another person except where due reference is made.

Acknowledgements

First and foremost, i would like to express my gratitude and appreciation to my thesis supervisor, Prof. DJENNAD M'hamed, for the valuable time he devoted for guiding me, his motivation, and specifically, the trust he placed in my personal abilities by allowing me to conduct my experimental research with his own tools and in the Laboratory that he instantly prepared for the benefit of PHD students. His constant monitoring and guidance helped me feeling with the true value of research throughout my PhD period, which ultimately resulted in my first publication in the research domain. I was extremely fortunate to be supervised by Prof. DJENNAD M'hamed.

Furthermore, my thanks are expressed to the members of the jury who consented to review the thesis and improve its quality. My heartfelt gratitude also goes to my co-workers for their presence in times of need, as well as their expertise in assisting with the publication of the article.

Many thanks to everyone, near or far, who contributed to the development of this thesis, including all the personnel of the university of Mostaganem, teachers, laborantins, and so on.

I would like also to express my sincere gratitude to my lovely mother, I would never be having success without her support. Also special thanks to my family and sisters, by keeping a great atmosphere to complete my thesis. I would like to thank my younger sister who directed me to pursue a doctoral degree program.

Finally, I'd like to express my gratitude to my wife for her patience and extensive knowledge in assisting me during the difficult days of my research. Certainly, this thesis and all of my successful work were a result of her; she was always close to me, supporting me throughout the doctorate period: traveling (Oran, Algiers...), purchasing tools, and years of travel for the purpose of the research. I'm glad we have such a wonderful story to tell our children.

INTRODUCTION

1.1 BACKGROUND & RESEARCH OBJECTIVES

Methane gas is an important fuel source for the production of electricity, heat, power, steam, electrical generation and vehicular fuel [1]–[3]. Additionally, methane gas is very light and by combustion, fewer hazardous emissions are released compared to coal and other fossil fuels [1]. Therefore, it is considered strongly as a clean gas and the best fuel source used for heating homes and fuelling vehicles [4], [5]. Methane gas is produced from many sources, both from natural and artificial, the main source is coming from natural gas industries, this later is classified as "fossil fuel" [6], [7]. Recently, methane gas has gained more attention since it became a "renewable source" fuel that can be produced continuously worldwide, from sources available anywhere, generally from landfills or through anaerobic digester biogas [7]–[10]. In addition, methane is a convenient greenhouse gas that has an estimated global warming potential of 28 to 36 times that of CO_2 over 100 years [11], [12]. Thus, further interest in methane gas arose for the purpose of reducing the impact of greenhouse gas emissions (GHG) [13]. Accordingly, the methane gas emitted by the biogas fields is recovered and processed for use as fuel [14], or injected into natural gas grids [15], [16]. Both main sources of methane, fossil or biogas, contain water vapour in their compositions. Therefore, they present several problems for transportation and processing, including hydrate formation, corrosion, erosion, slug flow, increased volume flow and a reduced calorific value [17]–[19]. For transportation uses, the methane gas is liquefied at lower temperatures [20], [21], where hydrates formation is more likely to occur and to avoid that many known processes are used for removal of water vapour, by scrubbing with glycol or by adsorption on silicates or molecular sieves (zeolites) [18], [22]–[25]. Membrane technology has been introduced in methane-water vapour separation, and it has shown several advantages [26]–[28] over other separation processes such as lack of demand for chemicals, lower capital and operation costs, higher energy efficiency, simple operability, low environmental impact and ease of scaling up [26], [27], [29], [30]. In the membrane fabrication process, the selection of the appropriate polymeric material plays an important role in the quality and efficiency of membrane separations, as presented by Lin et *al.*[26]: the study considered 12 polymers as representative for CH_4/H_2O separations, the permeability and selectivity are found much higher when using membranes based hydrophilic rubbery polymers whereas these two parameters were very low in the case of the selection of

membranes based on hydrophobic rubbers. Besides that, the addition of organic or inorganic components to the membrane structure has proven to be a very useful method to achieve the desired membranes [31]–[35]. Recently, many works presented additive materials where PEG material is considered one of the most widely used organic additives, it has received much attention as a promising polymeric organic additive for pore forming, the improving hydrophilicity, antifouling and improving pure water flux [36]–[40]. A review of the literature reveals other advantages of adding PEG: CHINNAN and PARK[41] found that water vapour permeability of hydroxypropyl cellulose (HPC) membrane increased significantly with increasing PEG content (400 mw). Lin et *al*.[42] reported that the PEG content affects the WVP of polyurethane films and higher water permeabilities occur at higher PEG contents. Similar results have been reported by Alakrach et *al*.[43] for PLA/HNT membranes.

In the present work, PET material was selected as a base polymer for preparing membranes for use in methane gas dehydration. As well known, the pure PET polymer has a hydrophobic character and exhibits more resistance to water transport [44] and moreover, it was used, first of all, due to its wide availability in the market, very low cost, high temperature and mechanical resistance [45]. Second, PET is one of the most well-known polymers used in the manufacture of bottles and, consequently, is considered one of the worst wastes for the environment after use [45], [46]. Many researchers have worked on the recycling of PET polymer mainly to keep it valuable for environmental improvement reason [47], [48]. Along the same lines, our thesis studied the use of the hydrophobic PET for the dehydration of methane gas to make PET attractive for future dehydration researches and encourage for retrieval of waste PET from the environment. In order to improve WVP of PET polymer against its hydrophobic character, a hydrophilic polyethylene glycol (PEG) material was used as a polymeric additive in different contents, 0%, 10%, 20%, 30%, and 40% (wt./wt.), where, different membranes are formed and named as M1, M2, M3, M4 and M5, respectively. All prepared membranes are tested by measuring MGP and WVP permeabilities and the results are compared and studied for their use in the separation of methane gas and water vapour, necessary for dehydration applications such as natural gas or biogas plants. The work of this thesis can be summarised in the graphical abstract shown in the Figure 0-1.

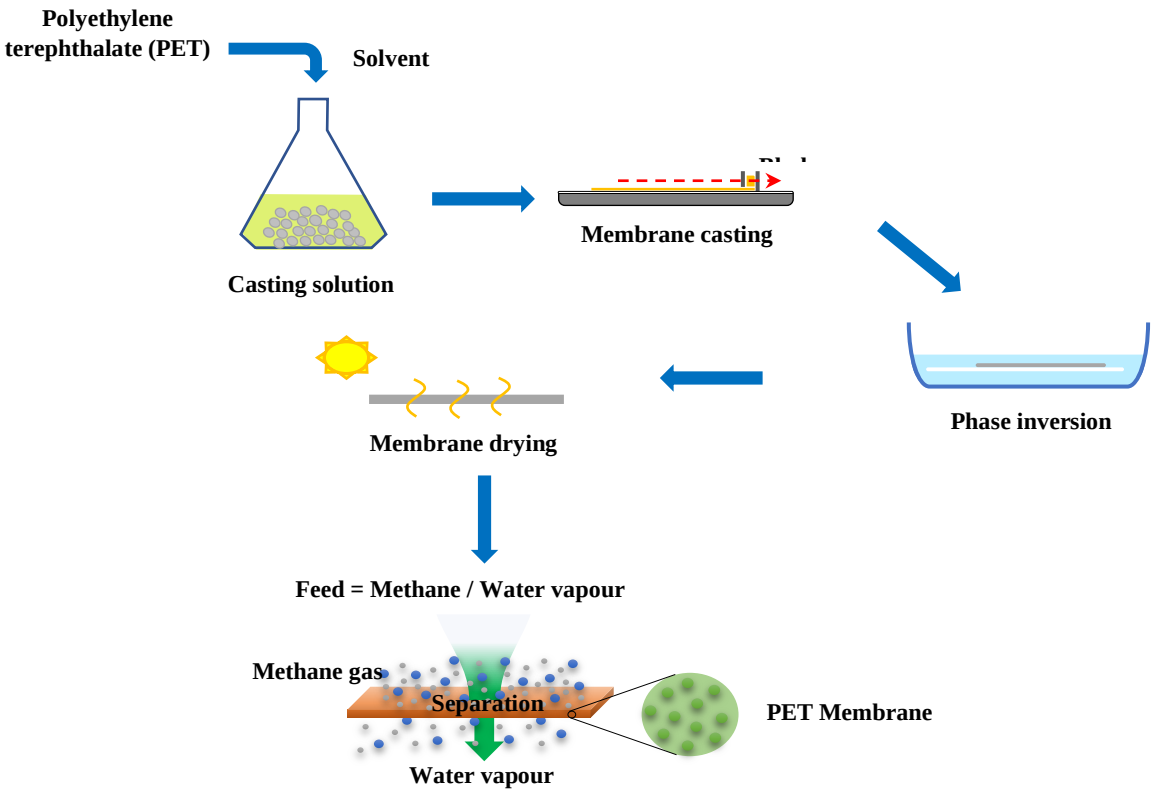

Figure 0-1. Thesis graphical abstract

1.2 FRAMEWORK OF THE THESIS STUDY

This thesis is structured into four chapters in order to emphasize the major topics and outcomes. The first chapter provides a review of the fundamental foundation required to understand the work in this thesis, including a review on key topics in the fields of gases and membrane technology. The second chapter explains all of the processes and materials used in the manufacture of PET membranes, such as polymers, solvents, and the equipment utilized, as well as the method for testing the permeabilities of water vapor and methane gas. The third and fourth chapters are devoted to discussing the acquired results; in the third chapter, the structure of the generated PET membranes is well shown and was studied in detail by characterisation using techniques such as SEM, EDS and deep SEM images analysis by ImageJ software. The fourth chapter addresses the relative nature of the structure of the generated membranes and their effect on the performance for methane gas dehydration, as well as a complete description of each membrane's separation capacity. Finally, a section headed "Conclusions and future perspective" summarizes the study's key results and suggests future avenues for research.

Chapter 1

Literature review

This chapter provides the fundamental background necessary to develop a basic understanding consistent with this thesis, including the main concepts in the field of gases, emphasizing the importance of methane gas, its dehydration for purification with gas separation techniques, and the main traditional gas separation processes used for that. In addition, a review of the main concepts of membrane technology, with an overview of the use of membrane technology in gas separation and in particular in the dehydration of methane gas. This chapter underlines the importance of membrane technology as a new concept for methane gas separation.

1.1 IMPORTANCE OF METHANE GAS

Methane gas is a flammable molecule, a lighter component and the cleanest hydrocarbon when burnt. In the past, most methane gas was produced from natural gas wells, which is a fossil fuel source in nature accumulated over millions of years. The old views assumed that due to the massive use of methane gas for energy production, the methane molecules are consumed, causing all fossil methane sources to disappear, this assessment made the methane gas losing its value and being considered to be replaced by another energy source component. These assumptions, however, were predicated on the idea that methane was exclusively created from fossil fuels in natural gas wells. In reality, the methane molecule has earned its prominence in recent years, owing to the fact that methane is not created only from fossil natural gas, but occurs spontaneously and constantly everywhere, mainly produced in biological fields, the concept is depicted in Figure 1-1, where, three relevant sources of methane are available naturally in the atmosphere for methane production: (1) from waste in landfills [49]; (2) emissions from livestock [50], [51]; and (3) wastewater treatment [52]. Based on its natural biological availability, methane is recognized as a renewable and ecologically pure energy source, rendering it a relevant subject for clean energy production and a suitable candidate to replace other fossil fuel sources, the fact that its production potential can reach 20-30% of the world's natural gas consumption [53]. Many attempts are underway to position it as a dominant energy source in the future, as evidenced by the growth indication in the number of biomethane plants in Europe from 367 in 2014 to 725 in 2019 [54]. Furthermore, because of the new

perspective of methane and its potential availability in nature through biological means, methane is valorised in many works, in particular converting it into other value-added chemicals such as the production of hydrogen H2 [55], ethylene [56] which is a monomer used for the production of polyethylene PE (plastics) [57], as well as the conversion of methane into liquid hydrocarbons using GTL technology under forms: kerosene, naphtha, gasoline, diesel and clean base oil [58]–[60].

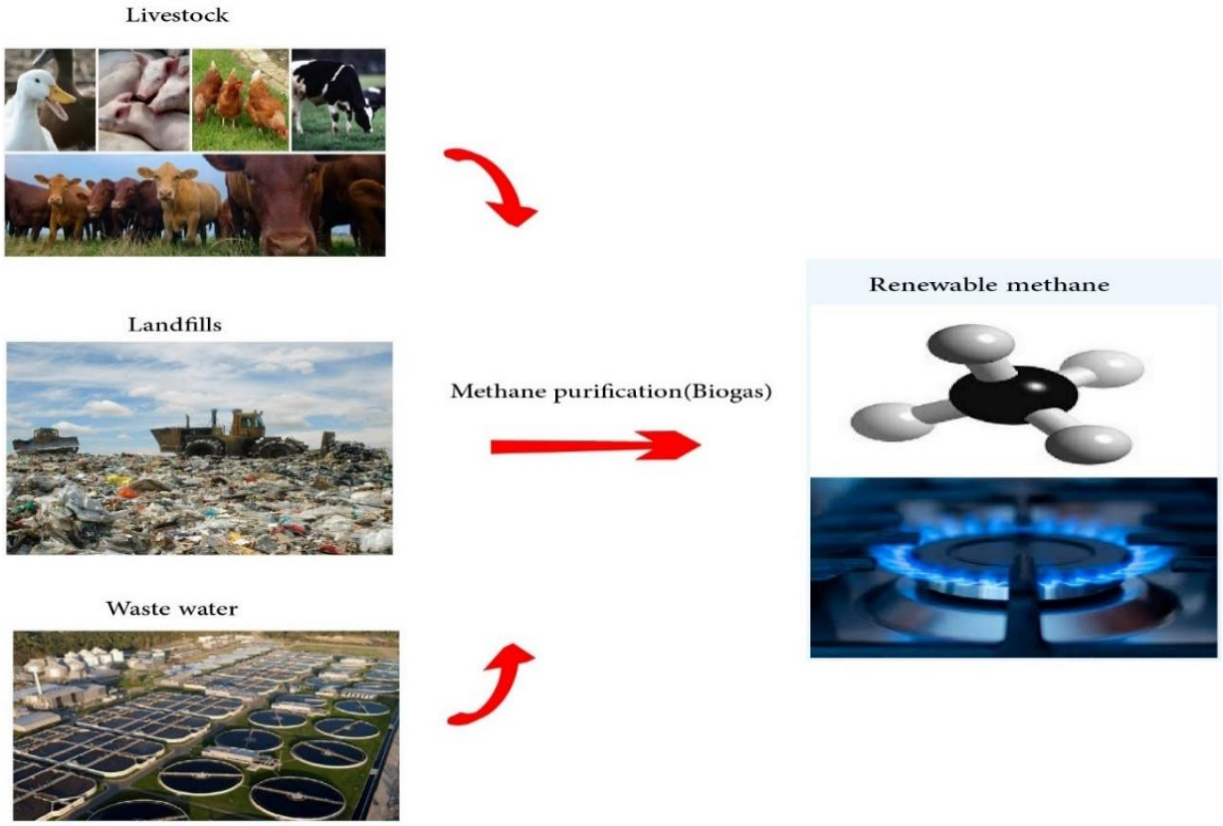

Figure 1-1. Relevant sources for renewable methane gas production

1.2 METHANE PURIFICATION FOR EFFECTIVE UTILIZATION

Raw methane contains other contaminants such as carbon dioxide, hydrogen sulfide, and water vapor; their concentrations vary depending on the source of raw methane; they are non-combustible and causing problems during production if not eliminated; therefore, purification of raw methane from these undesirable constituents is required to meet the specifications of methane use. Methane dehydration for water vapour removal is a crucial phase in raw methane gas processing facilities that prevents the formation of methane hydrates, pipeline corrosion if the gas contains acidic components such as carbon dioxide, hydrogen sulfide, and a loss in

methane gas heating value. To avoid these issues, the water content of raw methane gas must be decreased by the use of appropriate separation techniques [61].

1.3 CONVENTIONAL SEPARATION FOR METHANE GAS DEHYDRATION

Dehydration of raw methane gas can be achieved using a variety of separation techniques. The most frequent used are liquid desiccant dehydration, solid desiccant dehydration, and refrigerating by cooling the gas [62].

1.3.1 Absorption-based dehydration

Absorption is the most common method of drying gases, in which the water vapor in the gas stream is absorbed into a liquid solvent that has a high affinity for water, whereby glycols are the most commonly used absorption liquids [61]. However, this drying technique presents certain environment-related disadvantages due to the pollution caused by venting the BTEX (benzene-toluene-ethanol-xylene) into the atmosphere [61], [63]. In addition, it is energetically costly due to the necessary of distillation columns to regenerate the glycol, where the energy is consumed for the circulation and the heating of the glycol liquid [61]. Nonetheless, absorption is more cost-effective than other traditional dehydration processes since it consumes less energy, which is why absorption dehydration is commonly used to dry raw methane in the natural gas processing plants [62].

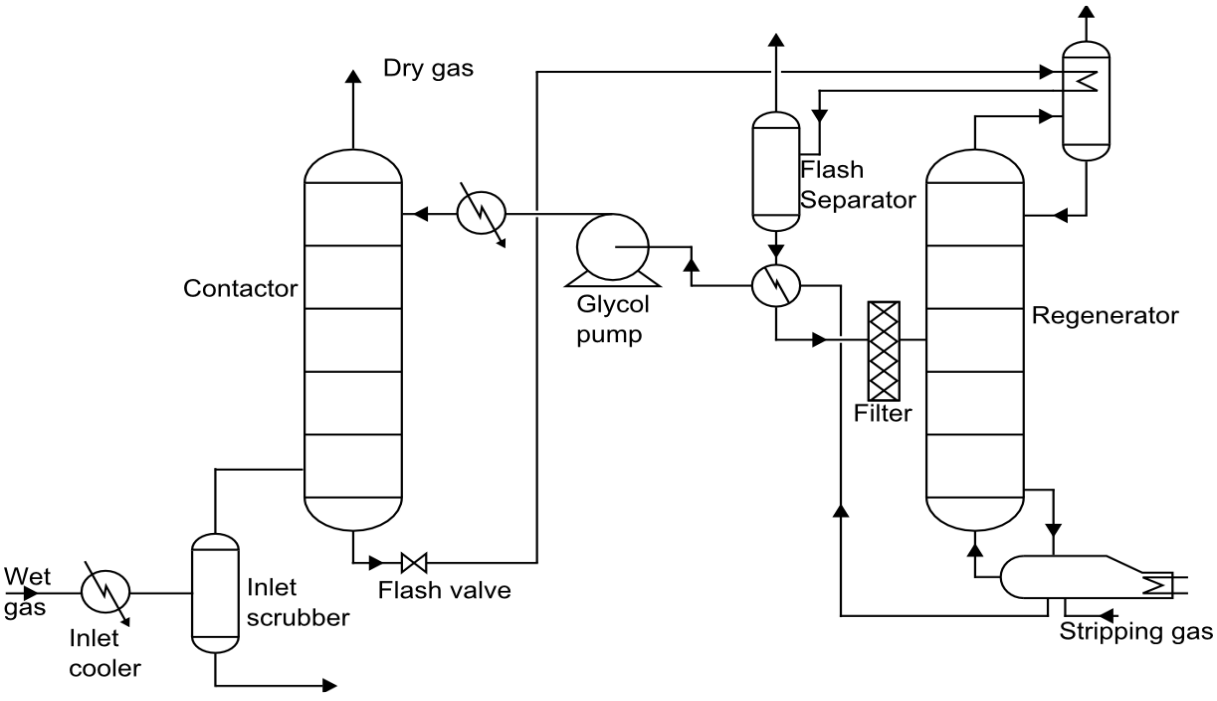

Figure 1-2. Absorption dehydration process

1.3.2 Adsorption-based dehydration

The dehydration of raw methane by adsorption uses solid desiccant for the removal of water vapour, it is carried out with a system of two beds, which are filled with adsorbents, usually by a molecular sieve, activated alumina, silica gel and silica-alumina gel. The gas is conducted through one of the adsorbents, allowing the water vapour to be removed by adsorption phenomena, while the methane passes through it and reaches a low water vapor content. The adsorbents are redundant, one is in operation for adsorption while the other is regenerated by hot gas to ensure continuous dehydration. The process is illustrated in Figure 1-3 [64], [65].

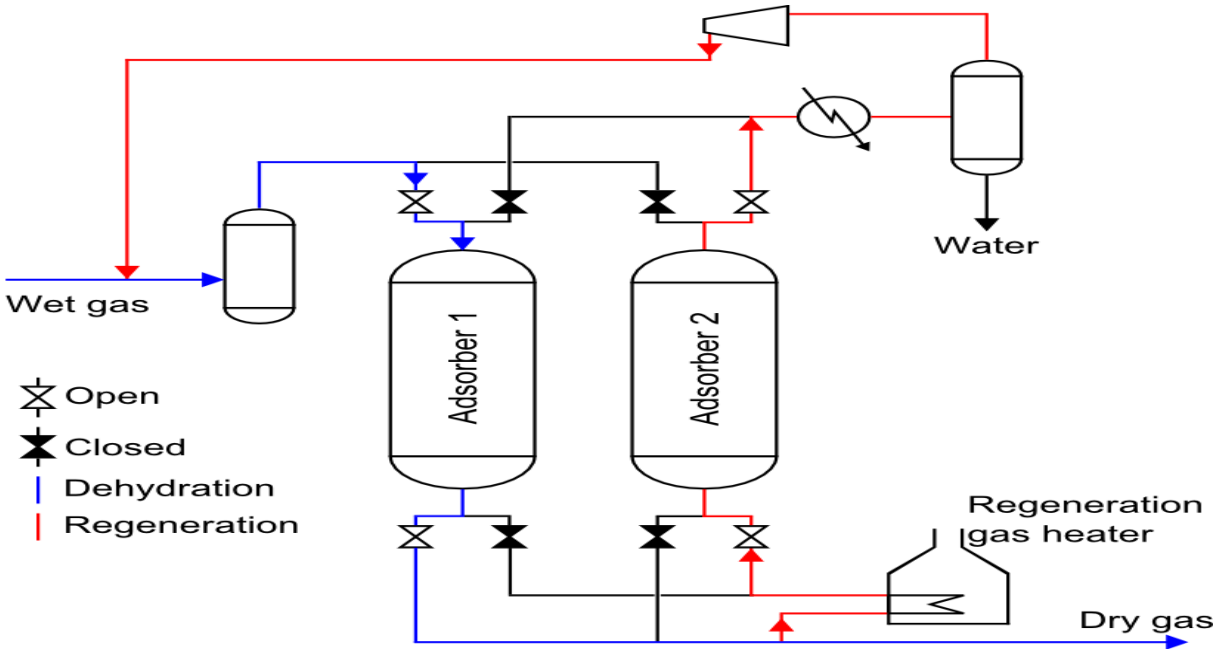

Figure 1-3. Adsorption dehydration process

1.3.3 Dehydration by refrigeration

Gas dehydration by refrigeration is a low-cost dehydration method. Water condenses when the gas is cooled; the water is then removed in a separator. The separation method can be conducted numerous times. The method is most efficient at high pressure. The amount of water removed in the refrigeration process is often insufficient. Because of the low cost the refrigeration process is often used before the other dehydration processes [66].

1.4 DEHYDRATION OF METHANE GAS USING MEMBRANES

The conventional methods of water vapor removal by absorption and adsorption may be regarded almost acceptable, although their disadvantages consist in the fact that these techniques consume a significant amount of energy and notably impact the environment. Accordingly, new innovative separation technology using membrane films have been developed and are under intensive research and development, which offers many advantages, such as separation of components at a lower temperature, reduction of thermal damage to the product, separation of the component in its own form, lower energy consumption, easy operation, less waste, cleaner environment. Membrane separation has been implemented in diverse separation applications, such as wastewater treatment, water recycling, enhanced oil recovery, separation of organic liquids, oil-to-gas conversion, and others. In this regard, this thesis was established to mainly contribute to the development of to the new membrane technology for methane gas dehydration, founded on many works that have been similarly developed for methane gas dehydration using membranes, the results are presented in Figure 1-4, where it is clear that the separation performance depends on the type of polymer-based membrane, such Nafion membrane, the dehydration performance of methane gas is significantly greater than that of the polyethylene (PE) membrane. Therefore, the selection of the right membrane based polymer is crucial for the gas separation efficiency [67].

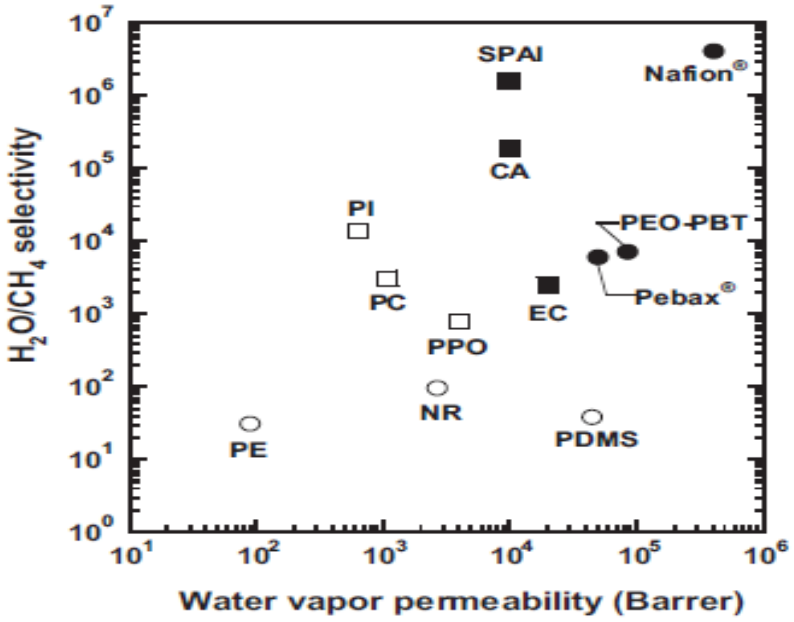

Figure 1-4. Water vapor permeability (extrapolated to zero activity) and H_2O/CH_4 selectivity at about 30 ◦C in various polymers [67]

1.5 PRINCIPLE OF MEMBRANE SEPARATION

Membrane is semi-permeable barrier, that serves as a filter to separate two phases that can be liquid, gas, or vapor. According to the membrane-based material and configuration, the membrane performance of the separation as consequence is varying. The principle of membrane separation can be presented in the Figure 1-5, where the feed stream is separated into two parts, permeate and retentate. The permeate is a term describing the molecules that are passed the membrane, while the retentate describes the feed stream which is captured by the membrane [68].

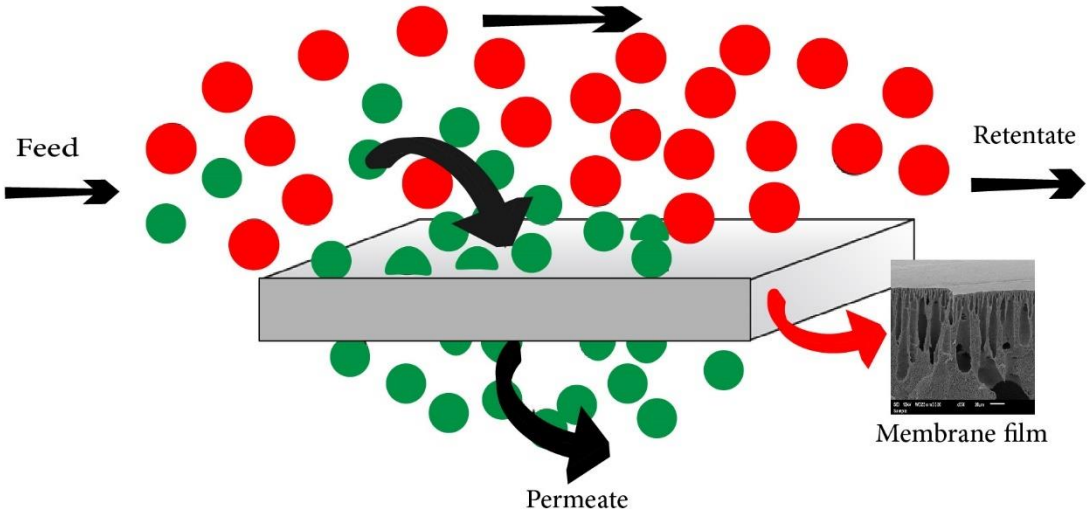

Figure 1-5. Membrane principal separation process

1.6 MATERIALS USED FOR MEMBRANE FABRICATION

The membranes are made from a wide variety of organic and inorganic materials.

1.6.1 Organic Membrane Materials: Polymers

The organic materials used in the preparation of membranes are polymers, which are characterized by a very long chain of small molecules or units called monomers. Polymers can be originated from natural or synthetic sources and their use offer benefits over other materials by availability, low cost, easily processed into a desired shape and structure for specific application [66], [69], [70]. Many works have used polymeric materials according to their application for separation, the most used polymers are polycarbonate (PC), cellulose acetate (CA), polyesters (PE), polysulfone (PSf), polyimide (PI), polyetherimide (PEI),

polytetrafluoroethylene (PTFE), polyamide (PA), polyacrylonitrile (PAN); polyetherimide (PEI), , polyether sulfone (PES), polypropylene (PP), poly(vinylidene fluoride) (PVDF) [66], [70].

1.6.2 Inorganic Membrane Materials

They have an excellent thermal and chemical stability, from ceramics to metals to inorganic polymers. The glass, metal, alumina, zirconia and zeolite membranes are examples of this type. Other inorganic materials such as silica, silicon carbide, nitride of silicon, titanium, cordierite, oxide of tin, and mica. Inorganic membranes have certain benefit in comparison to polymeric membranes, such as high chemical resistance, stable and well-defined pores with high operating resistances: for metallic membranes 500-800°C and for ceramic membranes over 1000°C. However, they are fragile, costly and difficult to scale [23].

1.7 MEMBRANE MODULES

Figure 1-6 shows the two most common module designs: flat sheet and hollow fiber modules. Due to the high compacity offered, the hollow fiber configuration is the most popular on the industrial level because of its high specific surface area. The hollow fiber module includes a hollow-fiber collection placed in the calendar. One fluid passes through the fibres, the other runs across the calendar. Flat sheet modules have a much smaller specific surface area than hollow fiber modules, but due to their simplicity of design and easy module configuration are preferred for laboratory testing [70].

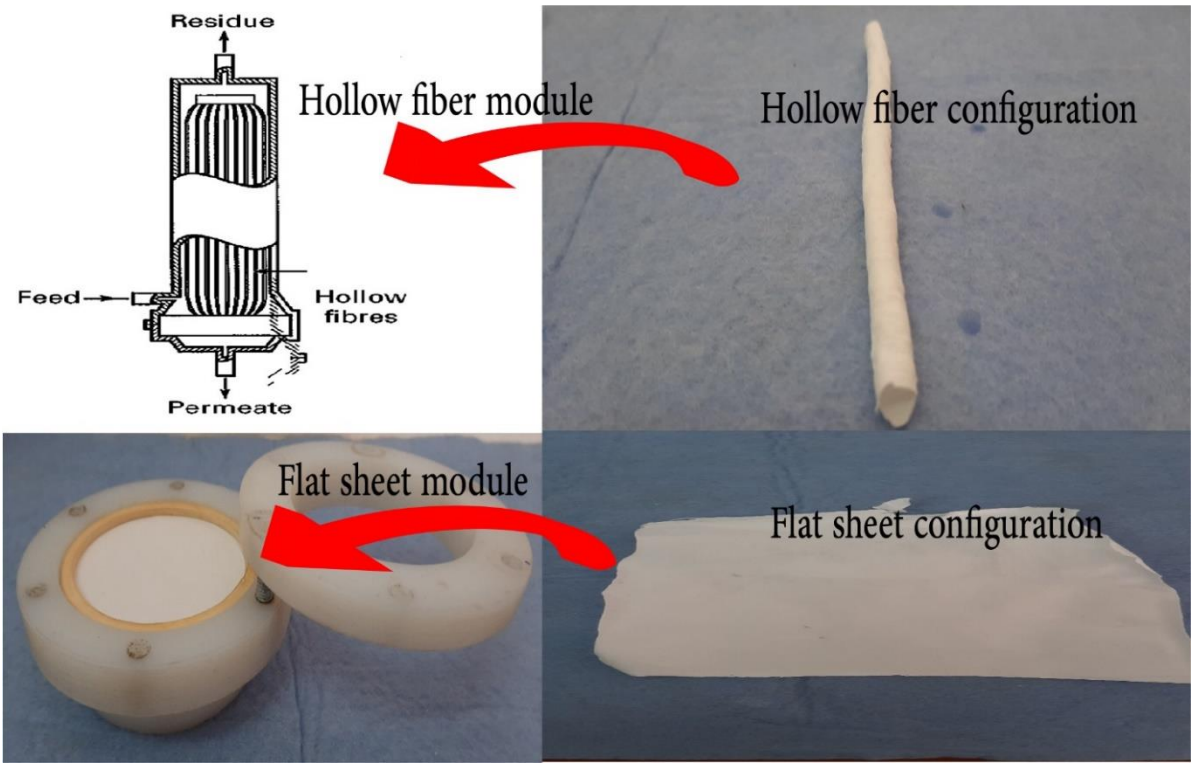

Figure 1-6. Membrane configuration types

1.8 MEMBRANE MORPHOLOGY

As shown in Figure 1-7, the membrane morphology can be divided into two types, isotropic or symmetric membrane and anisotropic or asymmetric membrane [70].

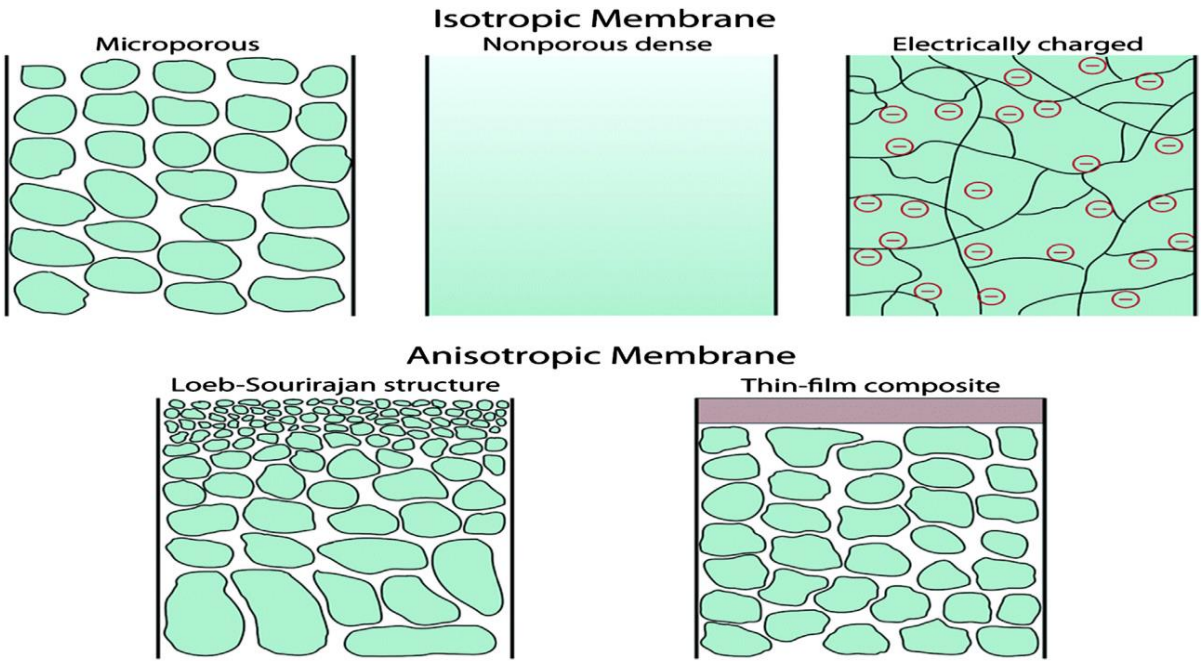

Figure 1-7. Isotropic and anisotropic membranes morphology

1.8.1 Isotropic Membranes

1.8.1.1 Dense nonporous isotropic membranes

Dense nonporous isotropic membranes are rarely used in membrane separation processes because the transmembrane flux through these relatively thick membranes is too low for practical separation processes. Isotropic (dense) membranes are usually prepared from solution casting by solvent evaporation or by extrusion of the melted polymer [70].

1.8.1.2 Isotropic Microporous Membranes

Isotropic microporous membranes have much higher fluxes than isotropic dense membranes and are widely used as microfiltration membranes. The most important type of microporous membrane is formed by the phase separation techniques, other techniques are able also to make it, the most important: track etching, stretching or leaching, and electrospinning.

1.8.2 Anisotropic Membranes

Anisotropic membranes typically have a very thin surface layer supported by a thick microporous layer. The thin layer is used as a selective layer to perform the separation while the thick microporous layer provides the strength to the membrane. The membrane fluxes are usually very high due to the thickness of the selective layer. The anisotropic membranes are mainly prepared by: Phase separation membranes, interfacial polymerization membranes, solution-coated composite membranes. The nonporous/isotropic membranes are used for gas separation, such as the dehydration of methane gas, the dense polymer layer contains no fixed pores, the separation is by solution-diffusion mechanism and occurs by the solubility differences of the permeant in the membrane material [70].

1.9 PHASE SEPARATION PROCESS FOR MEMBRANES PREPARATION

Many descriptions are often used; they all have a similar meaning to the phase separation process, named phase inversion process or polymer precipitation process. The term phase separation describes the process most clearly, namely, changing a one-phase casting solution into two separate phases. Where a liquid polymer solution is precipitated into two phases: a solid, polymer-rich phase that forms the matrix of the membrane and a liquid, polymer-poor phase that forms the membrane pores. The Precipitation to form the anisotropic membrane of the cast liquid polymer solution can be achieved in many ways:

A. **Water precipitation (the Loeb–Sourirajan process):** The cast polymer solution is immersed in a nonsolvent bath (typically water). Absorption of water and loss of solvent cause the film to rapidly precipitate from the top surface down.

B. **Water vapor absorption:** The cast polymer solution is placed in a humid atmosphere. Water vapor absorption causes the film to precipitate

C. **Thermal gelation**: The polymeric solution is cast hot. Cooling causes precipitation

D. **Solvent evaporation**: A mixture of solvents is used to form the polymer casting solution. Evaporation of one of the solvents after casting changes the solution composition and causes precipitation.

1.10 SOLUTION CASTING FILM APPLICATOR:

Solution casting is widely applied to generate small samples of membrane for laboratory characterisation tests, whereby, a suitable polymer solution is distributed onto a flat plate with a casting knife. The casting knife consists of a steel blade, sitting on two runners, designed to produce a precise gap between the blade and the plate onto which the film is cast, the necessary gap displays the membrane thickness. For casting application, common film applicators are frequently used, as depicted in below Figure 1-8.

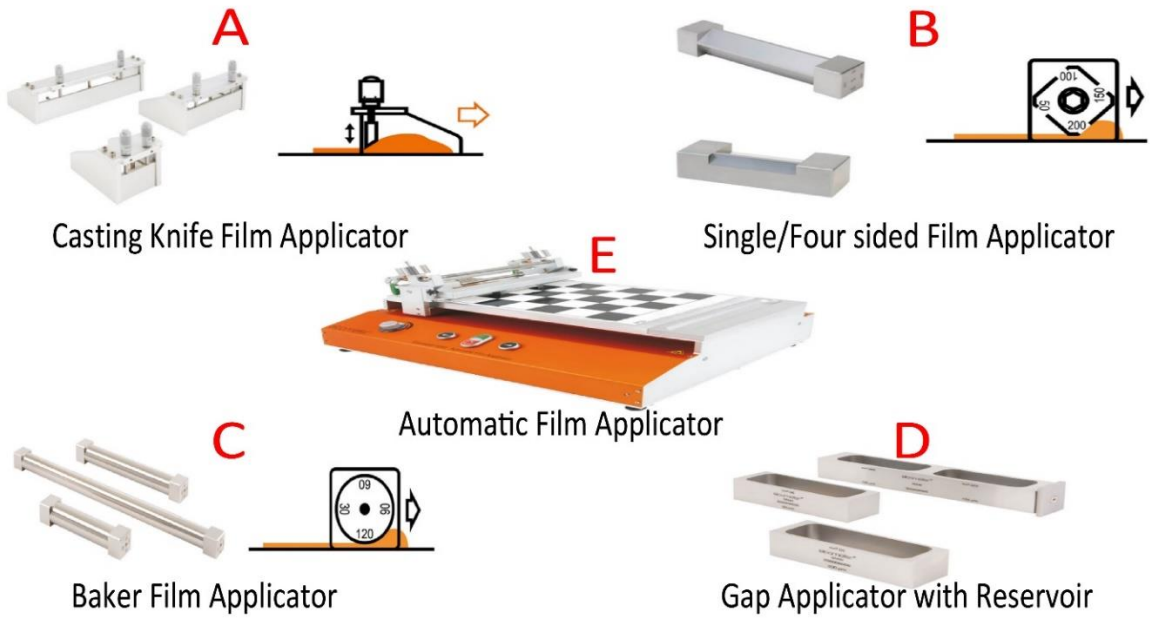

Figure 1-8. Typical film applicators widely used

1.11 GAS SEPARATION MECHANISM IN POLYMERIC MEMBRNES

The membrane consists of two morphological structures, dense membranes and microporous membranes. The separation by porous membrane is controlled by the variation in the pore's diameter whereas in dense membranes, the separation is carried out by diffusion, where the gas dissolves into the membrane material and diffuses across it, such as the dissolution of gas into liquid. In general, four basic mechanisms promote separation in both structures. Figure 1-9 clearly depicts them, including convective, Knudsen, sieving, and solution diffusion.

In the microporous membranes, if the diameter of pores is greater than 0.1 μm (100 nm), it is considered a large pore in gas separation; in this case, the gasses separation is carried across the membranes by convective flow without any separations, because the kinetic diameters of gas molecules are smaller than the pores diameter [71], [72]. When the pore diameter is less than 0.1 m (100 nm), the pore size is larger than the molecule gas size but smaller than the gas molecule's mean free path, allowing lighter molecules to preferentially diffuse through the pore, the diffusion is governed by Knudsen diffusion, gas molecules can be separated based on the inverse square root ratio of its molecular wight. These membranes are thus limited since they are better adapted to systems with high molecular weight ratios [71]–[74]. if the pores of porous membrane are on the order of sub-nanometres in the order of gases molecule diameter, then gases are separated by molecular sieving. Large molecules are excluded from the pores whereas gas molecules with smaller diameter can be transported through the membranes. The main limitation in this mechanism is that condensable gases such as water vapour cause fouling and directly affected the structure of the membrane [73].

In the dense membrane, the gas transport occurs through the following steps: absorption, diffusion, and release. In the first place, the penetrating gas molecules dissolve on the membrane upstream face (or at high pressure); second, the gas diffuse through the membrane; and third, it is released at the downstream (or low-pressure) [72].

As is well known, almost of gases molecule having a diameter of about 1-10 Å (0.1-1 nm), including methane and water vapor, with a dimeter of 3.8 Å for Methane and 2,65 Å for water ,therefore, for the separation of water vapor from methane gas by molecular sieving mechanism, it requires a porous membrane of a range 3 Å, nevertheless, the separation by sieving is performed with a lower performance, first raison is that the diameter of methane and water vapor molecules, they are close to each other, and secondly, the potential of water vapor

condensation within the pores; blocking the methane passage. For that raison, the dense membrane is ideal for methane gas dehydration than microporous membrane.

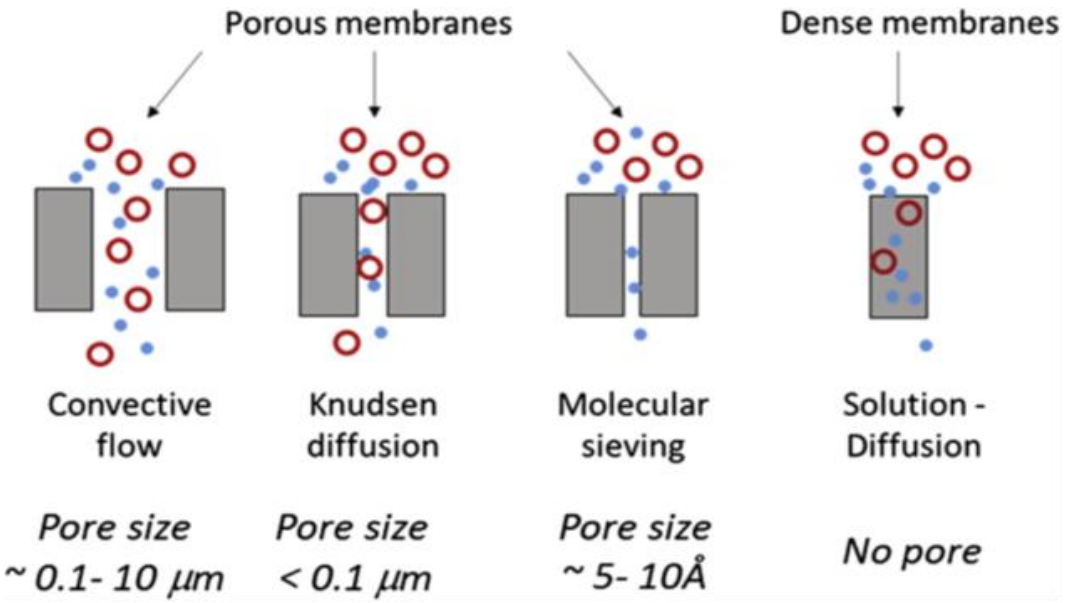

Figure 1-9. Gas transport mechanisms through membranes

Chapter 2

Materials and methods for PET membranes preparation

This chapter covers all materials used in this thesis, including polymers, solvents, and instrumentation, as well as methods for preparing PET membranes, blending PEG additives, and measuring water vapor and methane gas permeabilities to identify the membranes performance, even though materials and procedures used to characterize the membranes are also detailed in this chapter. The results are not explored in this chapter, alternatively, they are discussed in detail in the following chapters.

2.1 MATERIALS

2.1.1 Polymers

2.1.1.1 Polyethylene terephthalate (PET) polymer

The PET (CZ-302) shown in the Figure 2-1 has a molecular formula of $C_{12}H_{14}O_4$, it was used to make a PET film membrane, it is received from Jiangsu Xingye Plastic Co Ltd (China) in the form of chips, with an intrinsic viscosity of 0.80 ± 0.02 dL/g. The purchased PET polymer is suitable for bottle grade applications as well as a variety of packaging applications such as pure and mineral water bottles, distilled and drinking water, flavour and candy containers, and PET films. For more details of PET polymer, its specification is shown in the Table 2-1.

Prior to any use, the PET polymer is pre-washed with distilled water to eliminate any particles of dust and is then dried overnight in the furnace at a temperature of 60°C to ensure that any residual water and adsorbed moisture are completely removed.

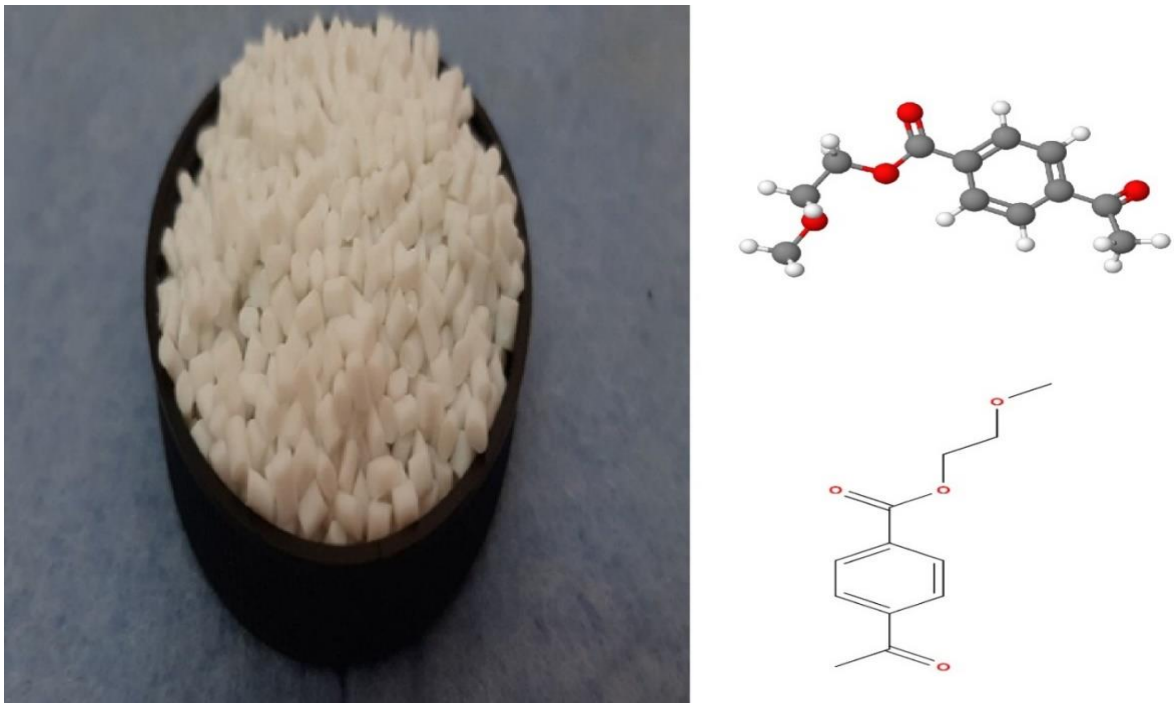

Figure 2-1. Polyethylene terephthalate (PET) polymer with chemical structure

Table 2-1. Polyethylene terephthalate (PET) specification

Form	Chips
Mol wt	222.24 g/mol
Ph	Not vailable
Melting point mp	250-255 °c
Boiling point bp	>170 °c (press: 10 torr)
Storage temp	Room temp

2.1.1.2 Polyethylene glycol (PEG) additive polymer

Polyethylene glycol (PEG) presented in Figure 2-2 has an average Mn ≈ 6000 of linear formula $H(OCH_2CH_2)_nOH$, it is packaged and received from Merck as flakes in a 1 kg plastic bottle, it was used as additive for making blended PET/PEG membranes. It may be emphasized that the PEG is a hydrophilic polymer, which is a convenient for biological applications since it does not induce an immune defence response. The main applications of PEG are the manufacturing of bioactive and immuno-insulating barriers for cell encapsulation. PEG did not undergo any further treatment; it is used as received quality.

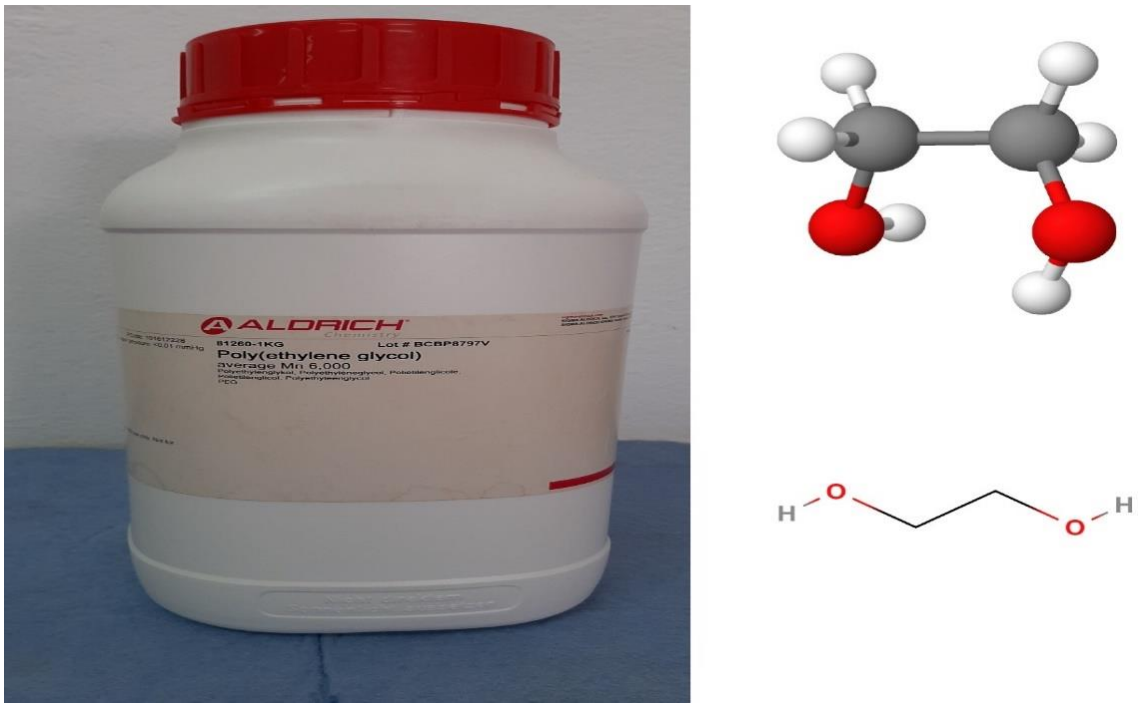

Figure 2-2. Polyethylene glycol (PEG) additive polymer with chemical structure

Table 2-2. Polyethylene glycol (PEG) specification (Specification Sheet: sigmaaldrich.com)

Form	Flakes
Mol wt	Mn 5,000-7,000, average mn 6,000
Ph	4.5-7.5
Boiling point bp	60-63 °c
Storage temp	Room temp

2.1.2 Pure methane gas

The methane gas is received in liquefied phase stored in cryogenic bottle with a purity of 99.8 percent; it is delivered from Sonatrach's GNL-2 facility in Arzew (Algeria). The pressure necessary for setup is increased by warming the bottle in the water bath; the temperature in the water bath should be gradually increased to avoid the cryogenic bottle collapsing by thermal chock.

2.1.3 PET membrane solvents

2.1.3.1 Dichloromethane (DCM) solvent

Dichloromethane (DCM) is received and purchased from Merck in liquid form in a bottle glass of 2,5 litters (Figure 2-3), it was used as a PET membrane solvent. Dichloromethane is a colourless liquid with a mild and sweet odour (ether-like odour) of the formula CH_2Cl_2. This volatile liquid is almost immiscible with water, a value of 13,2 g/l at 25 °C [75]. It is widely used as a solvent for membranes preparation [76]–[79].

Figure 2-3. Chemical structure of Dichloromethane (DCM)

Table 2-3. Dichloromethane (DCM) specification [75], [80]

Form	Liquid
Color	Colorless
Mol weight	84.93 g/mol
Ph	No data available
Density	1.325 g/ml at 25 °c (lit.)
Vapor density	2.93 (vs air)
Vapor pressure	584 hpa at 25 °c
Melting point (mp)	Melting point: -95 °c at 1.013 hpa
Autoignition temp	605 °c
Boiling point bp	40 °c at 1.013 hpa
Storage temp	Cool place, heat sensitive

2.1.3.2 Trichloroacetic acid (TCA)

TCA with the formula $C_2HCl_3O_2$, it has a stinging odour, was obtained as a crystalline powder in a 500 g glass bottle and was used as is to prepare the membrane solvent, purchased from EDEN LABO, SARL, Algeria (Figure 2-4). Trichloroacetic acid in solution phase appears as clear colourless crystals with corrosive character for metals and tissues [81].

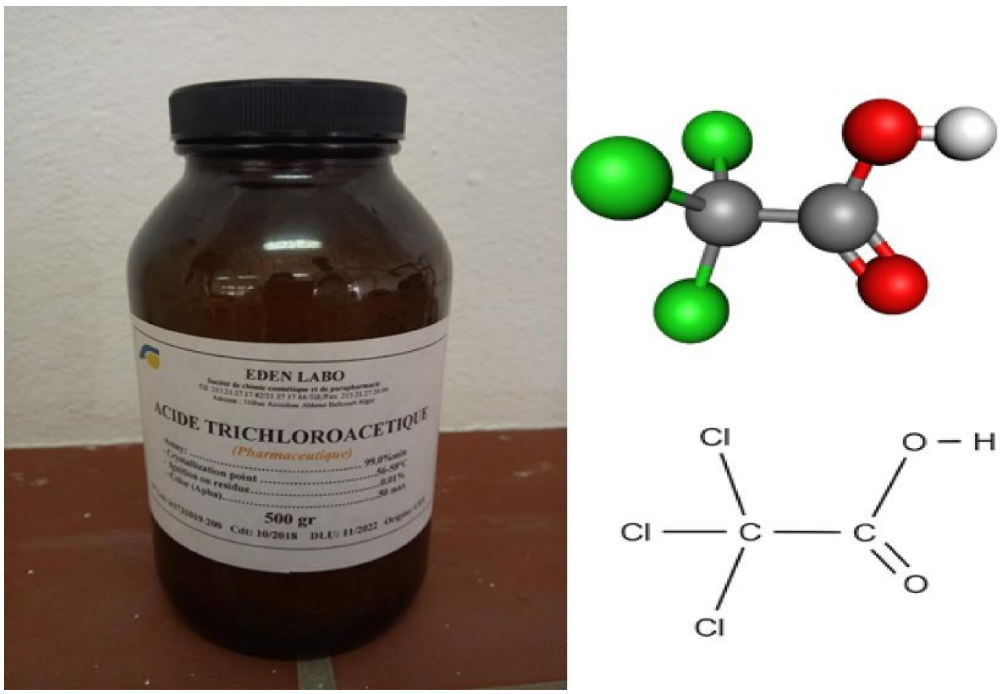

Figure 2-4. Trichloroacetic acid (TCA) with chemical structure

Table 2-4. Trichloroacetic acid (TCA) specification [81]

Form	Crystalline powder
Color	Off-white
Mol wt	163.39 g/mol
Ph	1 at 81,7 g/l at 25 °C
Density	1,62 g/cm3 at 25 °C
Vapor density	5,64 (vs air)
Vapor pressure	1 hpa at 51 °C
Melting point (mp)	54-58 °C (lit.)
Autoignition temp	Does not ignite
Boiling point bp	196 °C (lit.)
Storage temp	2-8°c

2.1.4 PET Membrane solvent mixture TCA/DCM

2.1.4.1 TCA Dissolving in DCM

TCA is suitable entirely for dissolving PET polymer, and was considered as a strong candidate to dissolve PET polymer by its own, nevertheless, TCA is available only in the form of a crystalline powder at atmospheric conditions, and it is not possible to use it in a solid form for dissolving. For that reason, the TCA crystal is dissolved in DCM solvent and transferred into a homogeneous mixing liquid of TCA/DCM solution. The main goal for dissolving TCA was to obtain a mixture solution which is able to dissolve the PET polymer. The DCM solvent was selected to produce a solvent of mixed homogeneous solution for PET polymer preparation, mainly used because when compared to the other solvents, first of all, it is a solvent for TCA, at the meantime, it partially dissolves the PET polymer, while water for example as a solvent has no advantage to dissolve the PET polymer.

Due to excessive corrosion of the TCA (PH=2.1), it was difficult to handle the TCA crystals during the solvent preparation, as precaution, during the preparation of the mixture solvent TCA/DCM, the TCA is dissolved at one time, the use of a lower quantity for repetitive preparation is prohibited, for example 500 g of TCA crystal as received is totally dissolved.

2.1.4.1.1 Saturation of DCM by TCA

A minimum volume of DCM solvent is required to completely dissolve the total amount of used TCA. Experiments were carried out with the aim of dissolving totally 500 g of TCA crystals in DCM solution, the findings are summarized in the points below, in which it is concluded that when using the total amount of received TCA of 500 g, at least 200 ml of DCM is necessary to dissolve it:

1. First experience: 100 ml of DCM is added to 500 g of TCA and well stirred overnight, however, it was not enough, the TCA is partially dissolved, and the rest was kept in a solid status at the bottom of the glass.
2. Second experience: 200 ml of DCM is added to 500 g of TCA under 24 hours of stirring, a homogeneous solution is obtained and used as reference for all experience calculation.

2.1.4.1.2 Selection of TCA/DCM ration

The membrane solvent was carefully prepared by dissolving the TCA crystal powder in DCM solution, the mixture was stirred at medium speed and at room temperature. In a test to select the appropriate proportion of the solvent of the mixture able to completely dissolving the PET granules, different proportions of TCA:DCM were prepared ((3:1), (3:2), (3:3), (2:3), (1:3)) and tested, the amount of PET was kept constant in the casting solutions at a concentration of 8 wt. %. The results carried out for dissolving the PET membrane with TCA/DCM solvent solution are shown in Table 2-5.

For a ratio (1:3), beams of PET remained even after keeping the solution stirred for 48 hours, while PET was completely dissolved in other proportions. In this study, the proportion (2:3) of TCA: DCM was chosen for the preparation of PET membranes, mainly for cost reasons. the price of TCA being 6 times that of DCM.

Table 2-5. Ratios of solvent solution TCA/DCM for dissolving of PET membranes

TCA:DCM ration(%)	Observation
3:1	24 hours of stirring, PET is totally dissolved
3:2	24 hours of stirring, PET is totally dissolved
3:3	24 hours of stirring, PET is totally dissolved
2:3	24 hours of stirring, PET is totally dissolved
1:3	48 hours of stirring, beams of PET are remained

2.1.5 Non-solvent solution

Distilled water is used as a non-solvent for PET membrane fabrication, other non-solvents such as methanol can be used to dissolve TCA/DCM solvents, and however, distilled water is chosen primarily due to its wide availability in the laboratory scale.

2.1.6 Instruments

2.1.6.1 Polymers-solvents mixing glass bottle

The mixing glass bottle is used to blend the mixture of polymers and solvents with the use of a magnetic stirrer, it can be pointed out that the use of 50-100 ml syrup glass bottles (Figure 2-5) that are used in package of midication liquid is the appropriate type since these bottles having the following advantages: firstly, the glass material does not react and does not stick with dope solution of polymers, secondly, the non corrosive allimunium screw cap with a silicone seal are not soluble with polymer solvents, it should be indicated that a special care must be taken when using the gaskets, particularly when the solution contains a light and volatile solvent such as DCM with a boiling temperature of 39.8-40 °C, if the sealing is defective, the results will not be accurate. Finally, the color of the glass bottle is amber, which preserves the solution from degradation and minimizes the effect of sunlight.

Before using the bottles for prepartion of the membrane dope solution, the collected glasses are first soaked in distilled water for a week, then washed with soapy water and rinsed thoroughly with distilled water, after which they are dried in an oven overnight at a temperature of 60°C to remove all moisture inside the bottles.

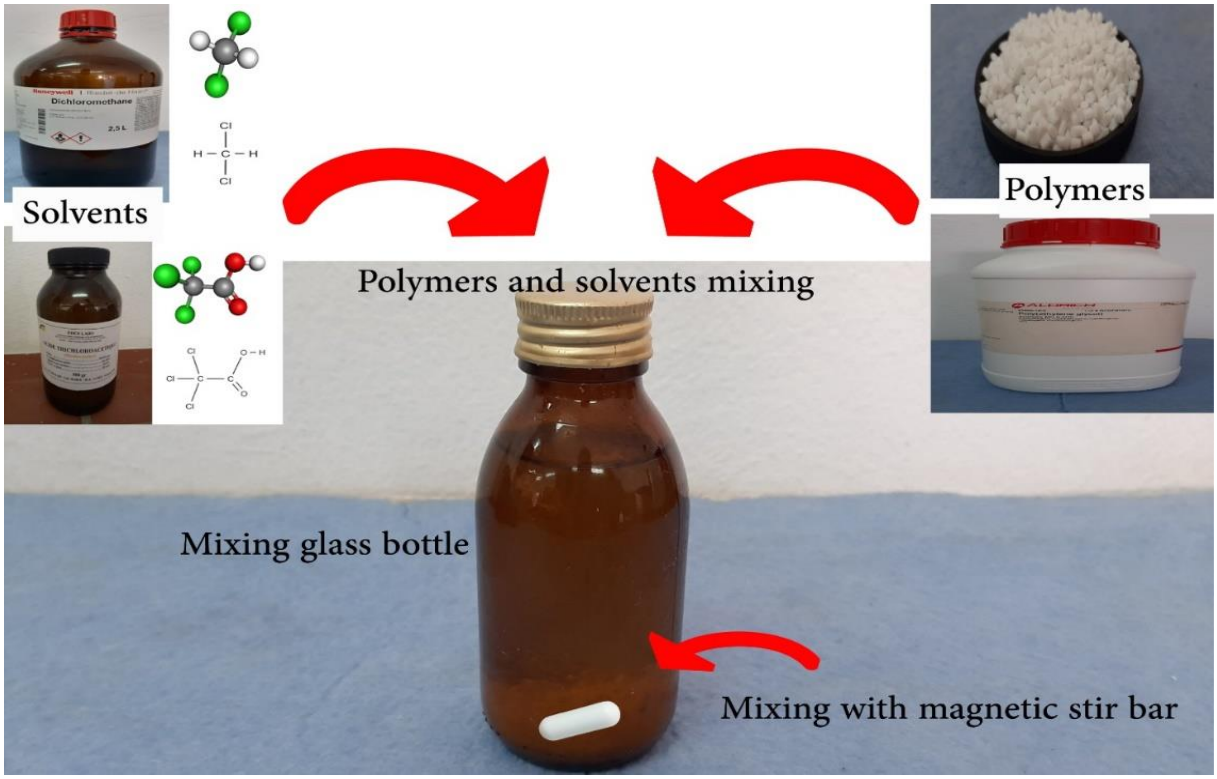

Figure 2-5. Polymers-solvents mixing glass bottle

Table 2-6. Mixing glass bottle properties

Material	Glass
Glass bottle Color	Amber
Cap material	Aluminum cap
Capacity	50-100 ml
Aluminum cap color	Gold
Cup gasket	Food grade silicone gasket
Type	Screw cap

2.1.6.2 Magnetic stirrer

For mixing PET membrane mixtures, a magnetic stirrer occupied by a heater with a different mixing speed option is used. Stirring is performed by means of a suitable stir bar with a diameter of 25 mm, which is introduced with the mixture into the glass bottle. The rate of speed was adjusted to the maximum rate at which the solutions should be in laminar regime and no turbulence observed producing bubbles. Figure 2-6 shows the process of stirring of the polymer-solvent mixture in the glass bottle, containing a magnetic stirring bar using a magnetic stirrer.

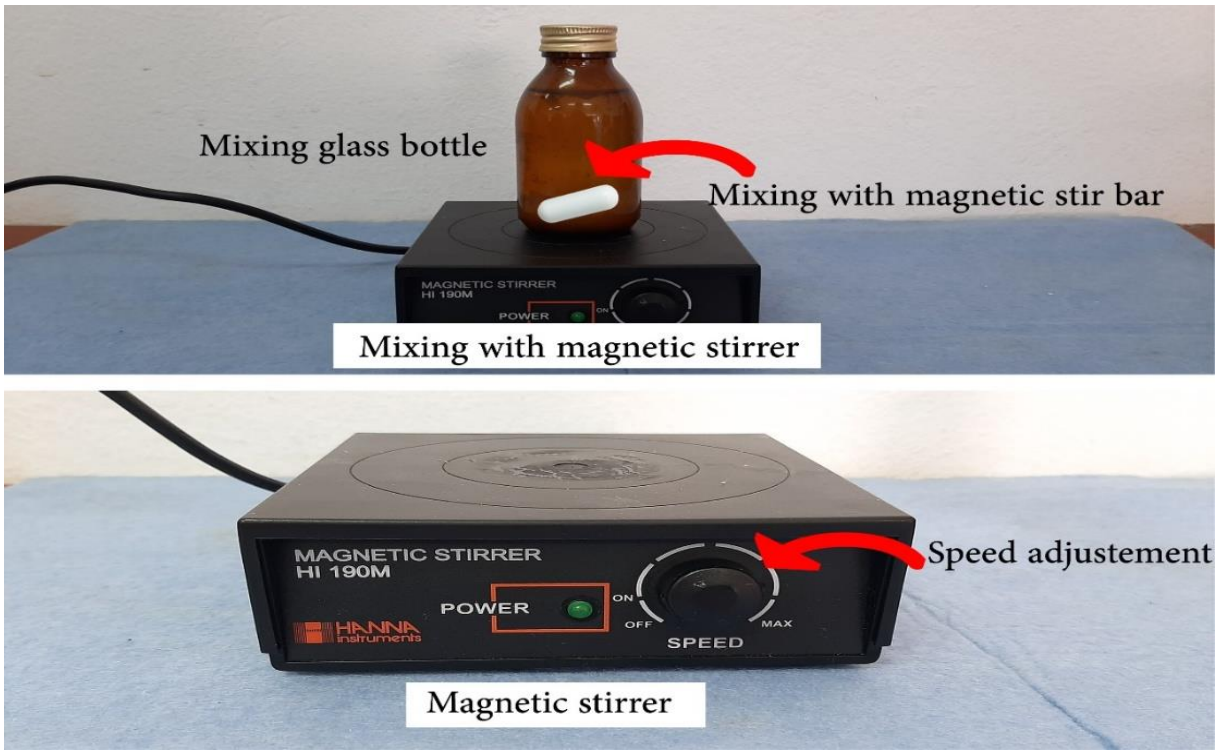

Figure 2-6. Mixing process with magnetic stirrer- stir bar

2.1.6.3 Dope solution flat glass plate

The glass plate (Figure 2-7) is used to receive on its surface the PET dope solution, for producing flat PET membranes. The material glass is chosen rather than other materials such as metals, wood, plastics, because the PET membranes once formed do not stick to its surface, thus providing a smooth and flat surface. Limited measures are required to accept the use of glass plate for the making of flat membranes. The glass surface should be free of mechanical grooves that could affect the development of the membrane, furthermore, it should be kept clean of any dust, it is preferable to clean it before use with an antistatic cloth to prevent any attraction of microfibers to its surface that would later affect the formed membranes.

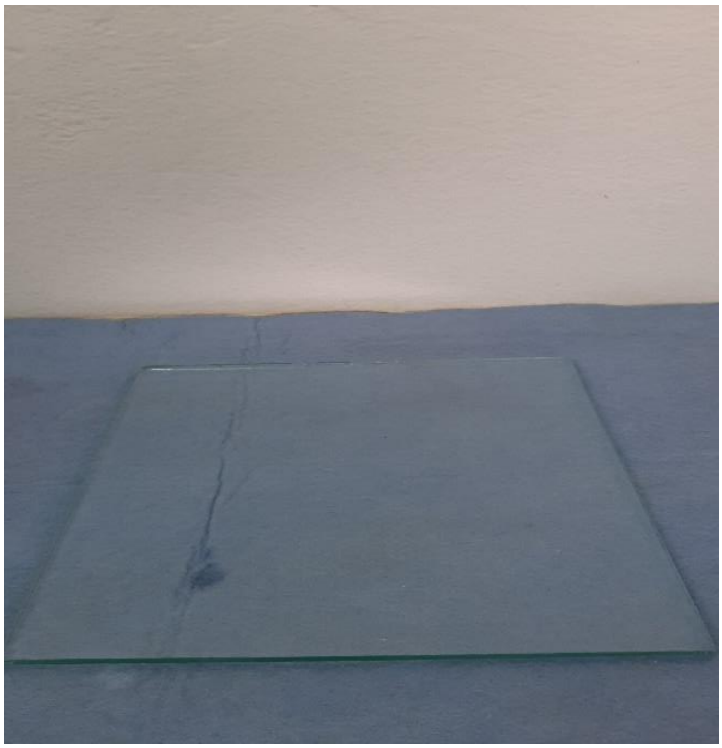

Figure 2-7. Flat glass plate for dope solution application

2.1.6.4 Coagulation bath

The coagulation bath (Figure 2-8) is a glass recipient containing the non-solvent solution which is distilled water. To obtain the structure of the membranes, the dope solution on the glass plate is soaked and kept inside the distilled water for removing all the solvents from the dope solution, nevertheless, a minimum level of distilled water is required whereby the entire dope solution should be covered and immersed in the water. The temperature of the bath is maintained at room temperature, usually the temperature of the climatic environment was on average of 24°C.

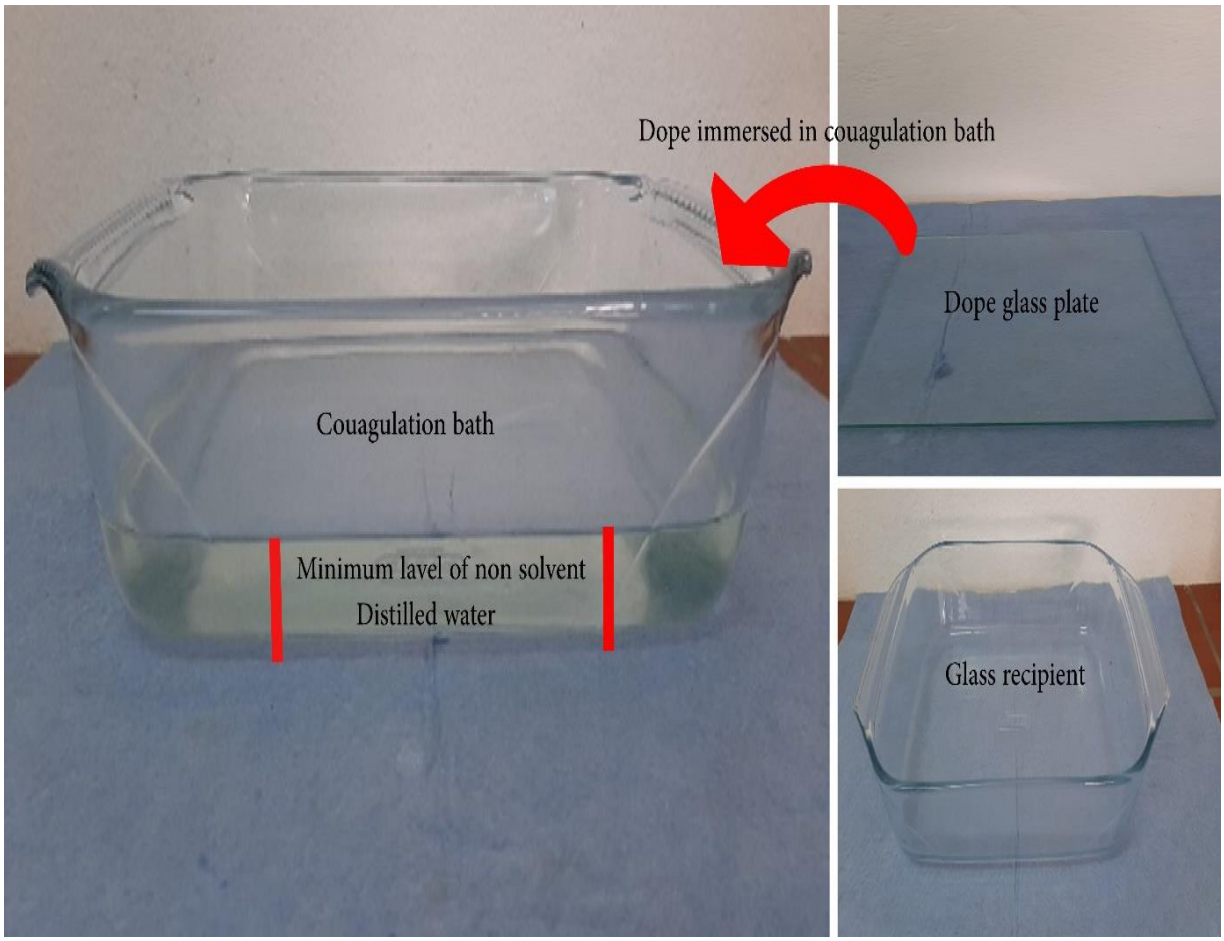

Figure 2-8. Coagulation bath filled with distilled water

2.1.6.5 Cup of water

The water cup also known as a test dish, is homemade fabrication with a circular shape design according to the recommendations of ASTM E 96, Figure 2-9 presents all the dimensions and layout details including the water cup on the left and its flange on the right.

The water cup shown in Figure 2-10 is necessary instrument in membrane technology, used in our work to perform water vapor permeability measurements of PET membranes to eventually determine the performance of PET membranes towards water vapor transport.

The structure of the cup of water is made by polyamide material, it has been chosen mainly over stainless steel because it is non-corrosive, impermeable to water or water vapour and specifically light, this last characteristic has the advantage of detecting small changes in weight during measurement and obtaining more accurate results. An external flange is also manufactured with a bolt clamping system, which is attached to the top surface of the water cup

that has a 5 mm strip left around the edge supported with the use of a Teflon gasket to properly seal the membrane film around the cup opening and prevent water vapor leakage.

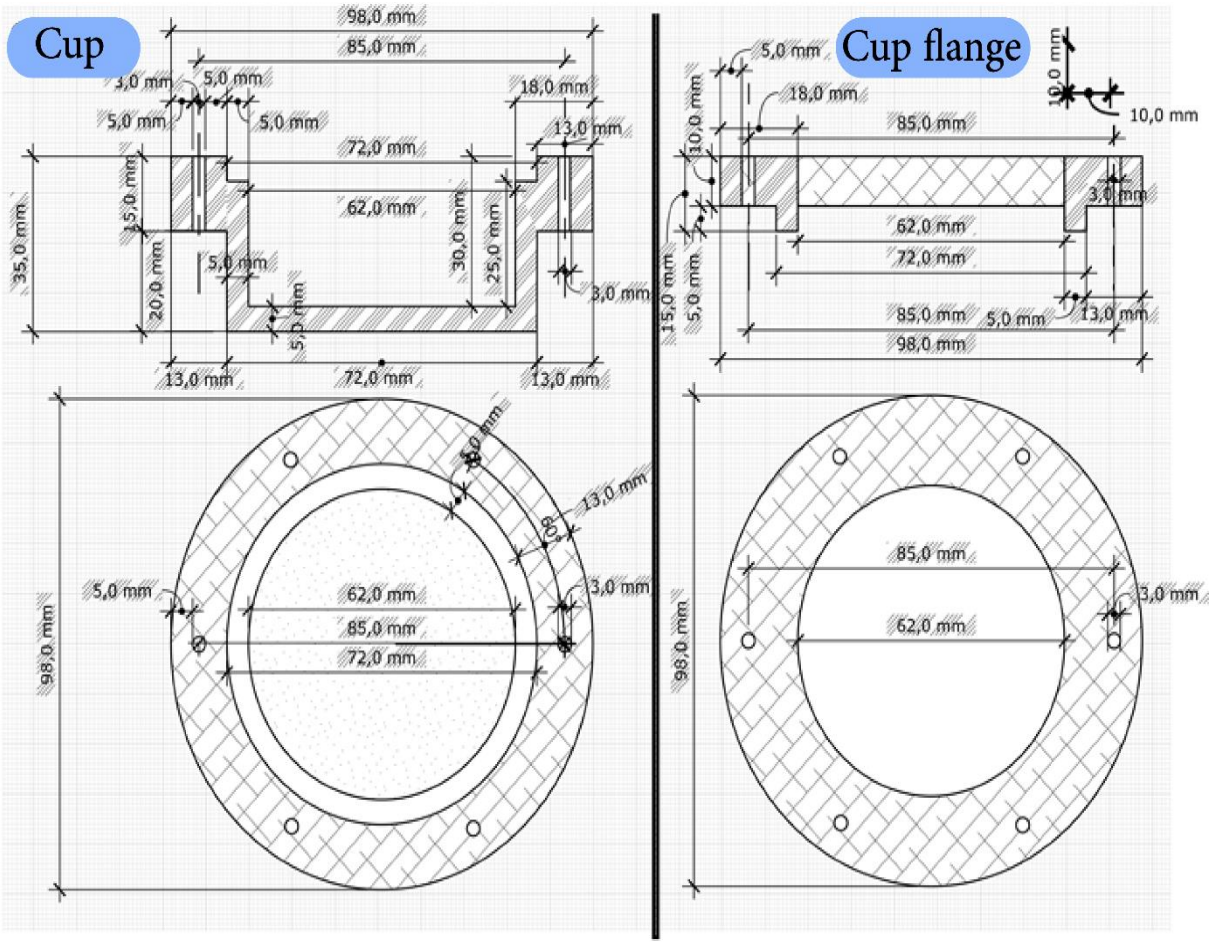

Figure 2-9. 2D layout structure of the water cup

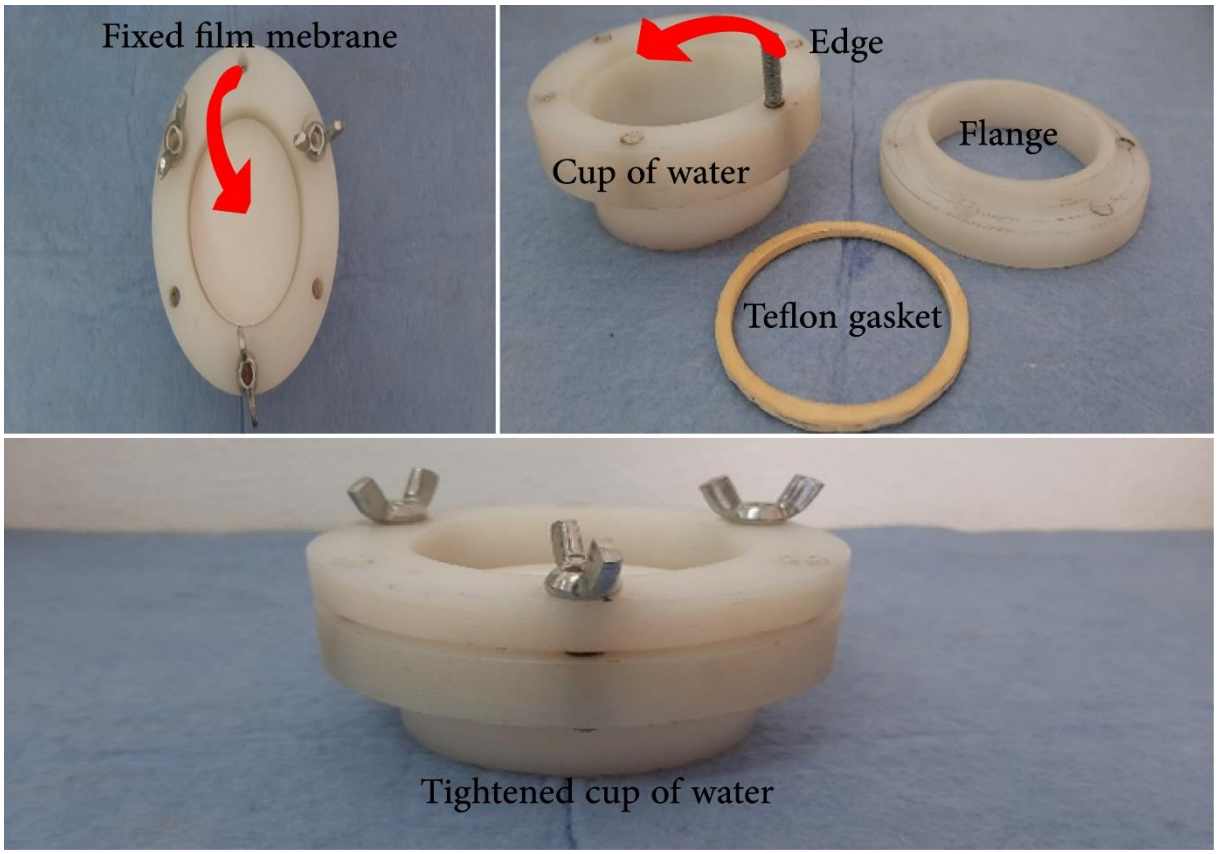

Figure 2-10. Water cup with main integrated elements

2.1.6.6 Flat membrane cell

The membrane cell is used for determining methane gas permeability of flat sheet membranes, it is made of stainless steel with a circular shape and a flat structure. The membrane cell presented in Figure 2-10 consists of two chambers, where the inlet chamber contains the gas supply, while the outlet receives the permeate gas. The inlet chamber part is equipped with a purge valve in which before supplying the methane gas in this part, the trapped air is purged from the valve to obtain more accurate results. In addition, a ledge is made in the middle of the two chambers where the circular membrane can be placed with the support of Teflon O-ring gasket to ensure the tightness of the membrane film.

2.1.6.7 Cutting flat sheet membranes

The cell membrane has a circular shape, requiring more attention when cutting the membrane film, hence, an appropriate tool should be used to cut the film into a circle similar to the opening of the membrane cell, it could be pointed out that the full roundness of the membrane film representing how the membrane will be fitted into the cell membrane and its ability to overcome

the gas leakage. A support disc made of porous stainless steel is used to hang the membrane film, it is a piece designed with the same diameter of the membrane cell opening, Figure 2-11 illustrates its shape as well as how to cut a suitable circular shape.

Before cutting the film, firstly a special latex glove is used mainly to avoid contaminating the membrane. Then, the flat film of the membrane is placed onto the surface of the disc and is cut along the edge of the disc with the scissor by holding the scissor at an angle in the direction of the center of the film to avoid undercuts. The resulting flat membrane should fit snugly without any curvature and protrude from the inner O-ring.

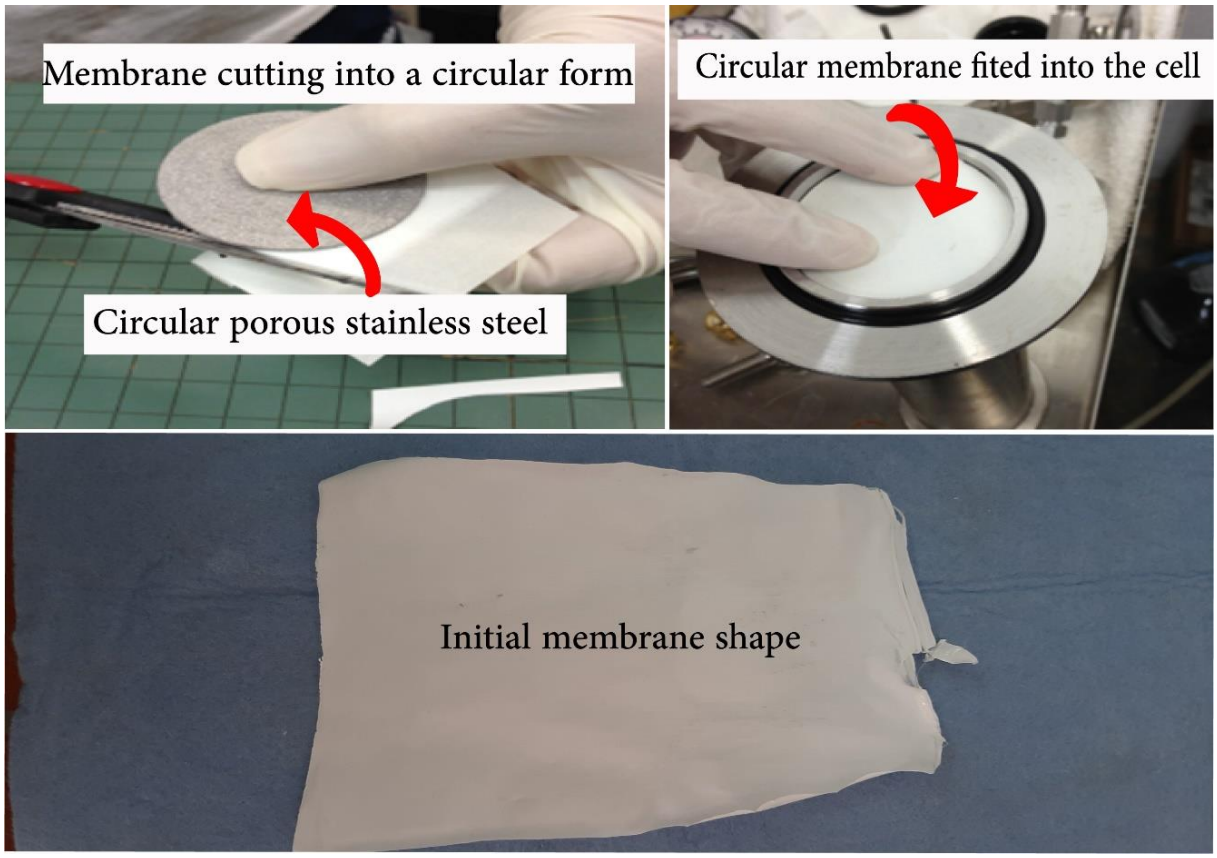

Figure 2-11. Cutting flat sheet membranes steps

2.1.6.8 Bubble flowmeter

The bubble flow meter is used to measure the volume flow rate of the permeate gas, where the flow rate is the change in volume over time. The Figure 2-12 illustrates a practical example of how the flow rate of gas is calculated.

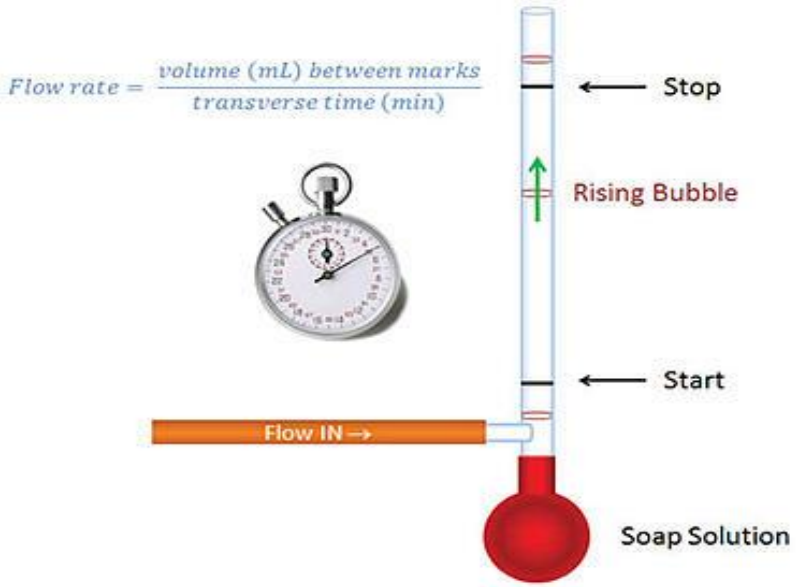

Figure 2-12. Schematic of bubble flowmeter

2.1.6.9 Film applicator

A film applicator is a wet coating device used to obtain flat sheet PET membranes, on this basis a homemade film applicator with a gap of 100 µm is made from a glass material whose design principle is based on the same design as the standard commercially available four-sided film applicator shown in Figure 2-13, where, two guide brackets supporting a glass rod used for straight application providing the desired thickness along the formed membranes. All parts of the homemade glass film applicator are bonded with silicone. The film applicator is thoroughly cleaned and washed with distilled water and dried before each use.

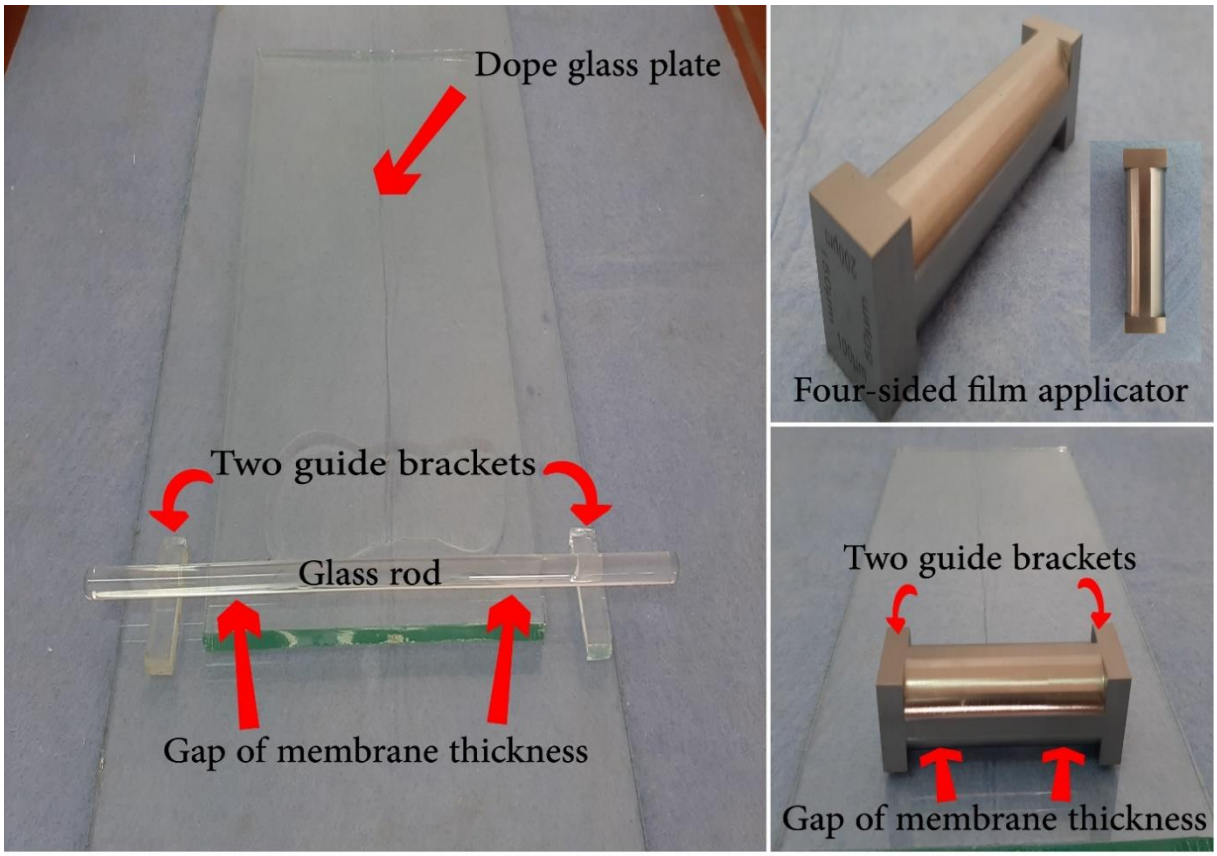

Figure 2-13. Home glass and four-sided film applicators design

2.1.6.10 Oven

The oven shown in Figure 2-14 is used to condition the water cup to a warm environment for measuring water vapor permeability of PET membranes according to E-96, it has two resistances, one at the top and one at the bottom, but only the bottom resistance is used, as it faces the water which absorbs the heat, causing the membrane film to be more protected while the top resistance is more likely to soften and damage the membrane, as it faces the membrane film. A temperature control unit with a residual steel sample occupies the oven and is set to the required temperature to comply with the measurement methods of the cup of water.

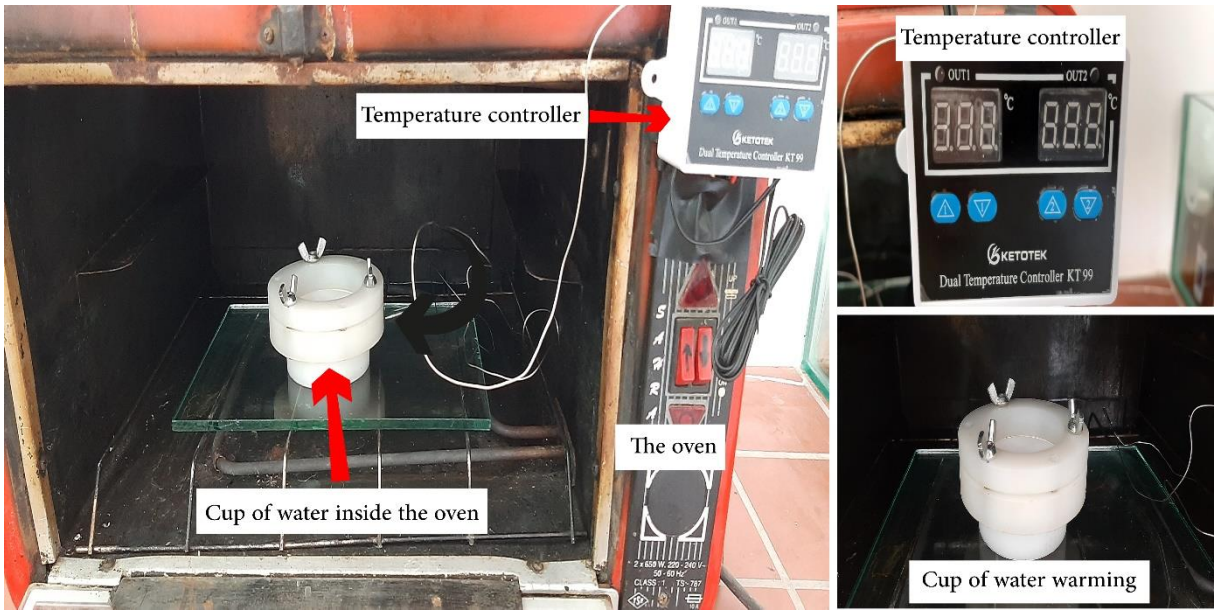

Figure 2-14. Oven structure with temperature controller

2.1.6.11 Thickness measuring gage

A certified INSIZE digital micrometer with a resolution of 0.001 mm (series 3109) shown in Figure 2-15 is used to measure the thickness of flat sheet PET membranes. For an accurate measurement, it is advisable to let the membrane dry completely and then make several measurements through the membrane, use the average value of the obtained thickness.

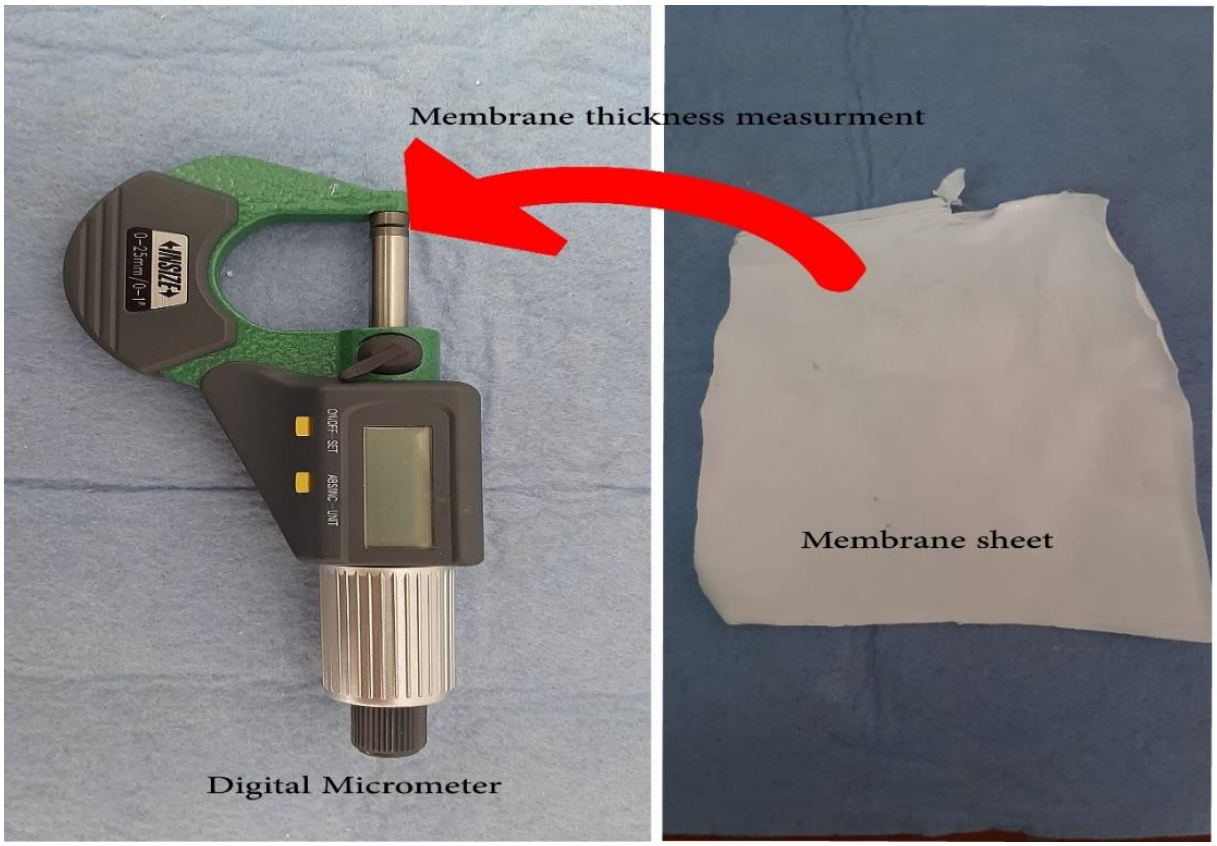

Figure 2-15. Measurement with digital micrometer

2.1.6.12 ImageJ software

ImageJ is a free program (Figure 2-16), open source, platform independent for image processing that is used as a support for SEM images mapping, it facilitates the processing of material surface topography for automatic detection and quantification of pores and cell populations, it represents a low cost and easy solution to use for counting compared to other methods, moreover if compared to manual visualization and counting, it is 10 times faster, and offers more reliable and consistent results [82]. Even though, due to ImageJ's program flexibility, its use as an automatic surface analysis and counting tool has recently spread to many other disciplines, including life sciences [83]–[86], astronomy, and physics [87]. Its primary application is solely dependent on the quality of the SEM images, which must be clear and high-definition for proper visualization. Following the selection of the SEM image, a dedicated step for pore detection and mapping should be followed, and then a feature of the ImageJ program allows counting of all the pores.

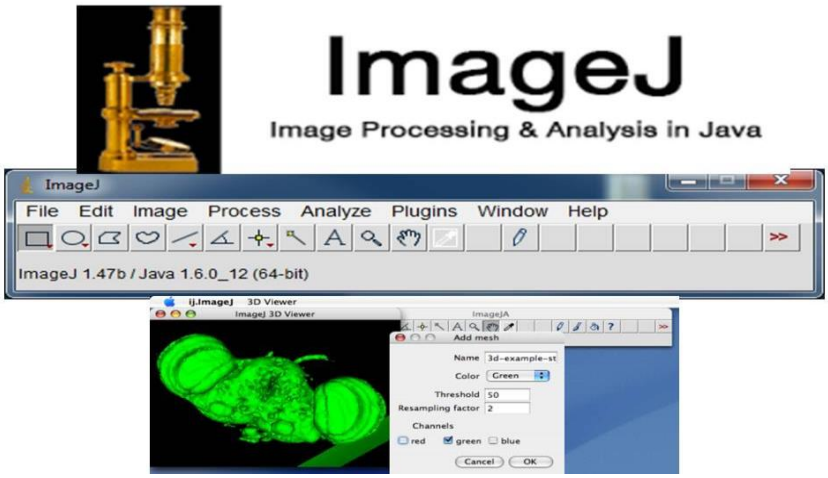

Figure 2-16. ImageJ program overview

2.1.6.13 Scanning electron microscope

The FEI Quanta 650 FEG SEM is a variable pressure microscope that provides high-resolution imaging scaling to less than 5 nm on a sample size up to 152.4 mm (6 inches). The FEI Quanta 650 FEG SEM illustrated in Figure 2-17, is equipped with a field emission gun (FEG) that allows for both bright and dark field imaging, it can be expanded up to 8 detectors for more sample imaging and analysis capabilities. For our analysis needs, the FEI Quanta 650 FEG SEM was equipped with an EDS analyzer (Bruker QUNATX EDS XFlash® 6|10), which was used also to analyse the porous surface elemental composition of the prepared PET membranes.

Before any analysis, the sample must be placed in a vacuum environment chamber to prevent air molecules from interference with the electrons reaching the sample. This feature is offered by Quanta FEG, which provides 3 vacuum modes for the analysis of large sample types:

• High Vacuum (HiVac)

• Low Vacuum (LoVac)

• Environmental SEM (ESEM)

The high vacuum (HiVac) mode, known as the conventional mode, allows the system to achieve the lowest possible pressure < $6e^{-4}$ Pa, and generally requires stable and electrically conductive samples, meanwhile if the substance is not conductive and has an electrical resistance greater than 1010 ohms, such as plastic, polymers, , the sample must be then coated with a conductive substance prior analysis, this attribution reduces beam penetration and provides a sharper

image, however, caution is necessary when x-ray analysis is required in this mode, the coating may mask elemental of interest for x-ray analysis, and makes inaccurate results.

Both Low Vacuum (LoVac) and Environmental SEM (ESEM) modes, operating at low vacuum, are suitable for imaging a non-conducting or wet sample by generating a gaseous atmosphere in the SEM chamber which is supplied by an auxiliary gas or water vapor from a built-in water storage tank. The internal pressure reaches a higher pressure in the vacuum mode, varying from 10 to 130 Pa in the Low Vacuum (LoVac) mode or between 10 and 4000 Pa in the ESEM mode. Low Vacuum (LoVac) mode is generally selected when the sample is not fragile and not conductive such as plastic, fiber. While for ESEM mode, it is usually selected in the case of biological specimens composed of materials containing relatively low boiling points such as water or other biological fluids which are non-vacuum compatible samples, often resulting in specimen destruction [88]–[90]. Water vapor (H2O) when used in imaging atmosphere mainly to promote charge suppression of nonconductive specimen and maintain sample moisture; alternatively, other gases such as carbon dioxide or nitrogen can be used instead [88]–[91].

The FEI Quanta 650 FEG SEM by accelerating voltage between 0-30 kV, for polymer and glass samples 2-6 kV works well and for metals or highly conductive surfaces 10-20kV will provide high resolution [88]–[90].

The FEI Quanta 650 FEG SEM (Scanning Electron Microscope) is used in our analysis, mainly to figure out the morphology of both the cross-section and the surface of the formed PET membranes, through allowing to observe the change of the morphology after each addition of PEG polymer.

Figure 2-17. FEI Quanta 650 FEG SEM equipped with an EDS analyzer (Bruker QUNATX EDS XFlash® 6|10)

2.2 METHODS

2.2.1 Blended PET/PEG flat membranes fabrication

2.2.1.1 Dope casting solutions preparation

Different proportions of blended PET/PEG polymers varying from 100%/0%, 90%/10%, 80%/20%, 70%/30% to 60%/40% were fabricated, named M1, M2, M3, M4 and M5, respectively, the composition of the doping solution of each membrane is summarized in Table 2-7.

First, a pure PET dope solution M1 was prepared with 0% of PEG content, where 3 g of PET flakes is weighted and introduced into a glass bottle of capacity of 50-100 ml, containing 17 ml of TCA:DCM solvent solution, the contents are then well mixed by using a magnetic stirrer for a total duration of 16 h. For blending of PEG into PET, the formed pure PET dope solution M1 was kept stirring whereby the desired percentage of PEG is added slowly to form M2, M3, M4, M5. The preparation of membranes was made by the process of wet/dry phase inversion.

Table 2-7. Compositions of dope casting solutions of PET membranes

Membrane code	Membrane composition (wt%)	
	PET	**PEG**
M1	100	0
M2	90	10
M3	80	20
M4	70	30
M5	60	40

2.2.1.2 Coating of PET membranes

The formed homogeneous casting solution was kept inside the glass bottle at room temperature for about 12 hours to remove air bubbles, then it was poured onto a glass plate at room temperature using a homemade glass film applicator with a gap of 100 µm (Figure 2-18-A). Prior to use of the glass plate, it is essential to ensure that it is not covered with dust or dirty. In particular, eliminate any source of airflow, such as the laboratory windows or other air generator source, to avoid micro-dust being blown in by airflow or projection of dusty air from the outside environment onto glass plate, an area that generates dust would affect the formation of the final shape of the membrane.

The poured dope solution is coated by pushing the film applicator towards the dope solution forcefully on the glass plate until the end to keep a constant gap (Figure 2-18-A). After coating, the pouring solution was kept for 5 minutes at room temperature and atmospheric conditions (Figure 2-18-B). Afterwards, it was immediately immersed into the coagulation bath of distilled water at room temperature for a period of more than 24 h to almost thoroughly remove the solvent and the water-soluble polymer (Figure 2-18-B).

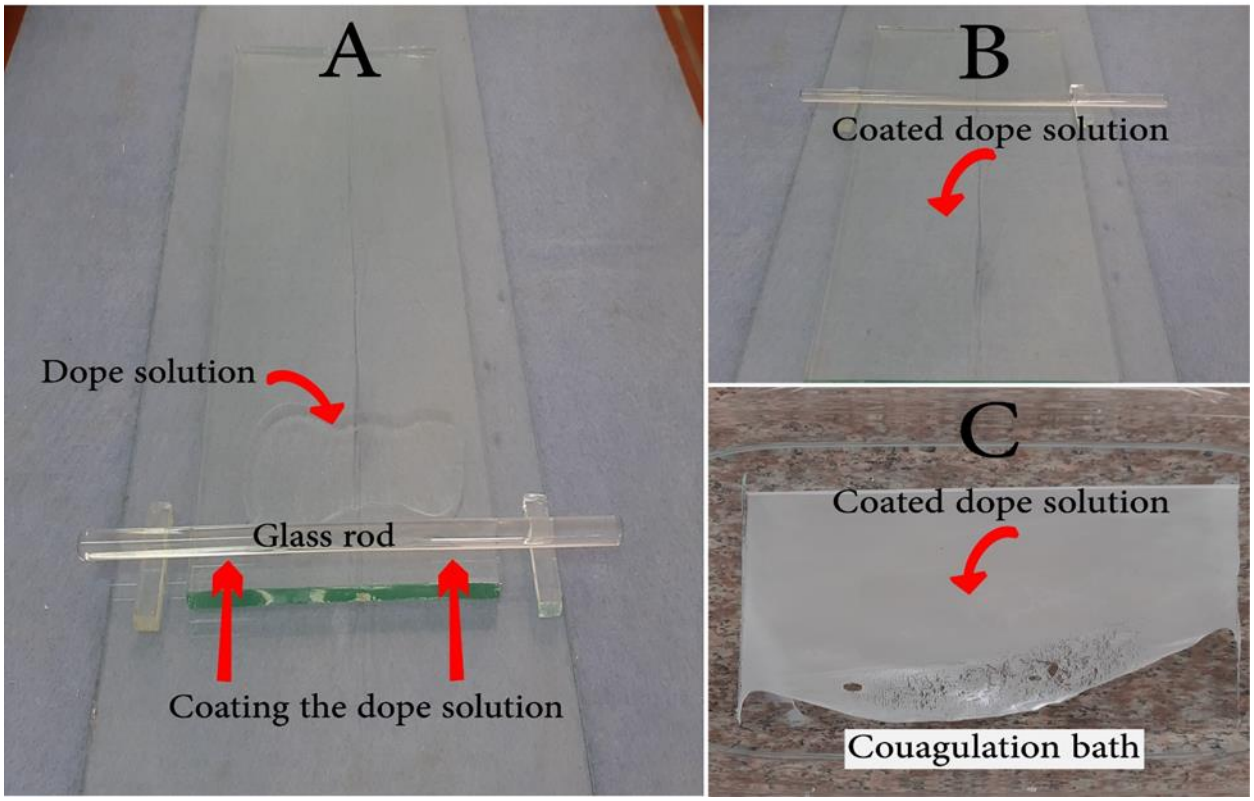

Figure 2-18. Coating of PET dope solution

2.2.1.3 Drying of PET membranes

The formed membrane inside the coagulation bath is removed and kept inside a water paper filter for a period of 24 hours for drying, after which the thickness was measured in 5 points by a certified digital, to check the consistency of the shape.

2.2.2 Membrane's characterization

For PET membranes characterization, three main characterizations are used: Scanning Electron Microscope (SEM), Energy Dispersion of X-ray (EDX) and Surface characterization

2.2.2.1 Scanning Electron Microscope (SEM)

The goal of the SEM characterization is to assess the development of the PET membrane morphology as a result of the PEG addition. SEM images are taken for all formed membranes M1, M2, M3, and M4, both on the surface and on the sectional profile, whereby the surface SEM is performed on the porous area that is later used for characterization of the pores and

their distribution, and the sectional images to validate the profile shape and, in particular, the development of pores deeply inside the membranes.

Initially, the membrane sampling is sliced into a 1cm square form and placed within the vacuum chamber on the specimen holder. Usually, for the best sampling results, keep the workplace clean at all times and use gloves when handling samples. Because the membrane is a polymer and is not conductive, a low vacuum mode with a water vapour atmosphere (H2O) is used as an imaging gas, and a high accelerating voltage of up to 20 kV is utilized throughout. It should be mentioned that if there is any uncertainty about the sample being contaminated with such as oil, grease, soil or liquid including touched human skin, the sample should be cleaned by immersion it into effective solvents like acetone or methanol solvent for 15 minutes and then is dried prior to loading for sampling [92].

2.2.2.2 Energy Dispersion of X-ray (EDX)

An EDS analyzer (Bruker QUNATX EDS XFlash® 6|10) integrated with a scanning electron microscope (FEI Quanta 650 SEM) presented in Figure 2-19 was used to identify the elemental composition of prepared PET membranes. The EDS data of the membranes are collected at the same time when performing the SEM image of the surface of the film membranes, and therefore the EDS mapping data was only for the membrane surfaces. EDS is performed to validate the use of the PET membrane and confirm that no interfering materials are incorporated for possible contamination during membrane preparation or handling.

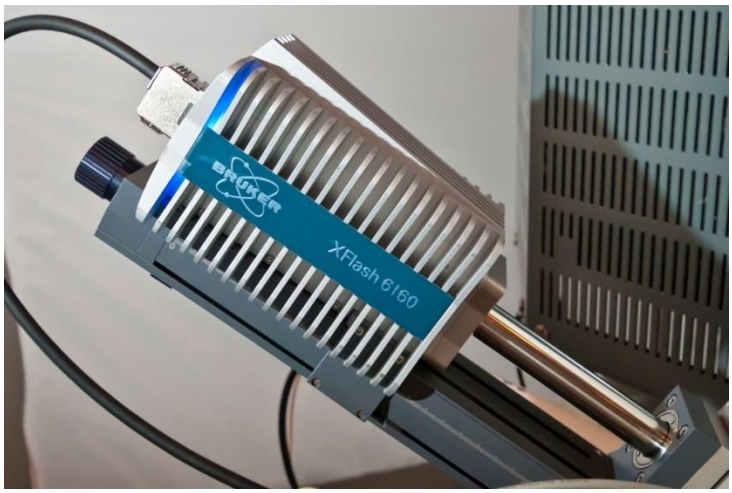

Figure 2-19. EDS analyzer (Bruker QUNATX EDS XFlash® 6|10)

2.2.2.3 Surface characterization

The purpose of the PET membrane surface characterization was to first determine the effect of the PEG additive on the pores size and distribution of the porous surface, and then to comprehend the relationship between these parameters and membrane performance. The size and distribution of pores are measured at each PEG polymer addition, where overall, only the sublayer surface was analysed, while the dense layer/skin was not, as it is considered non-porous.

In order to determine the pores size and distribution of the sub-layer surface of prepared membranes, the SEM images of porous surface are deeply analysed by the software (ImageJ)[93]. The principle of this method is based on extracting binary images from SEM images, and then distinguish the pores from the matrix, wherein a black component represents the pores and the white element represents the membrane matrix [94].

2.2.2.3.1 Procedure for SEM image analysis using image J

The purpose was to analyse the SEM surface images to determine the pores diameter of PET membranes. Four main steps are followed, which are listed below and well described in the Figure 2-20, Figure 2-21, Figure 2-22, Figure 2-23.

1. **Calibrate the SEM image**

The image calibration applies a conversion factor to SEM images by converting pixel distance unit to real metric distance unit. This information is later used in the SEM image analysis where all measurements are being expressed in µm.

a. **Steps to calibrate the SEM image**
   i. Select SEM image.
   ii. Choose straight line and scroll it on the SEM scale bar.
   iii. Select Analyse, then set scale, put the unit in µm, fill of the scale of the original SEM image in known distance field.

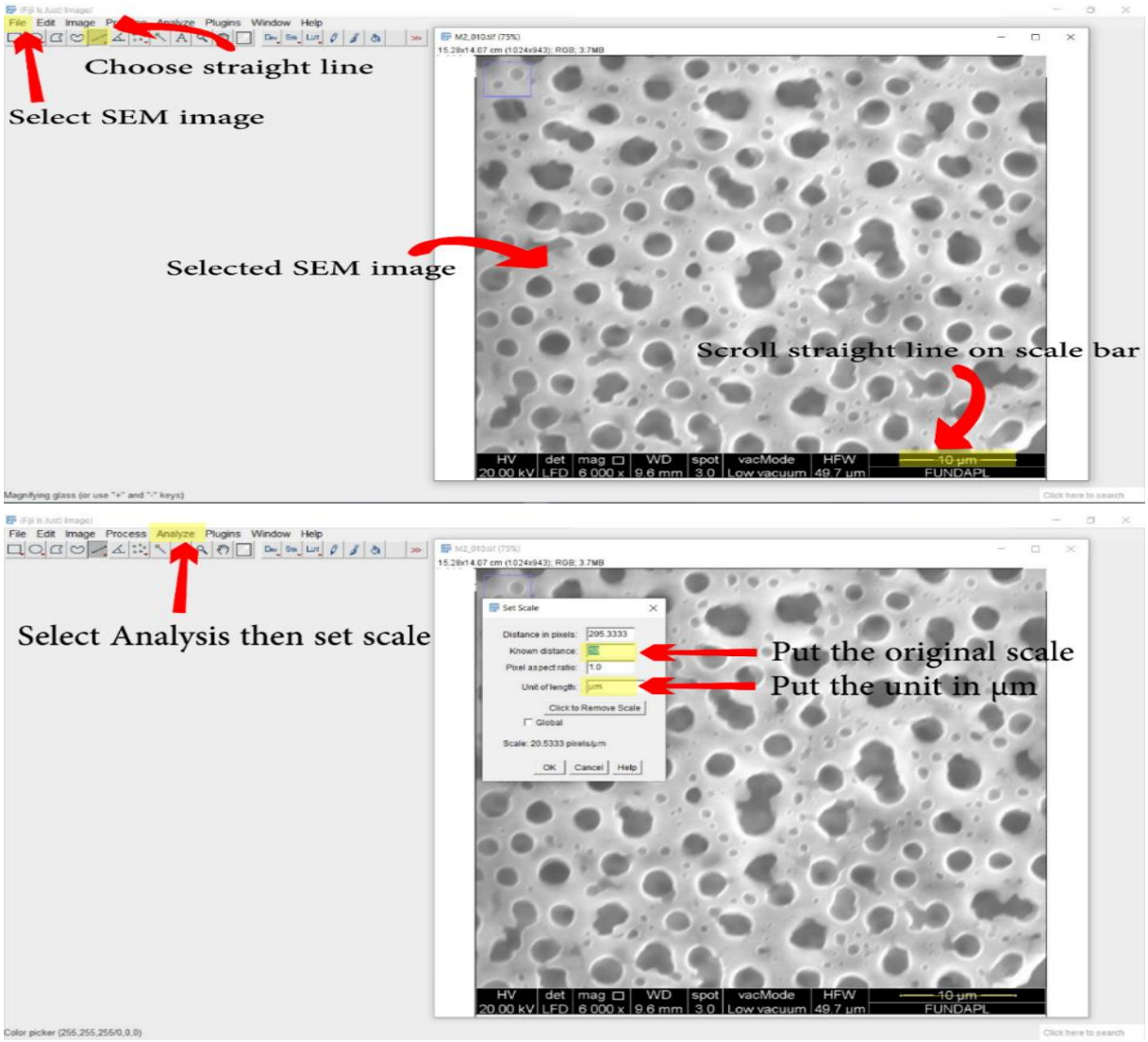

Figure 2-20. SEM image calibration

2. SEM image pre-treatment

Before scanning, the SEM image is pre-treated to retain only the porous area while removing the scale bar and any other included support information. This was mainly done to avoid interfering with the thresholding of the pre-treated images. Furthermore, the SEM image quality is adjusted to suit the automatic analysis.

a. SEM image pre-treatment steps

iv. Duplicate the calibrated SEM image by removing the scale bar. First, select the rectangle and frame the porous area of image without scale bar, right click on the image then select duplicate, the image will appear without scale bar.

v. Go to Image and select 8 bits.

vi. Go to Process » FFT » Bandpass filter and select a value greater than 100.

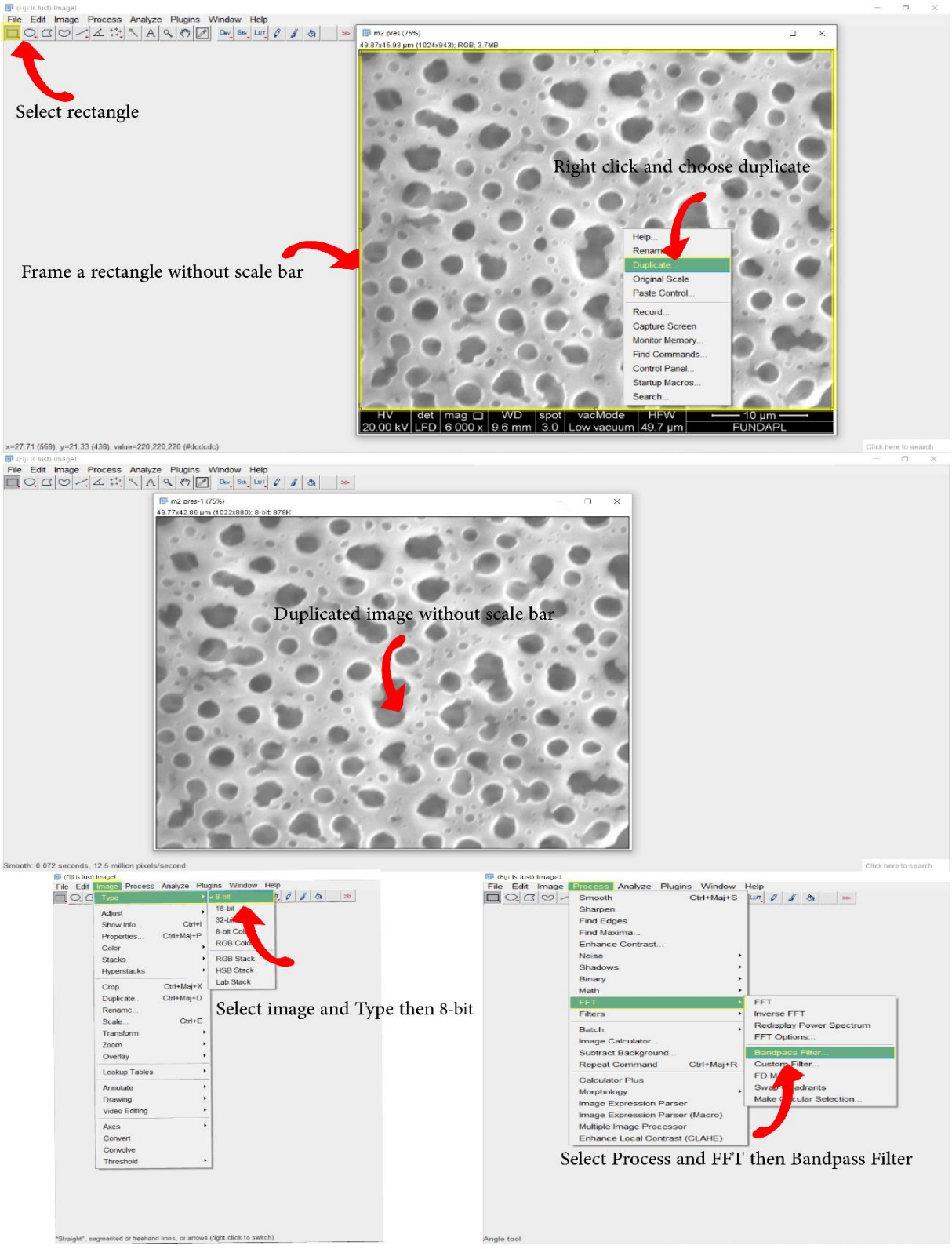

Figure 2-21. SEM image pre-treatment steps

3. Image Threshold

The threshold step is to convert the pre-treated SEM image into a binary image, which makes the pores of the membrane surface structure more visible and distinguishable.

a. Image Threshold steps

i. Go to Image » adjust » Threshold. In the box adjust the image to more visualize the pores, select dark background and black and white option, it is advisable to clean image before pores size distribution analysis.

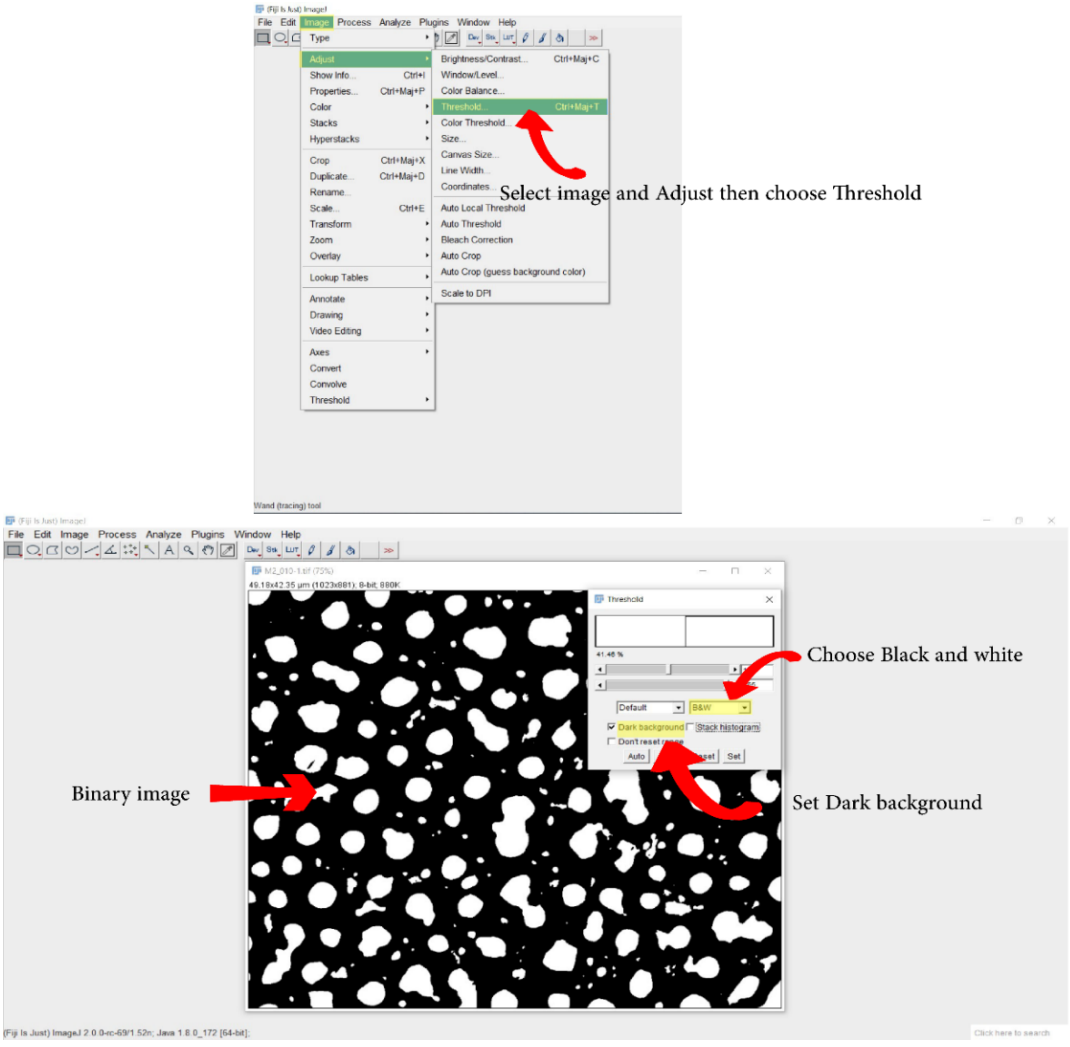

Figure 2-22. SEM image pre-treatment steps

4. Particles size analysis

In this step, the program examines the binary image to detect all of the pore's distributions, then converts them into data that includes the number of pores associated with their area dimension.

a. Particles size analysis steps

vii. Select Analyze » Analyze particles, then select outline in show type, then set display results and include holes.

viii. Save the results of the pores size distribution.

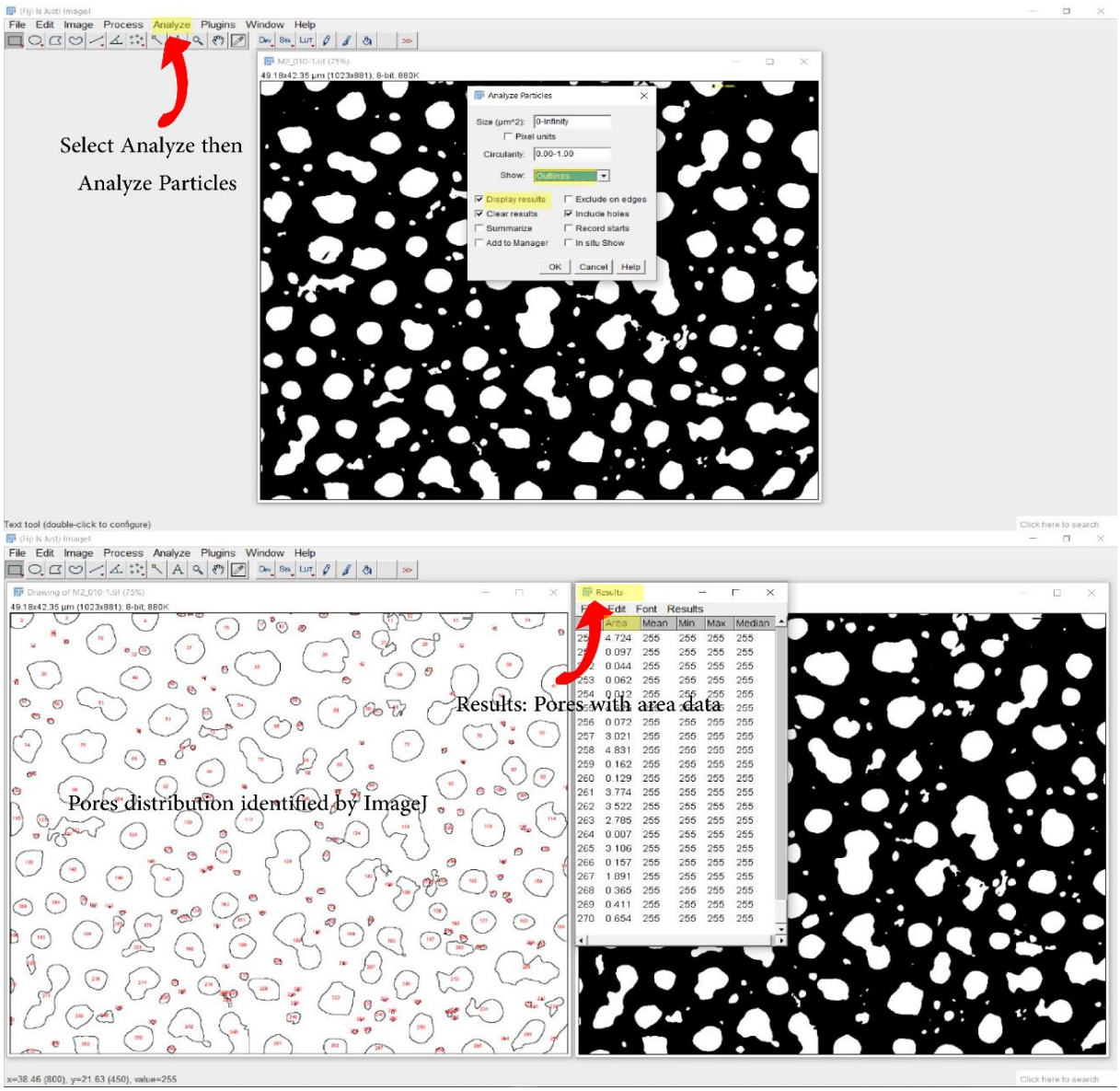

Figure 2-23. Pores size analysis steps

5. Pores size diameter calculation

From the ImageJ program, which well presented in Figure 2-23, the pores area size is automatically calculated and produced in a file that is downloaded and processed into the Excel file. Typically, the calculation of pores size diameter was based on the intensity of the pores

area form, which were globally in accordance with the processed images appear to be circular, accordingly, the formula for the circular area shown in the above equation (2-1) is used for the calculation of pores diameter, this formula is applied as a function in Excel to enable the automatic calculation of all pore's diameter, a typic Excel sheet model that is used, is illustrated in the Figure 2-24.

$$\mathbf{D} = \left(\sqrt{A/\pi}\right) \times \mathbf{2} \qquad (2\text{-}1)$$

Where: $\boldsymbol{A}$ is the aera of pores generated by ImageJ (µm)

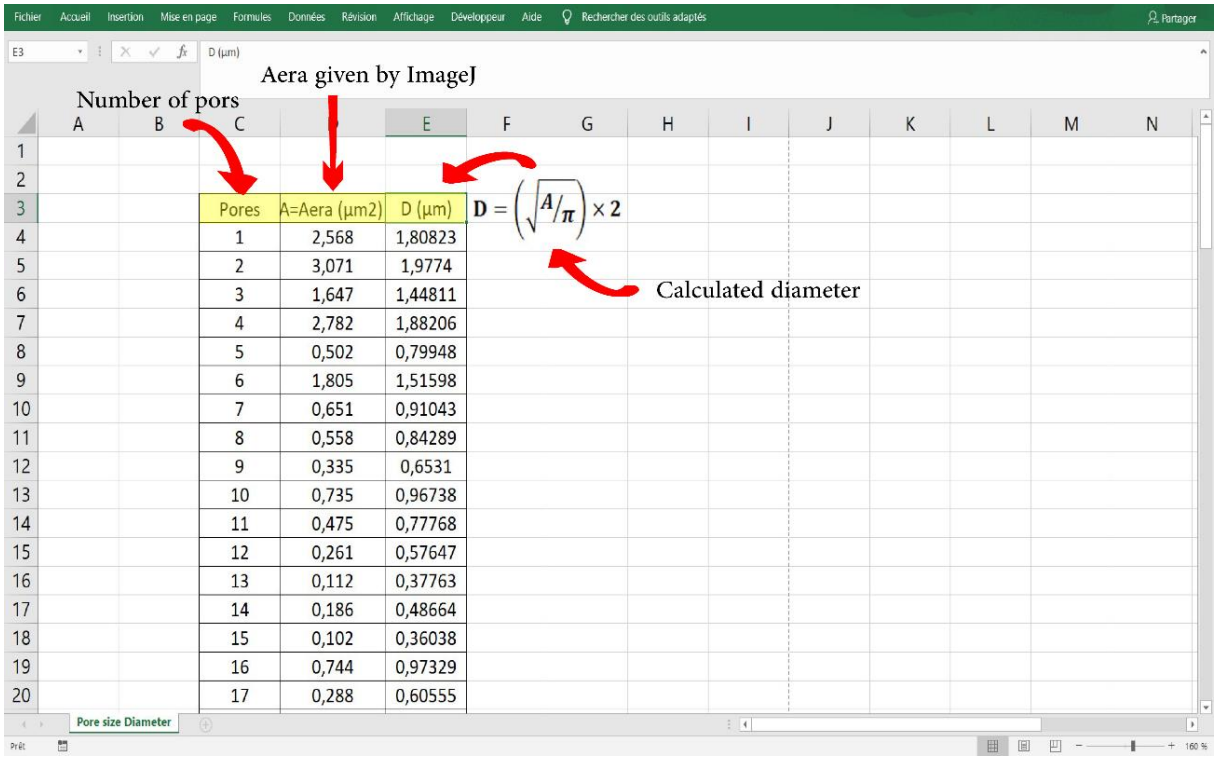

Pores	A=Aera (µm2)	D (µm)
1	2,568	1,80823
2	3,071	1,9774
3	1,647	1,44811
4	2,782	1,88206
5	0,502	0,79948
6	1,805	1,51598
7	0,651	0,91043
8	0,558	0,84289
9	0,335	0,6531
10	0,735	0,96738
11	0,475	0,77768
12	0,261	0,57647
13	0,112	0,37763
14	0,186	0,48664
15	0,102	0,36038
16	0,744	0,97329
17	0,288	0,60555

Figure 2-24. Excel model for calculation of pores diameter

6. Pore's diameter size distribution

After calculation of the pores size diameter in Excel, the data are transferred into Origin data, the function histogram diagram is used for figure out the distribution of the pores whereby the number of pores was adjusted as function against the pores size diameter.

2.2.3 Performance of the membranes

2.2.3.1 Water vapour permeability set-up

Two methods are commonly used to measure water vapour permeability: the “cup of water” and the dynamic moisture permeation cell (DMPC) [95]. Due to its availability and as it is easy to scale up, the ‘’cup of water’’ method was used in the present work where the water vapour transmission rate (WVTR) through the prepared PET membranes was calculated using the method described in ASTM E 96 [96].

First, the prepared PET membranes were shaped into a disk shape similar to the mouth of the cup with a thickness of between 60 and 130 μm (Figure 2-11), before placing the membranes, the test dish is filled with distilled water to the level (19±6 mm) above the specimen using a 20 ml syringe. An air space is left above the distilled water, principally to ensure that the water does not touch the specimen when handling the dish. It may be noted that some materials, when touched with water, can lead to inaccurate results of water vapour permeability. The depth of water should not drop below 3 mm to ensure coverage of the bottom of the dish throughout the test. As the water is filled, the shaped circular membranes were carefully placed around the edges of the cup and sealed with the support of a silicone gasket, the bolts are tightened at the end whereby an effective area of 30.19 cm2 is obtained. Afterwards, the cup assembly is initially weighed and then placed into the home-made oven where the temperature is kept by a controller around 37-39 °C (Figure 2-14). Humidity was also controlled around 30% by keeping the oven door open during all experiments. The dish was removed and weighed every 2-3 hours and was carried out in three replicates test whereby the values were recorded during weighting of water cup to measure the mass of water lost as a function of time and to calculate the WVTR in the equilibrium region. The water vapour permeability (WVP) is calculated when the permeance is identified from equation (2-4), it can be calculated by the raw formula presented by the equation (2-5) [96].

2.2.3.1.1 Water vapor transmission rate (WVTR)

The water vapor transmission rate of flat sheet PET membranes is determined by graphing the mass of water lost as a function of time and using the equation (2-2) illustrated above:

$$\mathbf{WVTR} = \frac{\mathbf{G}}{\mathbf{t} \times \mathbf{A}} = \frac{\mathbf{Flux}}{\mathbf{Area}} \quad (2\text{-}2)$$

Where:

G = weight change (from the straight line), g,

t = time, h,

G/t = slope of the straight line, g/h,

A = test area (cup mouth area), m2

WVTR = rate of water vapor transmission, g/h·m2

2.2.3.1.2 Water vapour permeance (*P)*

$$\boldsymbol{P} = \frac{\mathbf{WVTR}}{\Delta \mathbf{p}} = \frac{\mathbf{WVTR}}{\mathbf{S}\,(\mathbf{R1} - \mathbf{R2})} \quad (2\text{-}3)$$

Where:

Δp = Vapor pressure difference, mm Hg (1.333 × 102 Pa).

S = saturation vapor pressure at test temperature of 37 C˚, mm Hg (1.333 × 102 Pa).

R1 = relative humidity in the water dish.

R2 = relative humidity at the furnace.

At 37 °C, the saturation water vapor pressure is 46 mmHg (6254.436 Pa).

2.2.3.1.3 Water vapor permeability (WVP)

The permeability is the multiplication of permeance by membrane thickness. When the permeance is calculated and the thickness average is determined by the digital micrometer, the

water vapor permeability (WVP) then can be calculated from the equation (2-4) demonstrated below:

$$\mathbf{WVP} = \mathbf{Permeance} \times \boldsymbol{l} \tag{2-4}$$

Where:

l= Thickness, µm

By incorporating equations (2-2), (2-3), (2-4). The permeability can then be formulated in the following raw equation:

$$\boldsymbol{WVP} = \frac{\boldsymbol{G}.\boldsymbol{l}}{\boldsymbol{S}.(\boldsymbol{R1} - \boldsymbol{R2}).\boldsymbol{t}.\boldsymbol{A}} \tag{2-5}$$

Where: $\boldsymbol{G}$ is the weight change (g), $\boldsymbol{l}$ is the thickness of membrane specimen (µm), $\boldsymbol{S}$ is the vapour pressure at test temperature (37 °C), $\boldsymbol{R1}$ is the relative humidity in the dish (nominally 100% for the water), $\boldsymbol{R2}$ is the relative humidity inside the oven, $\boldsymbol{t}$ is the time (s), $\boldsymbol{A}$ is the test area (m^2).

2.2.3.2 Methane gas permeability set-up

The Methane gas permeability MGP of prepared PET flat sheet membranes was determined by the volumetric procedure described in ASTM D1434-82 (2015) [97], in this method, a volumetric gas transmission cell is used, which involves an upper and lower pressure chambers.

During the experiment for performance measurement, the upper pressure chamber is kept constant and the lower pressure chamber is kept at a pressure near to atmospheric pressure, the transmission rate through the test sample is derived by the difference pressure and reflected by means of downstream volume change measurement. The experimental setup of methane gas permeability measurement is adopted to the standard, which is shown in Figure 2-25 and is thoroughly depicted in Figure 2-26.

As shown in Figure 2-26, the PET flat sample is first placed between the two chambers of the cell membrane and clamped with the appropriate gasket support, after which the circuit is checked for leaks, this is further described in the next section. Methane gas is then delivered on its high-pressure side and held to flush out all air through the purge valve, a minimum of 10 minutes for the sweep is ensured at a flow rate of approximately 100 mL/min. Once the membrane circuit is ready, the methane gas control supply pressure is adjusted on the sample and held at the desired pressure of 37 cmH_2O, the permeate gas escapes from the low side at ambient pressure, and then fed into a bubble flow meter. The amount of gas escaping during the unit time was measured using the soap bubble method described in Figure 2-12. A straight line was obtained by plotting the position of the capillary soap against the elapsed time, the volume flow rate ($\boldsymbol{V_r}$) is then determined. The permeability to methane gas is given by the raw equation (2-10) [97], which is sort out from the permeance equation (2-6).

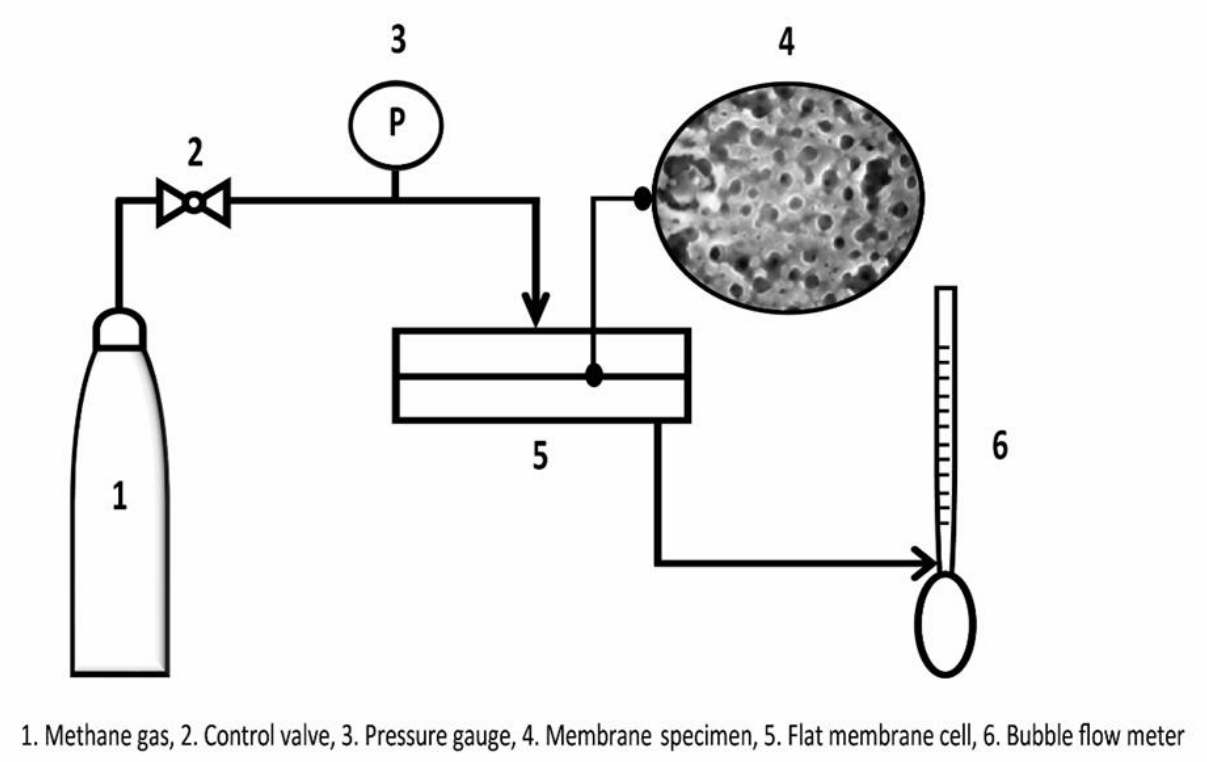

Figure 2-25. Experimental setup for MGP measurement cross PET membranes

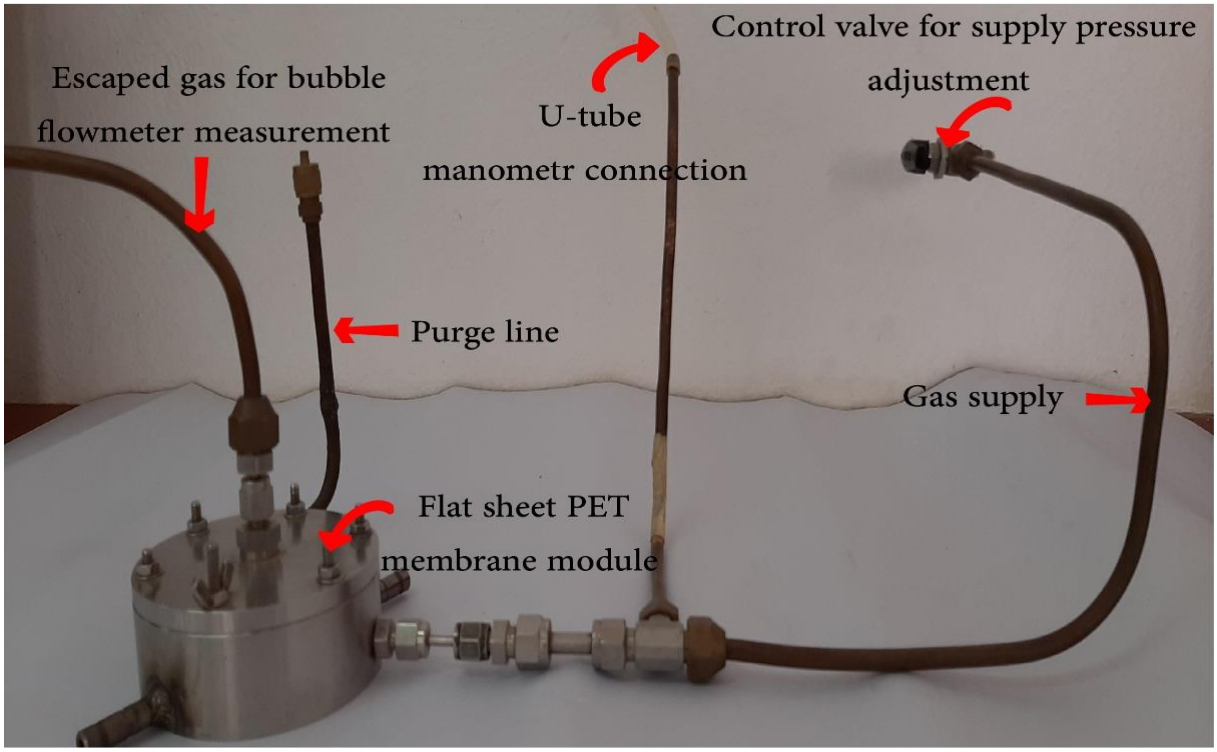

Figure 2-26. Practical experimental setup for MGP measurement

2.2.3.2.1 Cell chamber and connections sealing test

To ensure accurate and error-free results for permeability measurement, the cell membrane and all connections are checked for potential leaks. Two pressure gauges are installed upstream and downstream of the cell membrane in such a way that the tubing including the cell membrane is kept isolated by plugs, the downstream is closed by a plug.

First, the upstream gas is introduced from the high-pressure side, and when the circuit is pressurized until it is a little higher than atmospheric pressure, the gas supply is cut off. waiting for it to equal the upstream pressure, then the circuit is kept under pressure for 5 minutes to observe the pressure changes on both sides. If the pressure is held constant, identical in the upstream and downstream sides of the chamber, which indicates that there is no leakage, contrariwise, all joints and fixing points must be checked with soapy water, bubbles may be observed in the case of a non-tight connection which must be tightened to provide a leak-free circuit, the test should be repeated until no leakage is identified.

2.2.3.2.2 Volume-flow rate of methane gas (V_r)

The experimental data of escaped volume of methane gas versus elapsed time for each membrane is fitted in the equation (2-6). For more accurate results, the experiment is repeated three times for each membrane where the curve of the obtained points is drawn and then the best straight line is adopted.

$$\boldsymbol{V_r = slope \times a_c} \tag{2-6}$$

Where:

$\boldsymbol{V_r}$ = volume-flow rate, ml/s.

$\boldsymbol{slope}$ = rate of rise of capillary slug, mm/s.

$\boldsymbol{a_c}$= cross-sectional area of capillary, mm^2.

2.2.3.2.3 Methane gas transmission rate (*GTR*)

The methane gas transmission rate (GTR) of PET membrane is determined by the following equation:

$$\boldsymbol{GTR = 10^{-6} . \frac{P_0 . V_r}{ART}} \tag{2-7}$$

Where:

$\boldsymbol{GTR}$ = gas transmission rate ($mol \cdot m^{-2} \cdot s^{-1}$)

$\boldsymbol{V_r}$ = volume-flow rate (L/s)

$\boldsymbol{P_0}$ = is the ambient pressure (Pa)

$\boldsymbol{A}$ is the test area (mm^2)

$\boldsymbol{R}$ is the universal gas constant ($\boldsymbol{R} = 8.3143 \times 10^3$ L · Pa/mol · K)

$\boldsymbol{T}$ is the ambient temperature (K).

2.2.3.2.4 Methane gas permeance (*P*)

The methane permeance (*P*) is defined as the result of the ratio between the gas transmission rate and the differential pressure of the transmitted methane gas and is expressed by the following formula:

$$\boldsymbol{P = \frac{GTR}{(P - P_0)}} \tag{2-8}$$

Where:

$\boldsymbol{P_0}$ is the ambient pressure (Pa)

2.2.3.2.5 Methane gas permeability (MGP)

The MGP permeability is defined as the product of the permeance and the film thickness. It might be stated that the thickness of each membrane is measured at different points by a digital micrometer, an average for each specimen instead is used for the calculation.

$$\mathbf{MGP} = \boldsymbol{P.l} \tag{2-9}$$

By incorporating the equation (2-7), (2-8), (2-9), the above raw methane gas permeability (MGP) is presented in the following equation:

$$\mathbf{MGP} = \mathbf{10^{-6}}.\frac{\boldsymbol{P_0.V_r.l}}{\boldsymbol{(P - P_0).ART}} \tag{2-10}$$

Where: $\boldsymbol{P}$ is the upstream pressure (Pa), $\boldsymbol{P_0}$ is the ambient pressure (Pa), $\boldsymbol{l}$ is the thickness of membrane specimen (μm) , $\boldsymbol{V_r}$ is the volume-flow rate (L/s), $\boldsymbol{A}$ is the test area (mm^2), $\boldsymbol{R}$ is the universal gas constant ($\boldsymbol{R} = 8.3143 \times 10^3$ L · Pa/mol · K), $\boldsymbol{T}$ is the ambient temperature (K).

Chapter 3

Characterization of prepared PET-based membranes

In this chapter, the structure of the formed PET membranes is observed in depth by the characterization with media such as SEM images, the data are then scanned with ImageJ application. EDS analysis are performed for the confirmation of the structural components used in the formation of the membrane structure. Further discussion is considered on how the relative nature of the membrane structure affects the performance of methane gas dehydration.

3.1 FORMATION OF FLAT SHEET MEMBRANE

Figure 3-2 shows images of the prepared membranes M1, M2, M3, M4 and M5. It is mainly observed that the shape of the membranes M1, M2, M3, M4 is well developed while for M5 it is not correctly formed, the excess of PEG content (40%) led to the build-up of large holes in the range of 1 to 5 mm. This is explained by the higher solubility of PEG in the water coagulation bath, when the PEG content is high in the castled solution and is immersed in coagulation bath of distilled water, a part of PEG comes out of the castled solution and dissolves in distilled water, which results in getting final large holes in the membranes.

Several experiences are performed for the formation of M5 membranes, where the obtained data gave the same results, an appearance of holes through hole the membrane surface, Figure 3-1 demonstrates well the formation of holes in distilled water coagulation bath.

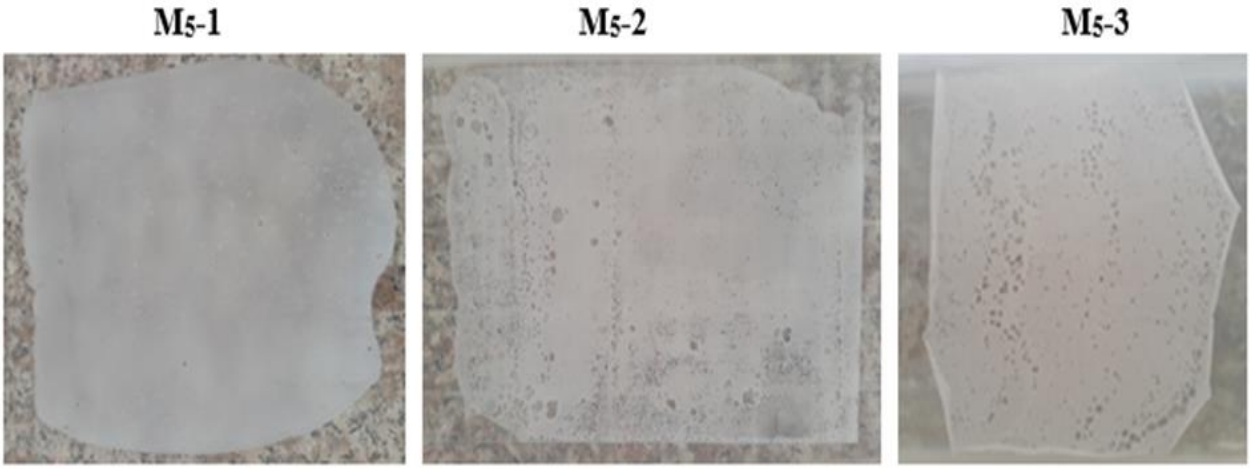

Figure 3-1. Holes build-up in distilled water coagulation bath for M5 membrane (60%/40%)

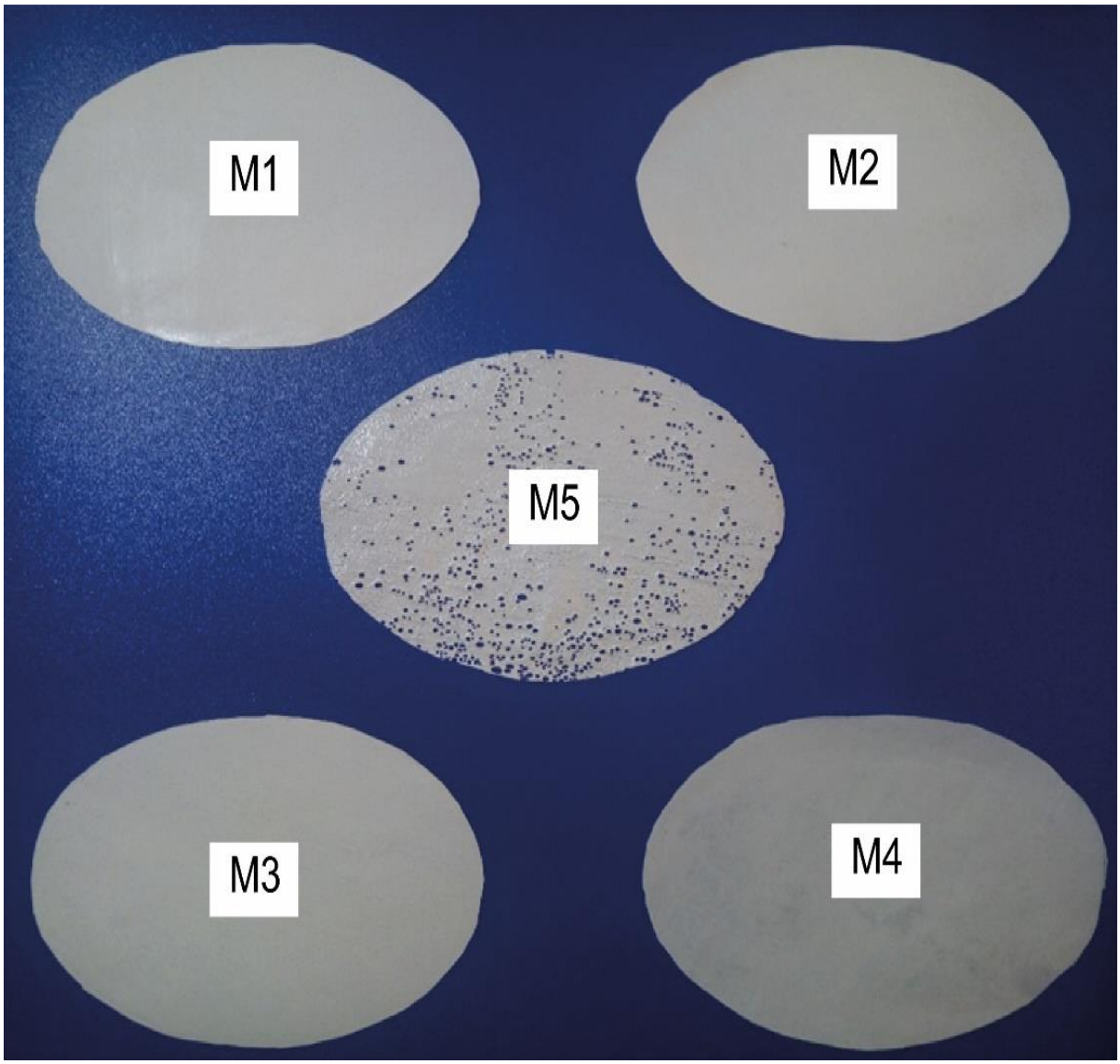

Figure 3-2. Build-up of PET/PEG membranes: M1 (100%/0%), M2 (90%/10%), M3 (80%/20%), M4 (70%/30%), M5 (60%/40%)

3.2 SECTIONAL AND TOP SURFACE MORPHOLOGY OF MEMBRANES

From SEM images of top surface of the membranes in Figure 3-3, the morphology of membranes is notably modified, in particular, half-sphere-shaped macro-voids are formed, and are distributed specifically in abundance on the surface of the membranes M3 and M4, their diameters increased with each increase in the PEG content, as such as, with an increment of 10% of the PEG content, the diameter of the macro-voids tripled from 35 µm in M3 to 100 µm in M4.

Sectional SEM images of membranes M1, M2, M3, and M4 are shown in Figure 3-4. All membranes clearly showed an asymmetric structure: thin, dense top layer and a sponge-shaped sub-layer structure. The resulting change in the morphology of the prepared membranes is due to the delayed de-mixing process. It may be noted that the delay in the de-mixing process leads to the formation of a spongy structure, while an instantaneous de-mixing facilitates the formation of a finger-like structure [98]. One of the factors that contributed to the spongy morphology was specifically the presence of DCM solvent with a higher content ratio in the TCA/DCM solvent mixture (2:3). The solvent dichloromethane (DCM) is basically a solvent with a lower miscibility power with the non-solvent (distilled water), its presence with a higher proportion in the solvent of the mixture of TCA/DCM (2:3) made the mixture also gain lower miscibility [99], this property provided the exchange rate in a slow process, thus leading to the formation of a spongy morphology and a dense top layer [100].

The SEM cross-sectional image of the pure PET membrane M1 shows the formation of a light porous layer which does not appear in abundance. By varying the concentration of PEG in the casting solution, the membranes showed changes in their morphology: an increase in the PEG content makes the top layers thicker and a more porous sub-layer is produced [101], the addition of 10% PEG content (M2 membrane) resulted in a spongy sub-layer with clearer pores compared to M1, a similar observation is noted for M3 and M4 membranes. In conclusion, the addition of PEG induced a substantial increase in the porous area [5], [6]. It seems interesting to underline the same observation found by Samuel et al.[103], when PEG additive is added, the PET membranes generated more porous area. In fact, the PEG is a water-soluble polymer and it is considered as a pore former, useful to control the morphology and the porosity of the resulting membranes [104]. The increase in porosity suggested to be due to the leaching of the PEG additive from the PET dope solution. PEG is hydrophilic polymer and has a good affinity and solubility with the non-solvent (water), when mixed with the dope solution and immersed in the coagulation bath, most of the PEG additive leach out of the polymer solution and diffuse into the water bath, leaving spaces that become micropores, which induce a porous membrane. This is in good agreement with the SEM cross-sectional results (Figure 3-4) and the observations of increased porous surface area in the obtained PET membranes [105], [106].

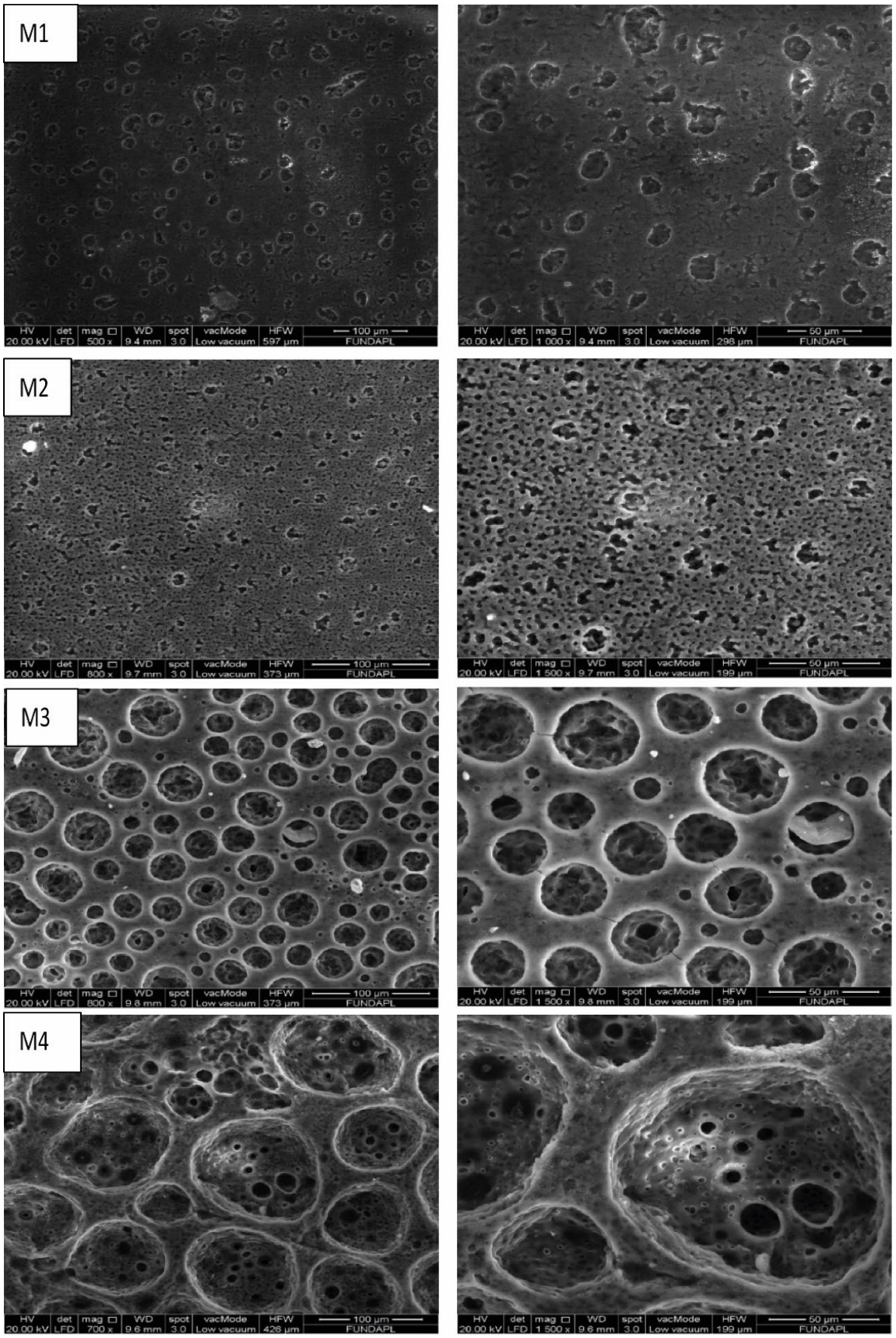

Figure 3-3. Scanning electron microscopy images of the porous sub-layer surface of PET membranes. (M1, no added PEG; M2=10% PEG; M3=20% PEG, M4=30% PEG)

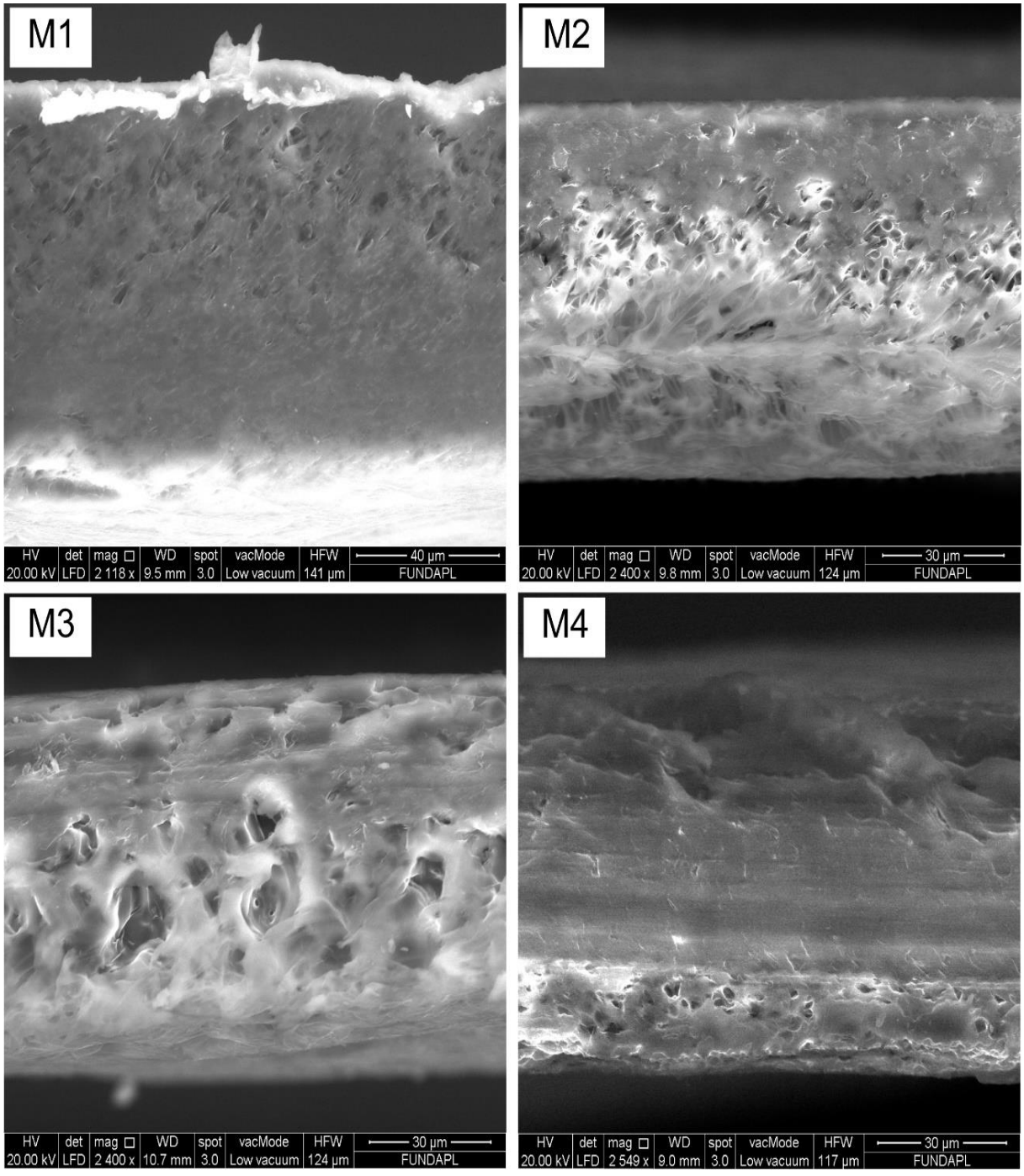

Figure 3-4. Scanning electron microscopy images of membrane cross sections. (M1, no added PEG, M2=10% PEG, M3=20% PEG, M4=30% PEG)

3.3 SURFACE CHARACTERIZATION

The results of SEM sub-layer surface of the membranes that are analysed using ImageJ software are presented in Figure 3-5, where the data of the pores size and distribution of the membranes are shown in Figure 3-5A and the images analysis of the surface of the membranes in Figure 3-5B. From the results of the sub-layer surface analysis shown in Figure 3-5B

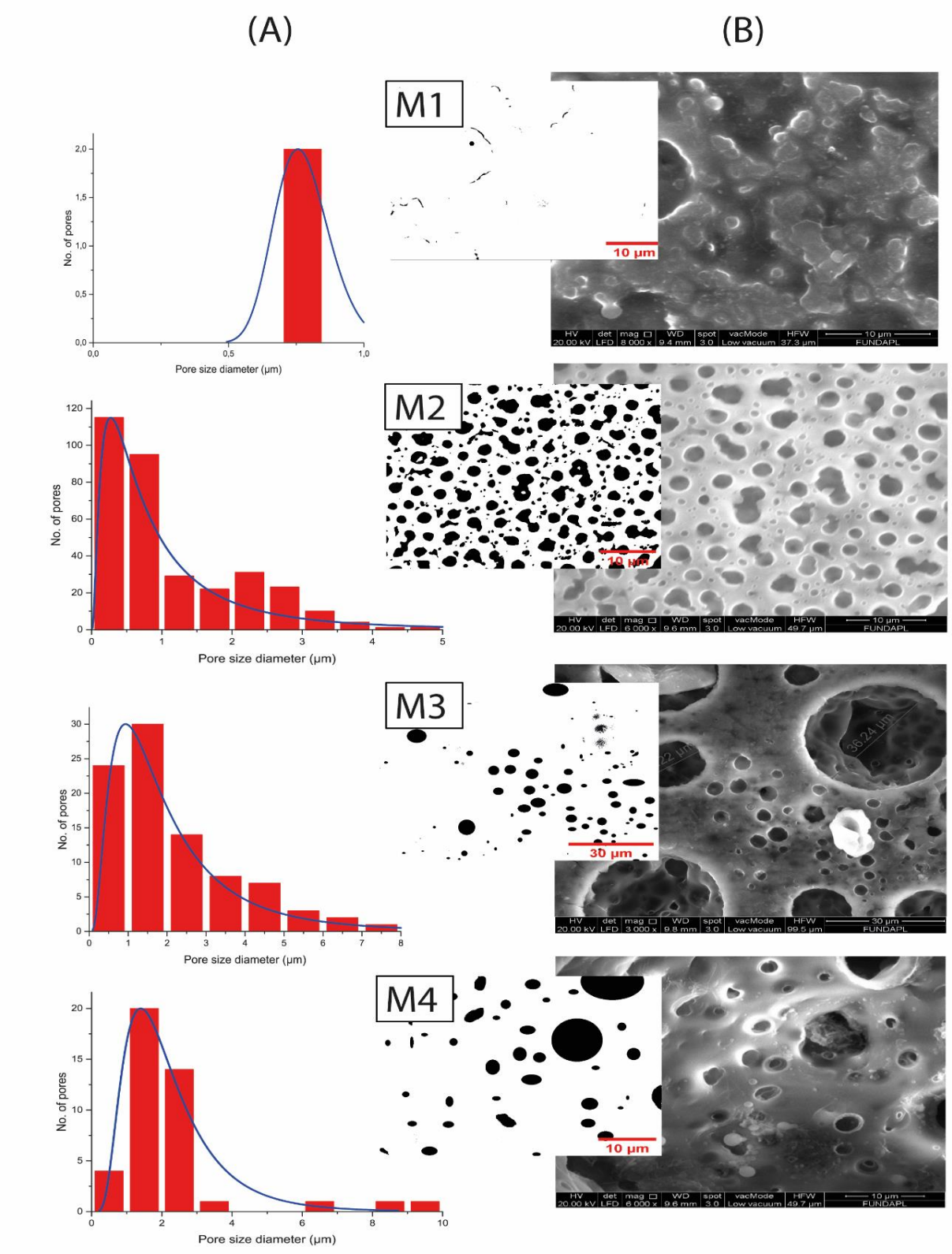

Figure 3-5. SEM suface analysis of membranes : A- Pores size distribution of membranes, B- Detected pores in binary SEM images: black = Pores, white = membrane matrix

3.3.1 Membranes M1

Four areas, A, B, C, and D, were subjected to SEM examination, a scale up to 10 µm is adjusted in order to uncover precisely the geometry of the membrane surface. All of the collected images are shown in Figure 3-6, where it is visible that, on the surface of the pure PET (M1) membrane sub-layer, the pores are mostly unformed in all SEM cases A, B, C, and D, with detection only one pore. Constantly, the formation of macro voids is not observed, which makes the membrane more solid, the surface of the membrane seems rough with deep and steep edges.

Based on the ImageJ scan shown in Figure 3-5B, the surface of the membrane appears having pores diameter in the range of 0.7-0.84 µm.

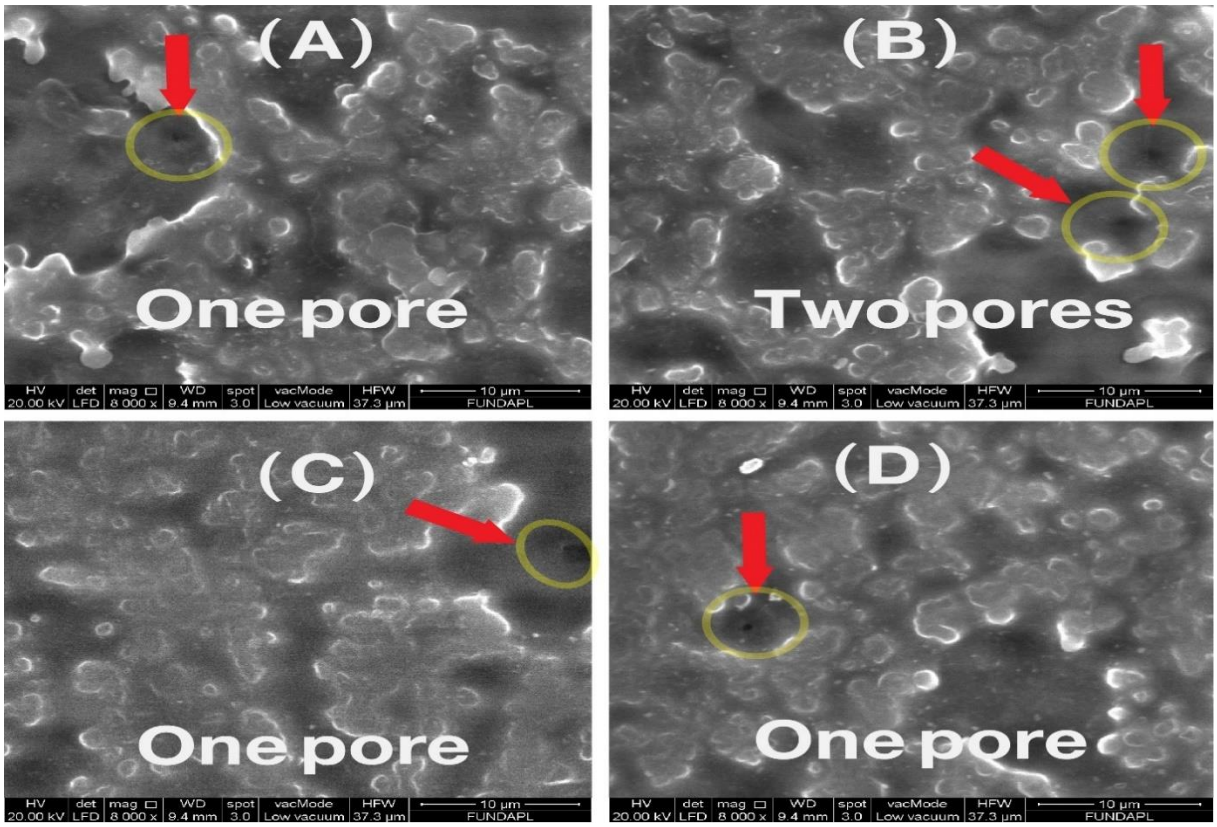

Figure 3-6. M3 SEM image of sub-layer surface

3.3.2 Membranes M2

In comparison to the M1 membrane, M2 membrane has become significantly porous through all of its surface, as presented in Figure 3-7**Figure 3-7.** M2 SEM image of sub-layer surface, the pores distributed symmetrically, it might be noted that this change of the pores development

was a result of the addition of PEG, the pores diameter is in the range of 0.05 µm to 5 µm, most of the pores formed having diameters in the range of 0.05 µm to 1 µm.

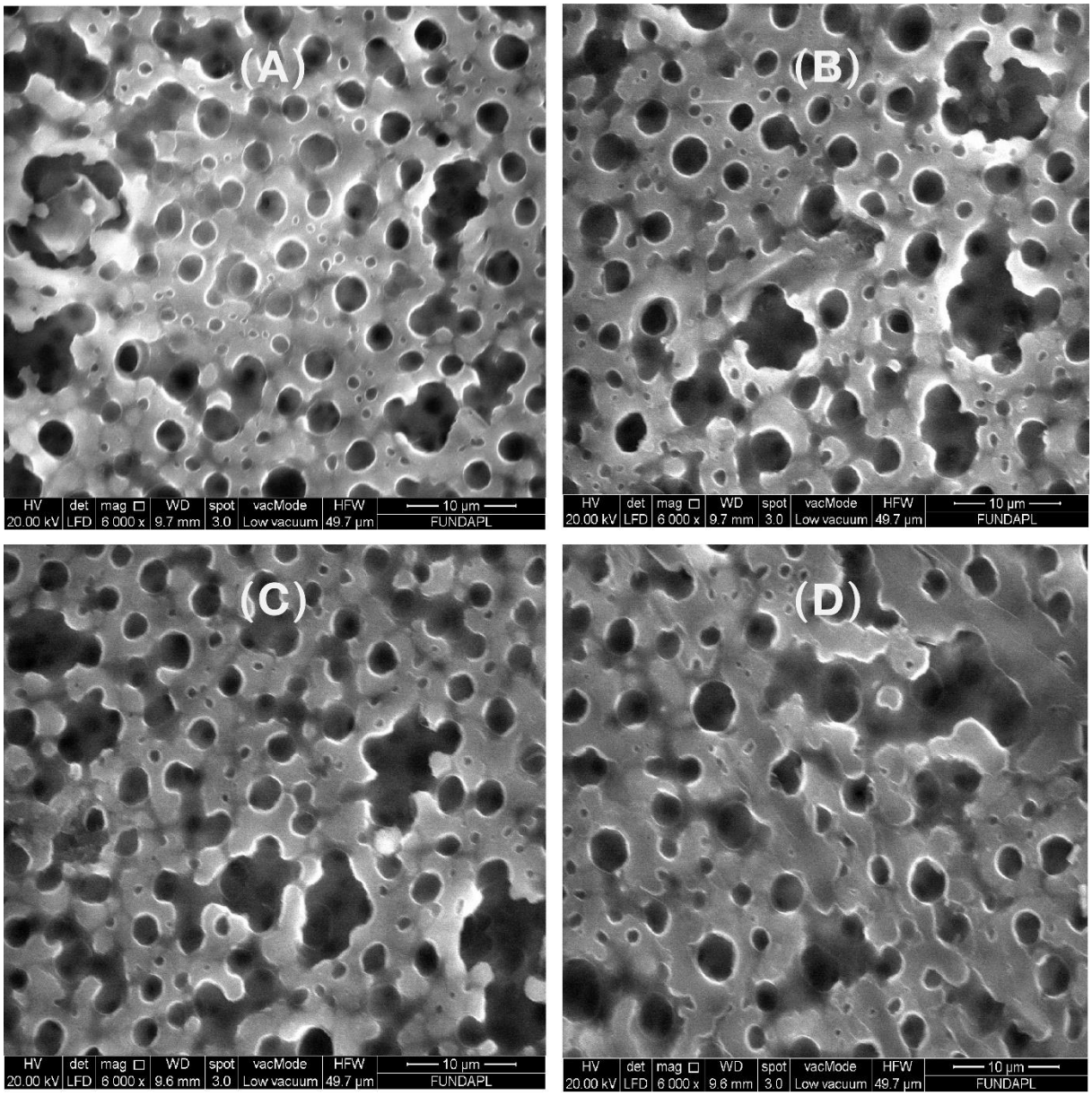

Figure 3-7. M2 SEM image of sub-layer surface

3.3.3 Membranes M3

The obtained sublayer surface SEM images of M3 membrane are presented in the Figure 3-8, the image zoomed out up a scale of 10 µm, to focus on the shape details of the membrane surface, it is observed a development of macro-voids of half-sphere shape on the surface of the sub-layer of M3 membrane, the pores are also formed and they are intensely developed compared to the membrane M2, they are located inside the walls of macro-voids structure and

on the flat surface of the sub-layer. It can be concluded that most of the pores are located inside the macro voids.

By analysing M3 membrane surface with ImageJ, the obtained results are presented in Figure 3-5B, where the size diameter of the pores is found distributed in the range of 0.3 to 7.47 µm, most diameters vary from 0.3 to 3 µm.

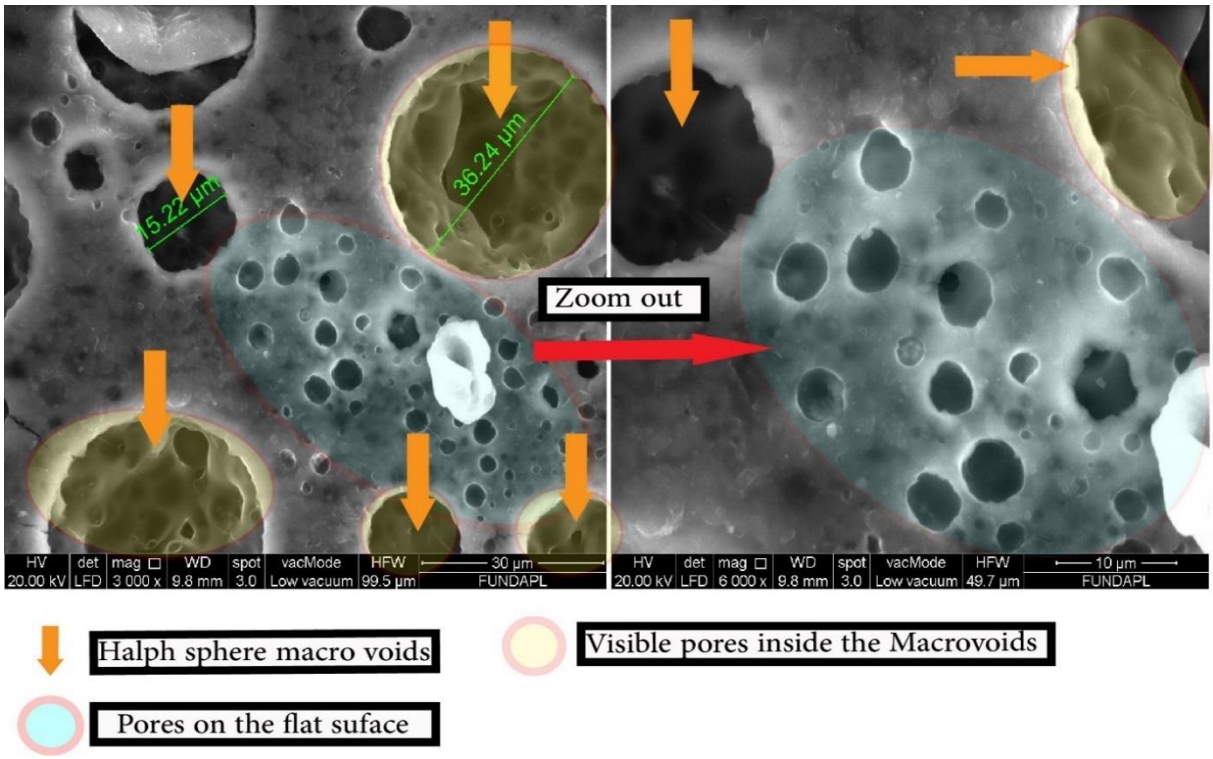

Figure 3-8. M3 SEM image of sub-layer surface

3.3.4 Membranes M4

For the M4 membrane, it might be expressed that the surface of the sub-layer is almost occupied by large half-sphere-shaped macro-voids with diameters of up to 100 µm, and that the pores formed are found located almost inside the macro-voids (Figure 3-9). For this reason, the surface analysis was focused inside the macro-voids, the pores diameter is found ranging from 0.7 to 9.46 µm and most of them having diameters between 0.7 and 3 µm.

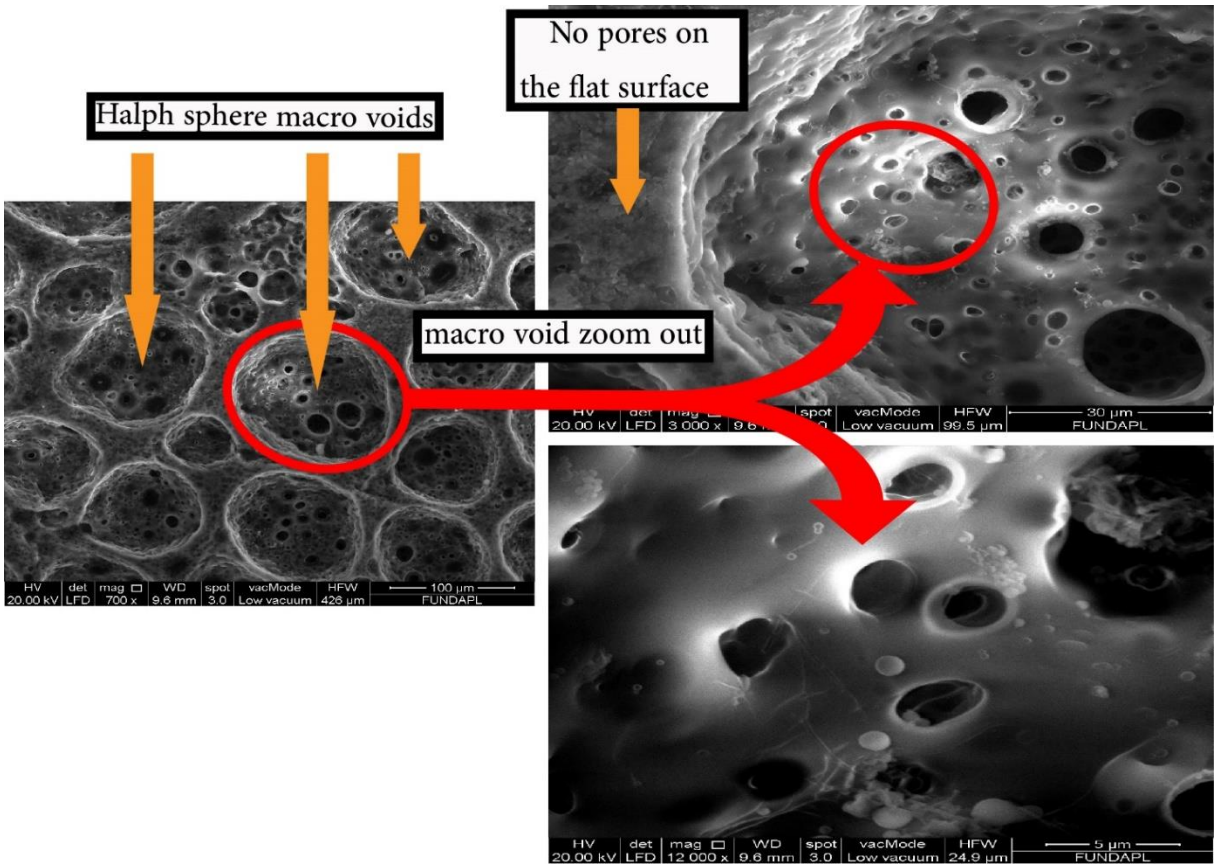

Figure 3-9. Zoom out inside the macro voids of M4 membrane sub-surface

3.3.5 Membranes mean pore diameter

Based on the findings of pores size, the mean pore diameter is calculated and the data is shown in Figure 3-10, it is observed that the mean pore diameter of the sub-layer surface increased with the increasing of PEG content, such as this result is also attributed to the formation of macro-voids structure on the sub-layer surface that favours the increase of the membranes pores diameter. A similar observation has been reported by Yunos et *al*.[107] using PEG as additive in polysulfone membranes.

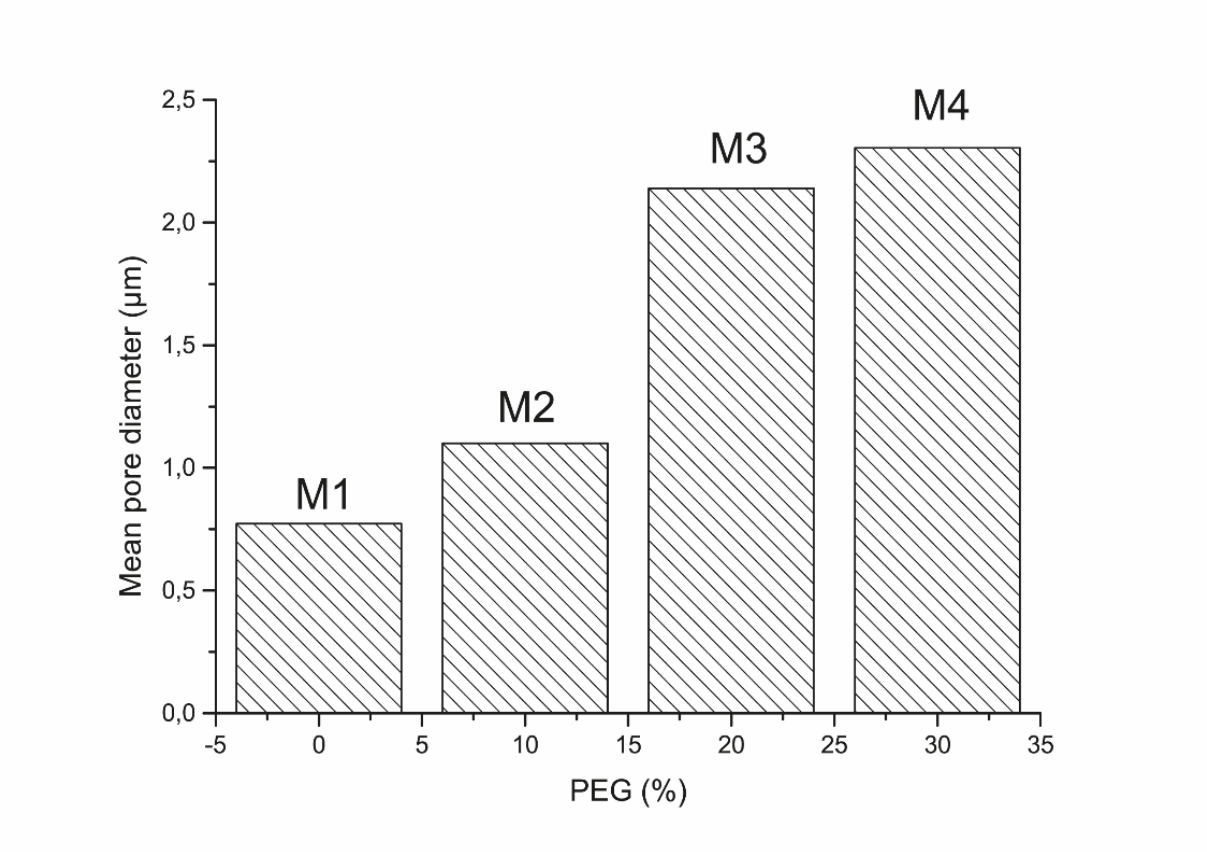

Figure 3-10. Sub-layer mean pore diameter of PET/PEG membranes

3.4 ENERGY DISPERSIVE X-RAY SPECTROMETRY

Figure 3-11 shows the intensity of X-ray generated per second relative to the projected energy beam for the membranes M1, M2, M3, M4. The location of the energy of pick intensities is useful for qualification, hence provides the identification of the corresponding element in the sample. From the spectrums obtained from the membranes, three energy picks are identified, carbon (C), oxygen (O) and chlorine (Cl). Indeed, exempted (H), all the elements of the products used for the preparation of the membranes are captured: chlorine atoms (Cl) are mainly sourced from used solvent mixture of Dichloromethane (DCM)/Trichloroacetic acid (TCA) of chemical formula CH_2-Cl_3 /Cl_3-COOH respectively, while carbon (C) and oxygen (O) are found in addition to the solvents: in the PET polymer (−OOC−C_6H_5−COOCH_2−CH_2−)n and PEG (H-(O−CH_2−CH_2)n−OH). The hydrogen (H) is not identified in the spectrum. Generally, EDS does not work for elements with a low atomic number, hydrogen is light with no core electrons which can be removed to allow X-ray emission and detection by EDS [108], [109]. On the other hand, the intensity of the X-ray peaks allows establishing the concentration of the element, the results obtained are summarized with the graphs of the spectrum in Figure 3-11, there might not be a

significant change in the distribution of the elements, an average value of C: 59%; O: 34% and Cl: 5.50%.

The variation in x-ray intensity in the spectra is believed to be the effect of the surface morphology of the membrane sub-layer. Figure 3-3 shows macro-voids distributed along the surface of the membranes, which contributed in making the surface rougher, this later compared with the intensity of x-rays from a smooth surface is not constant. Specifically, x-rays from lower parts of deep macro-voids may not reach the detector analyzer due to a shadow effect. The depth is variable in correlation with the geometry of each macro-void, which could lead to a variation in the intensity of the received X-ray [110].

According to all of the EDS materials detection data, no material contaminant is found that is not used in the preparation and formulation of PET and PEG polymers.

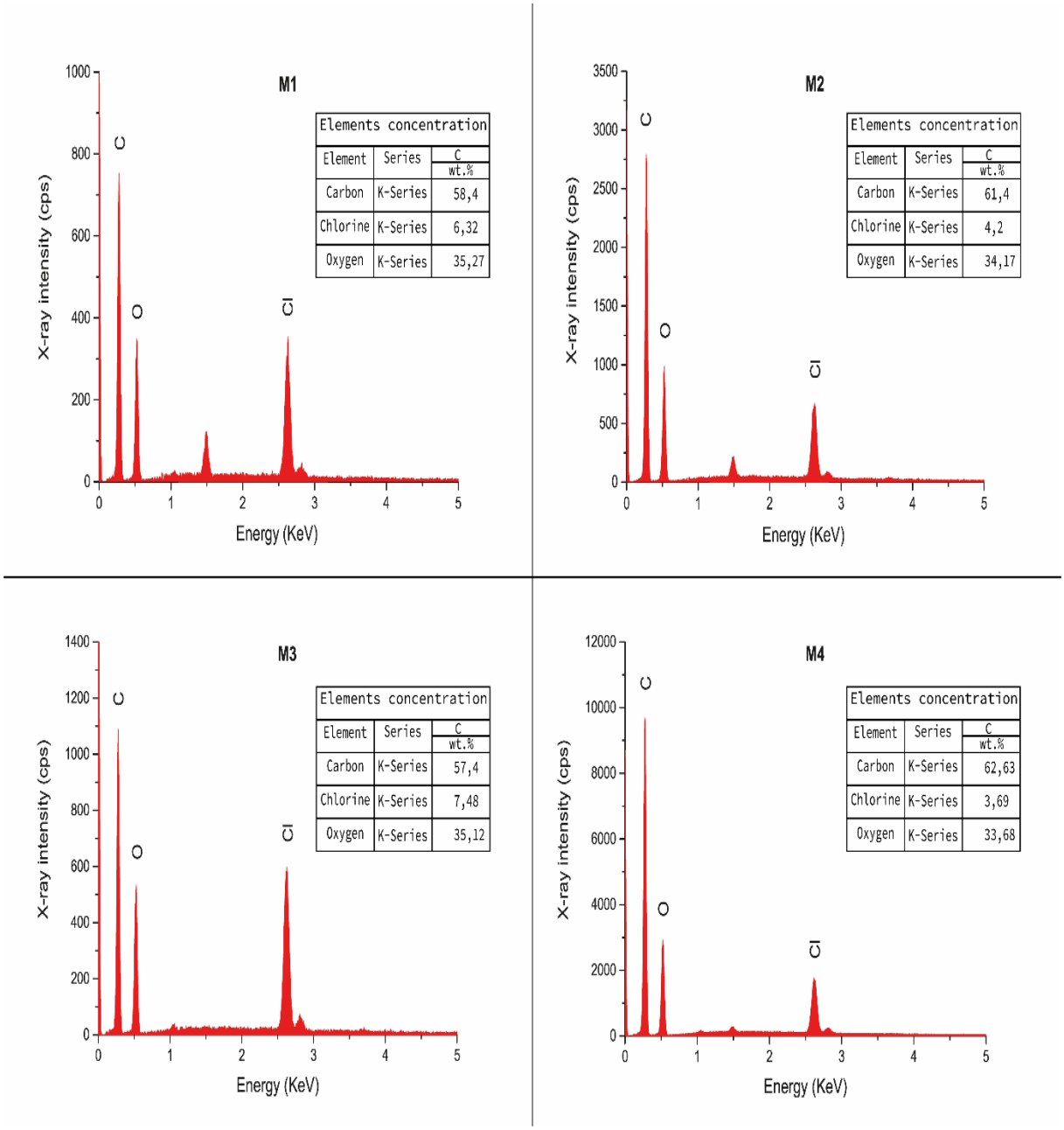

Figure 3-11. Energy dispersive X-ray spectrometry images of the sub-layer surface of PET membranes. Series = characteristic X-ray lines, C [wt. %] = the concentration in weight percent of the element

Chapter 4

Methane gas dehydration by PET-based membranes

The measurement of the permeability of the water vapour (WVP) and methane gas for the obtained PET membranes M1, M2, M3, M4, is shown in this chapter. The results are thoroughly examined to determine the performance separation of each membrane for removing the methane gas from water vapor (methane gas dehydration). All influencing parameters on separation performance, such as the effect of the PEG addition, are thoroughly discussed.

4.1 WATER VAPOR PERMEABILITY MEASUREMENT (WVP)

4.1.1 Membrane's thickness

A duplicate measurement is undertaken for each flat sheet membrane M1, M2, M3, M4 to calculate the water vapor permeability (WVP). It should be noted that the used membrane cannot be reused for another experiment, because it loses its original thickness and characteristics after the permeability test, an example of the thickness loss of the M2 membrane is shown in Figure 4-1, a loss of 15 µm is observed. This phenomenon was observed on all prepared membranes after the water permeability test of the membranes. This variation can be explained by the continuous force of water vapor during the WVP measurement, which causes the membrane to elongate.

In comparison, M1 shows more considerable thickness loss, which matches the water vapor permeability results, it might be note that a higher resistance to water vapor permeance, leading to greater thickness loss due to greater expansion by water vapor pressure. As the PEG additive increases, the water vapor permeability increases and the resistance is lower, leading to little thickness loss.

The used membranes to calculate the water vapor permeability (WVP) have such a circular form with an affective area that fits the cup water of 0,003019 m2, the thickness is measured at various points, the sequential numbering of the membranes with the average value of thickness is presented in

Table **4-1**.

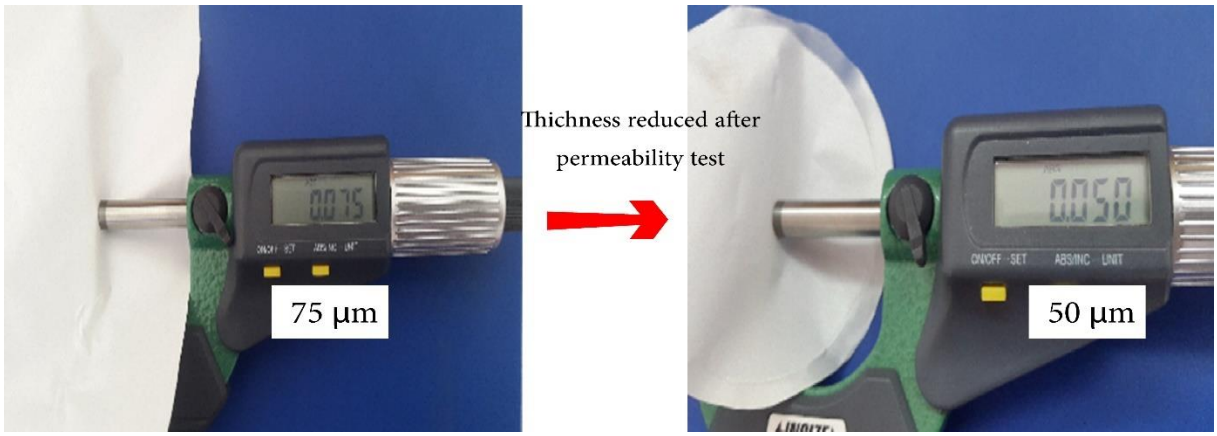

Figure 4-1. Membrane thickness loose after water vapor permeability test

Table 4-1. Average thickness of membranes

Membrane	Average thickness (µm)
M1-1	90
M1-2	80
M2-1	120
M2-2	75
M3-1	120
M3-2	110
M4-1	110
M4-2	110

4.1.2 Water vapor transmission rate (WVTR)

The water vapor transmission rate (WVTR) of flat sheet PET membranes M1, M2, M3, M4 is determined using the equation (2-2), defined as the flux across a membrane effective aera. The flux is calculated by plotting the weight loss of water vapor of membranes as a function of time, then using the function for the best fit of the results to find the slope value.

Based on the similarity of equation (2-2) with the equation of line Y=ax+b of the weight loss, the flux is considered equal to the value of the slope. All the water weight loss data of the membranes are listed in the tables below: Table 4-2, Table 4-3, Table 4-4, Table 4-5.

4.1.2.1 M1 Membrane flux

The data recorded from the experiment of the cup of water for the membrane M1 are shown in the Table 4-2.

Table 4-2. Weight loss vs time data of M1 membrane

M1-1		**M1-2**	
Thickness: 90 µm		Thickness: 80 µm	
Weight loss (g)	Time (min)	Weight loss (g)	Time (min)
0	0	0	0
0,3	120	0,2	120
0,4	240	0,4	240
0,6	360	0,6	360
0,8	480	0,7	480
1	600	1	600
1,3	720	1,2	720
1,5	840	1,4	840
1,8	960	1,6	960
2	1080	1,7	1080

By graphing the data presented in the Table 4-2 of the weight loss versus time, the Flux is determined which represents the slope value, the results of the best fit are illustrated in Figure 4-2 where the value of slopes are determined:

M1-1 Slope=0,0018, Adj. R-Square R2=0,99217
M1-2 Slope=0,0016, Adj. R-Square R2=0,99499

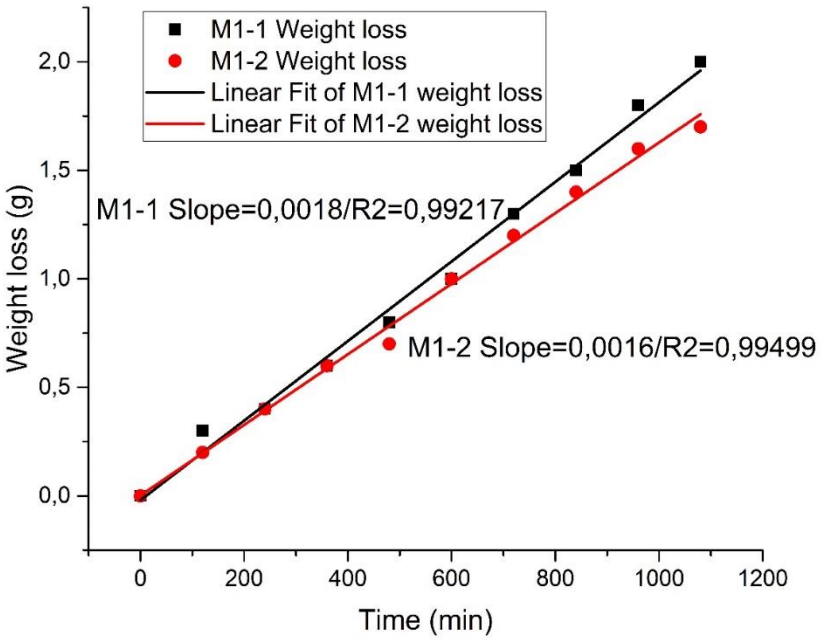

Figure 4-2. Weight loss slope of M1 membrane

4.1.2.2 M2 Membrane flux

Table 4-3, shows the data taken from the cup of water experiment for membrane M2.

Table 4-3. Weight loss vs time data of M2 membrane

M2-1		**M2-2**	
Thickness: 120 µm		Thickness: 75 µm	
Weight loss (g)	Time (min)	Weight loss (g)	Time (min)
0	0	0	0
0,3	120	0,3	120
0,5	240	0,5	240
0,8	360	0,9	360
1,2	480	1,3	480
1,6	600	1,6	600
1,9	720	1,9	720
2,2	840	2,4	840
2,5	960	2,7	960
2,8	1080	3,2	1080

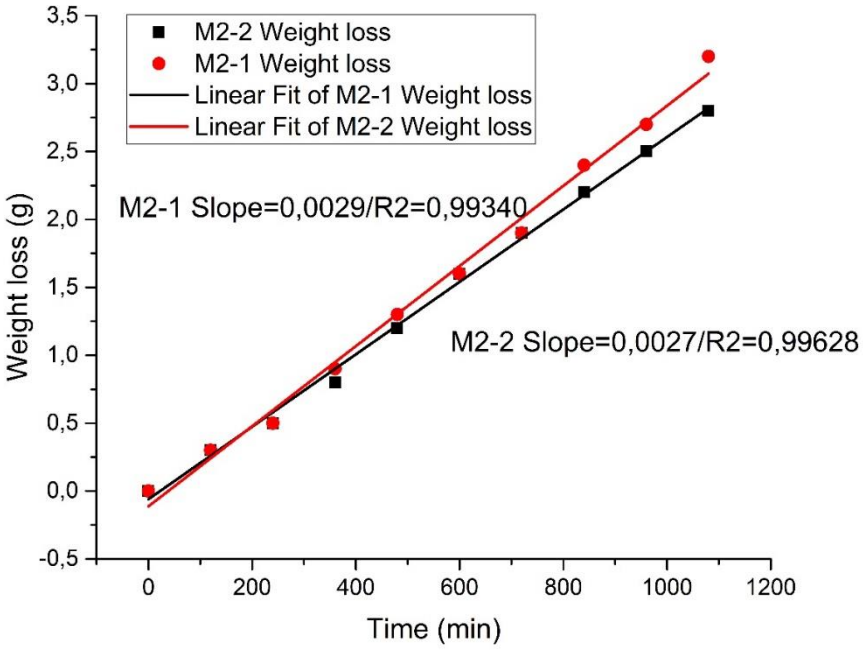

Figure 4-3. Weight loss slope of M2 membrane

4.1.2.3 M3 Membrane flux

Table 4-4, shows the data taken from the cup of water experiment for membrane M3

Table 4-4. Water weight loss of M3 membrane

M3-1		**M3-2**	
Thickness: 120 µm		Thickness: 110 µm	
Time (min)	Weight loss (g)	Time (min)	Weight loss (g)
0	0	0	0
0,4	120	120	0,4
0,8	240	240	0,8
1,3	360	360	1,3
1,8	480	480	1,8
2,4	600	600	2,4
3	720	720	2,9
3,6	840	840	3,7
4,1	960	960	4,2
4,5	1080	1080	4,7

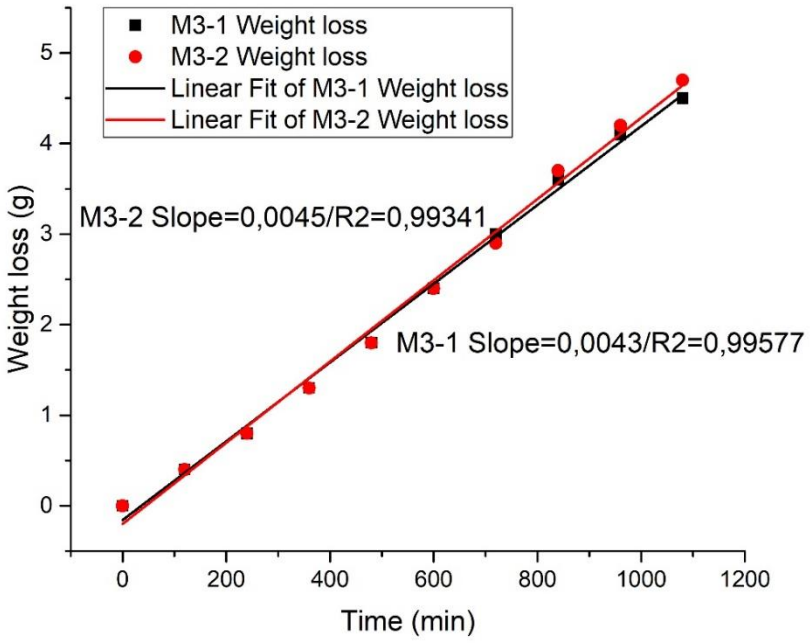

Figure 4-4. Weight loss slope of M3 membrane

4.1.2.4 M4 Membrane flux

Table 4-5. Water weight loss of M4 membrane

M4-1		**M4-2**	
Thickness: 110 µm		Thickness: 110 µm	
Time (min)	Weight loss (g)	Time (min)	Weight loss (g)
0	0	0	0
120	0,6	120	0,6
240	1,3	240	1,3
360	2,1	360	1,9
480	2,7	480	2,7
600	3,6	600	3,3
720	4,1	720	4
840	4,9	840	4,7
960	5,6	960	5,5
1080	6,1	1080	6,3

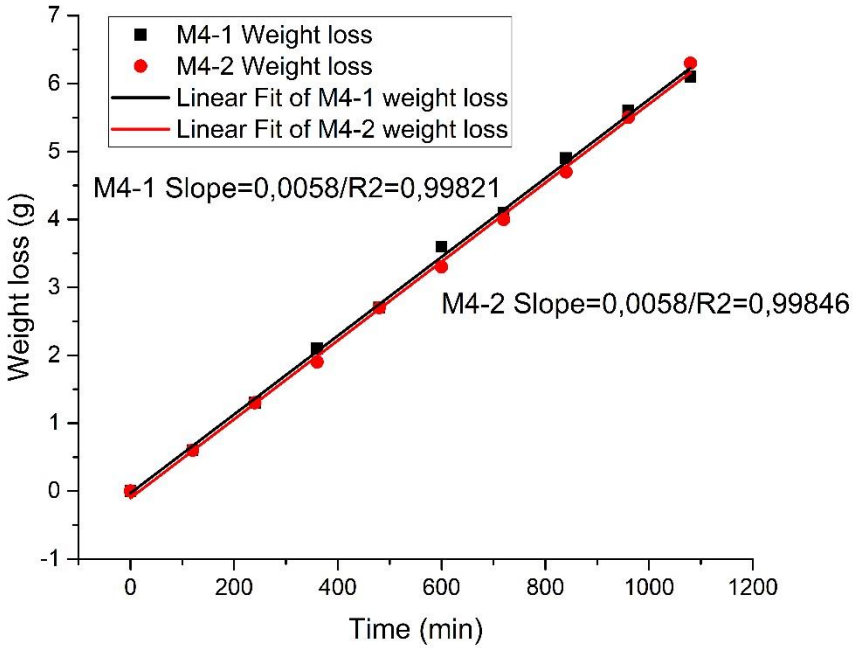

Figure 4-5. Weight loss slope of M4 membrane

4.1.2.5 Membranes average slope-Flux

The average slop-Flux of each membrane is the average of the flux of used membrane in each experiment, are calculated and listed in the Table 4-6.

Table 4-6. Average slopes of membranes

Membrane	Flux=Slope, $(\Delta G/\Delta t)$ (g/min)		Average slope $(\Delta G/\Delta t)$ (g/min)
M1	M1-1	0,0016	0,0017
	M1-2	0,0018	
M2	M2-1	0,0027	0,0028
	M2-2	0,0029	
M3	M3-1	0,0043	0,0044
	M3-2	0,0045	
M4	M4-1	0,0058	0,0058
	M4-2	0,0058	

As the membranes average slope-Flux is obtained, the water vapour transmission rate (WVTR) can be then determined, by dividing the average slop over effective area which is presented by the equation (2-2). The effective area of the membrane when attached in the cup water is 0,003019 m^2.

Table 4-7. Water vapour transmission rate (WVTR)

Membrane	Average Slope $\Delta G/\Delta t$ (g/min)	WVTR ($g.min^{-1}.m^{-2}$)	WVTR ($g.d^{-1}.m^{-2}$)
M1	0,0017	0,563100364	810,8645247
M2	0,0028	0,927459424	1335,54157
M3	0,0044	1,490559788	2146,406095
M4	0,0058	1,921165949	2766,478967

4.1.3 Water vapor permeance (*P)*

The permeance is then resulted in the Table 4-8 by using the equation (2-3), where R1 the saturation water vapor pressure inside the cup of water is 100 %, R2 the saturation water vapor pressure inside the oven is measured by a digital hydrometer, S is the saturation water vapor pressure at 38 °C, is 46 mmHg (6254.436 Pa),

Table 4-8. Water vapor permeance (*P*)

Membrane	WVTR ($g.d^{-1}.m^{-2}$)	R2 (%)	(R2-R1) (%)	Permeance (*P*) $g \cdot m^{-2} \cdot d^{-1} \cdot Pa^{-1}$	Permeance (*P*) $ng \cdot m^{-2} \cdot s^{-1} \cdot Pa^{-1}$
M1	810,8645	32,6818	0,673182	0,192587298	2229,019649
M2	1335,5416	27,7639	0,722361	0,295607179	3421,379385
M3	2146,4061	24,6250	0,753750	0,455298706	5269,660948
M4	2766,4790	18,9250	0,810750	0,545572244	6314,493568

4.1.4 Water vapor permeability (WVP)

Table 4-9 displays the water vapor permeability values determined from equation (2-4) by multiplying the permeance by the thickness.

Table 4-9. Water vapor permeability (WVP)

Membrane	Permeance $(ng \cdot m^{-2} \cdot s^{-1} \cdot Pa^{-1})$	Average thickness (µm)	Permeability (WVP) $(ng \cdot m^{-1} \cdot s^{-1} \cdot Pa^{-1})$	Permeability (WVP) Barrer $x10^{+2}$
M1	2229,019649	85	0,1895	314,1007536
M2	3421,379385	98	0,3353	555,7677186
M3	5269,660948	115	0,6060	1004,459402
M4	6314,493568	110	0,6946	1151,316008

4.2 EFFECT OF THE PEG ON THE WVP

Figure 4-6 shows the slop of PEG percentage in each membrane against the water vapor permeability. It is observed that WVP is significantly increased where pure PET membranes M1 (WVP = 314.10x10^{+2} barrers), M2 (WVP = 555.77x10^{+2}), M3 (WVP = 1004.46x10^{+2}) and M4 (WVP = 1151.32x10^{+2}). This increase in WVP is attributed to the change in morphology affected by the addition of the PEG additive. Indeed, the morphology of the formed asymmetric membranes consists of two layers, a thin and dense layer supported by a porous sub-layer, their morphologies contributing both to limiting or improving the transport of water vapour. According to the previous results stated above, the addition of the PEG additive resulted in: an increase in the mean diameter of the pores of sub-layer top surface (Figure 3-10), build-up of macro-voids of the order of 35 μm in M3 and reaching 100 μm in M4 (Figure 3-3) and an increase in the porous surface area of the sub-layer (Figure 3-4). This change in morphology resulting from the addition of PEG makes the sub-layer providing less resistance to the transport of water vapour, thus contributing to the increase in the permeability of the water vapour [107], [111], [112]. In addition, it is also believed that WVP increased due to the addition of the hydrophilic PEG polymer in hydrophobic PET membranes that improved the wettability of water vapour on the membrane surface, thereby contributing to the improvement of the water vapour diffusion rate through the membranes. This result is consistent with the reported literature [36], [107]. Moreover, the thin layer of the asymmetric membrane is also influenced by the PEG additive, the thickness increased but did not slow down the WVP, this behaviour can be explained in particular by the incorporation of the PEG additive in this layer, which gave it a better hydrophilic character, and therefore a better water vapour transport [107].

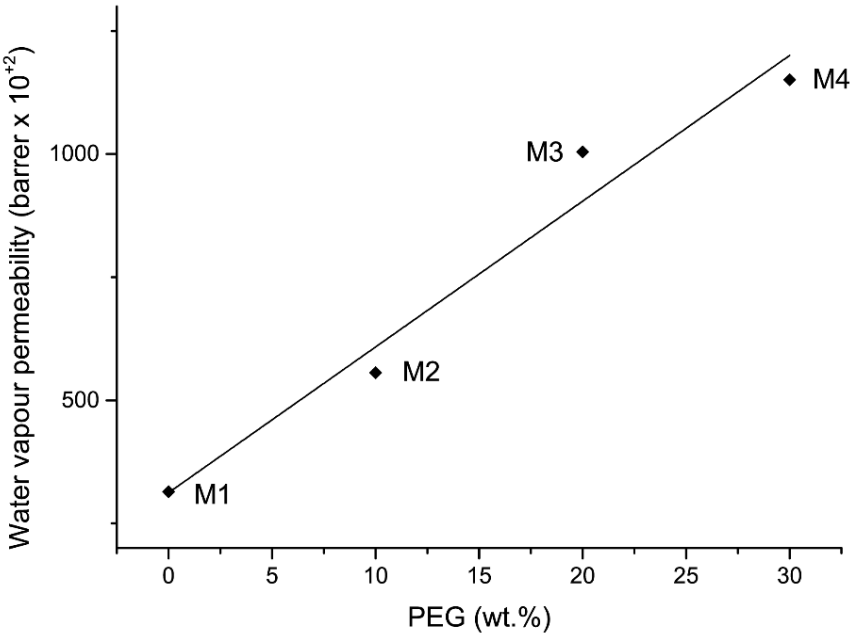

Figure 4-6. Water vapour permeability of PET/PEG membranes: M1 (100%/0%), M2 (90%/10%), M3 (80%/20%), M4 (70%/30%). *(R square =0.9497)*

4.3 METHANE GAS PERMEABILITY MEASUREMENT (MGP)

Methane gas permeability (MGP) measurements of the prepared membranes M1, M2, M3, M4 are calculated by determining the methane gas volume flow rate (V_r), gas transmission rate (GTR), and permeance. For each membrane, the methane gas transmission experiment is performed three times to allow accurate results where the same membrane remains attached during all three experiments since the membrane was not influenced during each test.

4.3.1 Methane gas volume-flow rate (V_r)

The methane gas transmission experimental data of escaped volume of methane gas versus elapsed time for each membrane are recorded in Table 4-10, Table 4-11, Table 4-12, Table 4-13, and all are graphed. The volume-flow rate of methane gas (V_r) is calculated using the equation (2-6), where the slope, defined as flow rate in volume changed over time, is calculated using the regression line of the recorded data, are shown in Figure 4-7, Figure 4-8, Figure 4-9, Figure 4-10.

Table 4-10. Water weight loss of M1 membrane

M1			
Volume (ml)	Time exp 1 (s)	Time exp 2 (s)	Time exp 3 (s)
0	0	0	0
1	46,81	44,82	44,989
2	91,737	89,05	88,397
3	138,762	134,988	135,37
4	183,251	181,801	181,648
5	228,29	226,43	226,805

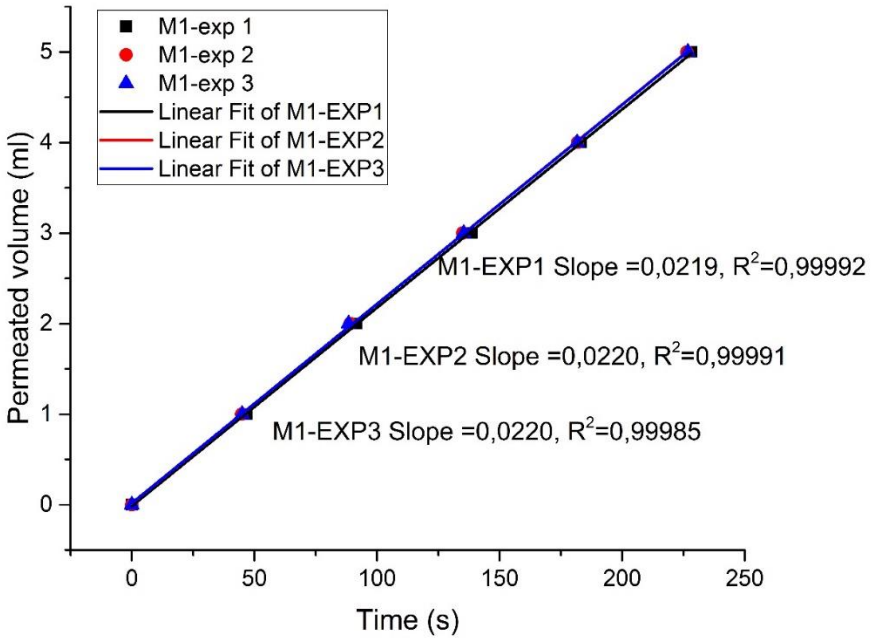

Figure 4-7. M1 Membrane escaped methane volume regression line with slopes

Table 4-11. Water weight loss of M2 membrane

M2			
Volume (ml)	Time exp 1 (s)	Time exp 2 (s)	Time exp 3 (s)
0	0	0	0
1	26,34	24,124	22,292
2	51,502	47,545	45,081
3	77,102	72,948	69,13
4	101,861	96,325	93,145
5	126,706	119,342	116,454

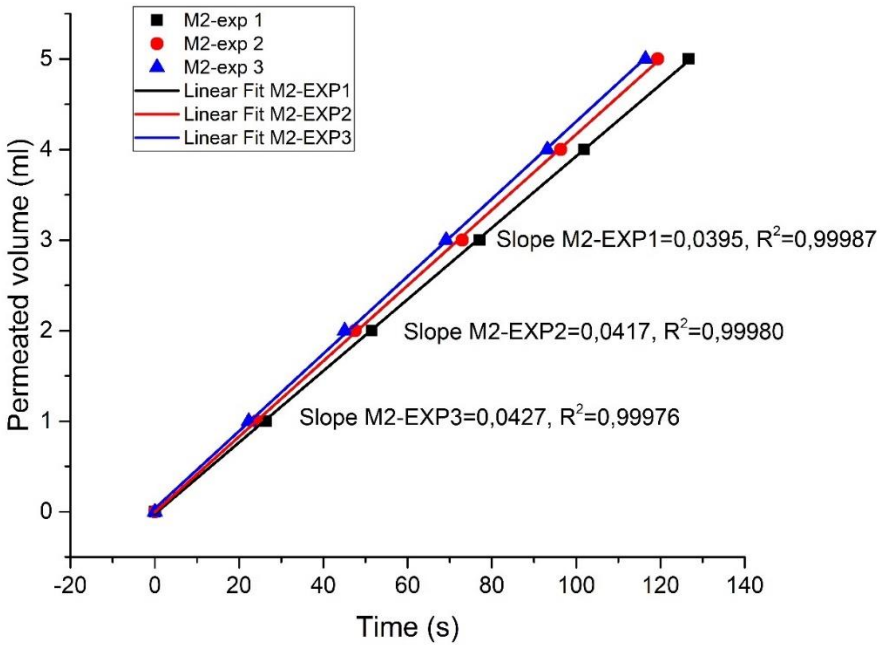

Figure 4-8. M2 Membrane escaped methane volume regression line with slopes

Table 4-12. Water weight loss of M3 membrane

M3			
Volume (ml)	Time exp 1 (s)	Time exp 2 (s)	Time exp 3 (s)
0	0	0	0
1	21,825	24,127	22,294
2	44,611	47,012	43,812
3	68,479	69,827	67,099
4	90,835	92,639	89,463
5	112,801	115,066	110,731

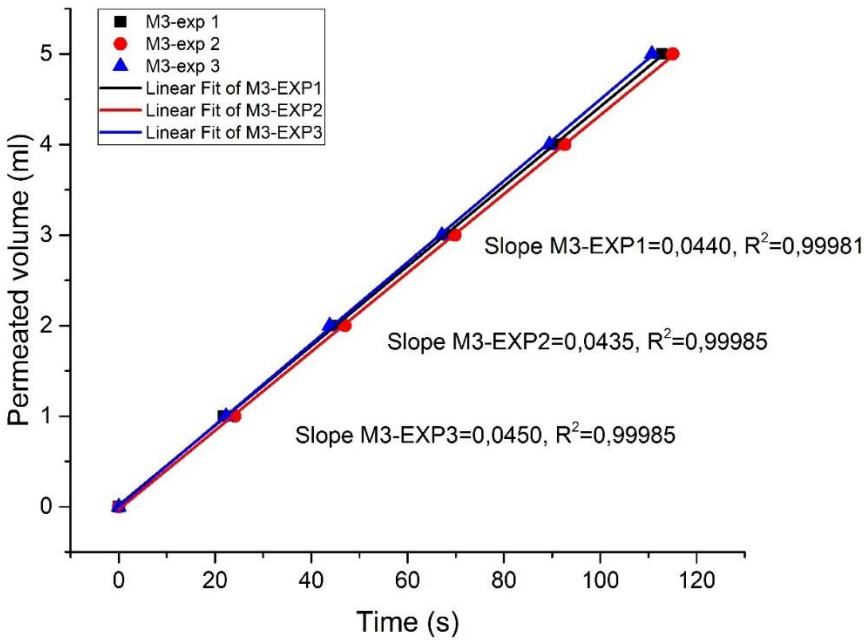

Figure 4-9. M3 Membrane escaped methane volume regression line with slopes

Table 4-13. Water weight loss of M4 membrane

M4			
Volume (ml)	Time exp 1 (s)	Time exp 2 (s)	Time exp 3 (s)
0	0	0	0
1	25,285	24,969	24,685
2	49,073	48,282	48,12
3	75,037	73,248	72,389
4	99,061	97,307	96,016
5	121,216	120,474	118,623

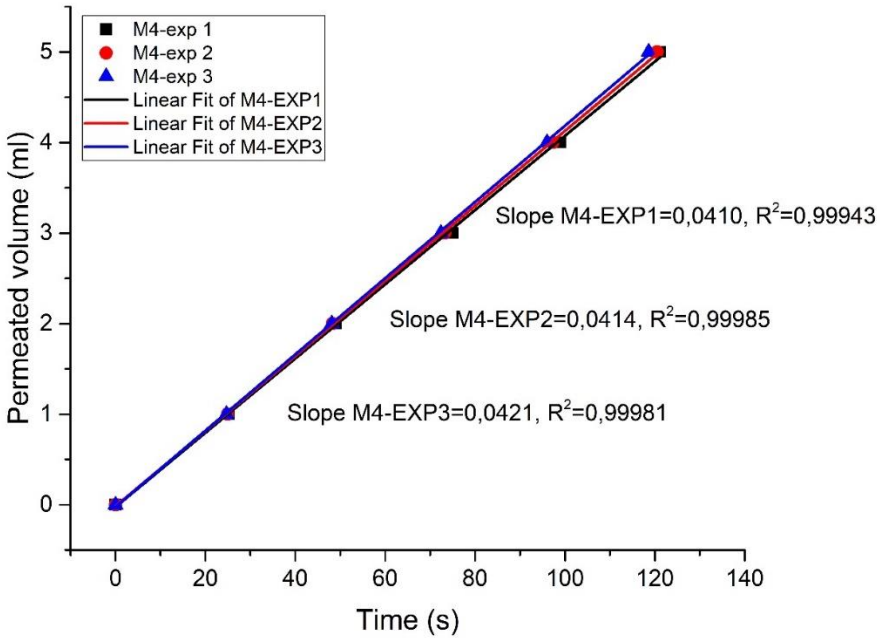

Figure 4-10. M4 Membrane escaped methane volume regression line with slopes

4.3.2 Average Methane gas volume-flow rate (V_r) of membranes

The Average Methane gas volume-flow rate (Vr) of membranes is calculated by taking the average value of three experiments of each membrane.

Table 4-14. Average Slope=V_r of membranes

Membrane	Slope=V_r (ml/s)		Average V_r (ml/s)	Average V_r ((L/s))
M1	M1-exp1	0,0219	0,021966667	2,19667E-05
	M1-exp2	0,0220		
	M1-exp3	0,0220		
M2	M2-exp1	0,0395	0,0413	0,0000413
	M2-exp2	0,0417		
	M2-exp3	0,0427		
M3	M3-exp1	0,0410	0,044166667	4,41667E-05
	M3-exp2	0,0414		
	M3-exp3	0,0421		
M4	M4-exp1	0,0410	0,0415	0,0000415
	M4-exp2	0,0414		
	M4-exp3	0,0421		

4.3.2.1.1 Methane gas transmission rate (*GTR*)

The methane gas transmission rate (GTR) of PET membranes is determined from the equation (2-7), the Table 4-15 resumes the obtained results.

Where:

Membrane raduis (mm)=	31
A (mm2) =	3019,07054
R (L·Pa/mol·K) =	8314,3
T (K)=	298,15
P0 (Pa)=	101325

Table 4-15. Methane gas transmission rate (GTR)

Membrane	V_r ($L.s^{-1}$)	GTR $mol \cdot m^{-2} \cdot s^{-1}$
M1	2,19667E-05	2,97E-16
M2	0,0000413	5,59E-16
M3	4,41667E-05	5,98E-16
M4	0,0000415	5,62E-16

4.3.2.1.2 Methane gas permeance (*P*)

The methane permeance (*P*) is expressed by the equation (2-8), the results are listed in the Table 4-16.

Table 4-16. Methane gas permeance (*P*)

Membrane	GTR $mol \cdot m^{-2} \cdot s^{-1}$	Permeance (*P*) $mol \cdot m^{-2} \cdot s^{-1} \cdot Pa^{-1}$
M1	2,97404E-16	8,19643E-20
M2	5,59156E-16	1,54103E-19
M3	5,97967E-16	1,64799E-19
M4	5,61864E-16	1,54849E-19

4.3.2.1.3 Methane gas permeability (MGP)

Methane gas permeability (MGP) expressed by the equation (2-9), is determined by multiplying the permeance by the thickness of the membrane, the obtained results are listed in the Table 4-17.

Table 4-17. Methane gas permeability (MGP)

Membrane	Thickness (µm)	Permeance (*P*) $mol \cdot m^{-2} \cdot s^{-1} \cdot Pa^{-1}$	Permeability (MGP) $mol \cdot m^{-1} \cdot s^{-1} \cdot Pa^{-1}$	Permeability (MGP) Barrer
M1	100	8,19643E-20	8,20E-24	2,45E-08
M2	95	1,54103E-19	1,46398E-23	4,37E-08
M3	90	1,64799E-19	1,48319E-23	4,43E-08
M4	80	1,54849E-19	1,23879E-23	3,70E-08

4.4 EFFECT OF THE PEG ON THE METHANE GAS PERMEABILITY

The MGP of all membranes with different PEG contents is presented in Figure 4-11. The results showed that M1 membrane has the best barrier to methane gas with a lower permeability of $2.45x10^{-08}$ barrer. By increasing the PEG content, the permeability of M2 seems to increase, this is assumed to be due to the increase in the porous area of the sectional and top surface of the sub-layer of M2. With higher PEG contents (≥20%), a sharp decrease in permeability is observed, where M2 and M3 membranes maintained higher close values, while a lower value is achieved for M4. Compared to M2 and M3 membranes, M4 showed a higher resistance to methane gas transport, this behaviour is attributed to the increase in the thickness of the skin/dense layer. The addition of PEG content leads to an increase in the thickness of the skin/dense layer and, therefore, greater resistance to the transport of methane molecules, resulting in a decrease in MGP. Indeed, the build-up of skin layer acts as a separating layer for gases, whereas this is not the case for the water vapour [36], [111], similar observation reported by Liu et *al* [111], the thickness had little influence on WVP, while the permeability to nitrogen gas decreased sharply with increasing skin layer thickness. The results clearly illustrate that even with the increase in the porous surface area of the sub-layer, mean pores diameter and build-up of macro-voids, the MGP is not affected by this gain of decrease in the resistance of the sub-layer, it is kept down mainly due to the additional thickness that acted as a separation layer.

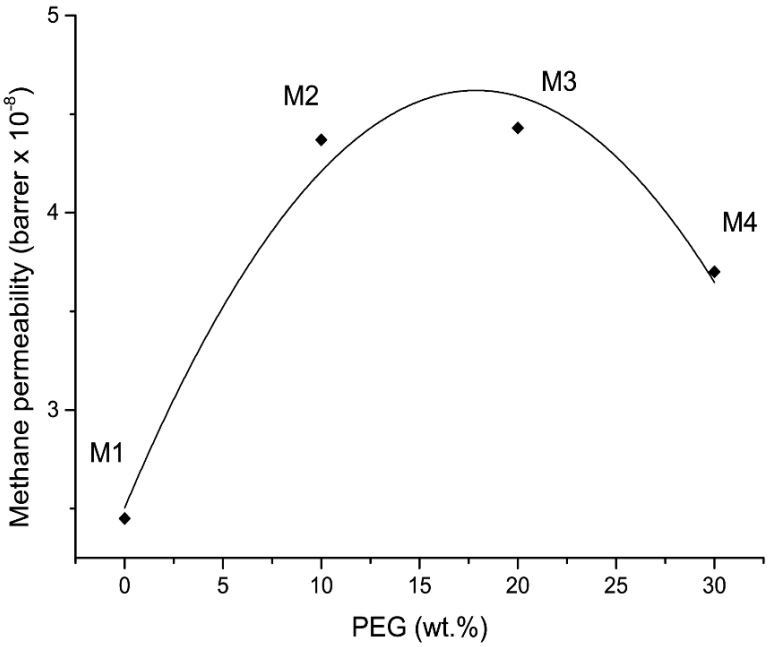

Figure 4-11. Effect of PEG additive on gas transport properties of methane gas, (*R square=0.9323)*

CONCLUSIONS AND FUTURE PERSPECTIVE

a. CONCLUSIONS

In this thesis, PET-based membranes were prepared in different compositions and were modulated by incorporating the hydrophilic polymer PEG into the PET membranes for the reason of improving the properties and performance of the prepared membranes, for use in methane gas and water vapour separation. The PEG additive was found to play a key role in the performance of the membranes for the dehydration of methane gas, the results showed an improvement in WVP and a reduction in MGP. In particular, the addition of PEG to the membranes led to the formation of macro-voids on the surface of the sub-layer, which facilitated an increase in pore size diameter and consequently, led to an increase in the WVP of the membranes. Another advantage of the addition of PEG, it led to an increase in the thickness of the skin layer which resulted in the production of high resistance to methane gas transport and low influence on WVP. The same is valid for M4, the high PEG content of 30% compared to M2 and M3, it showed more barrier to methane while showing a higher WVP, this last data makes M4 the best separator for the dehydration process. Moreover, with a maximum addition of 40% of PEG, the prepared membranes are deformed and massive holes are formed.

In summary, the results in this thesis validate the conclusion that an excessive content of PEG is not appropriate, but when used at an acceptable level, it serves a high performance to the prepared membranes for the separation of methane gas and water vapour.

b. FUTURE PERSPECTIVE

In order to have a good mastery when using PET membranes for future methane gas dehydration applications, the following recommendations should be taken into account by future researches:

- ✓ The produced membranes in this thesis are flat in shape, they are used for laboratory tests, and have proved good performance for methane gas dehydration, however, to develop PET membranes for use in industrial applications, the shape of PET membranes should be made as hollow fiber, it is effective for large flow rates. A study should be conducted for the manufacture of PET hollow fiber with their application results.
- ✓ The PET membranes produced in this thesis were made from a new PET polymer, for future application improvement, a suggestion to investigate and use a recycled PET for the natural gas dehydration, this thesis aimed to improve the environment, and the investigation would be a benefit and a complementary result.
- ✓ The PET films application was handled with fabricated home-made blade, sometimes the produced films are rejected, due to the errors by unfamiliar operator, to manually adjust both the speed and the thickness, the errors are minimized with practices. A recommendation to use an automatic film applicator, it is relevant tool that enhance the quality of films, it offers an accurate thickness as a function of time for coating application, it can be delivered with a heating system for temperature control, in addition, the speed rate is adjusted automatically. All these elements contribute in providing a rough, consistent and reproducible coating film. The automatic film applicator can be purchased from suppliers or, preferably, manufactured locally by the master student.

Bibliography

[1] Kavitha. Shanmugam, Mats. Tysklind, et V. K. K. Upadhyayula, « Use of Liquefied Biomethane (LBM) as a Vehicle Fuel for Road Freight Transportation: A Case Study Evaluating Environmental Performance of Using LBM for Operation of Tractor Trailers », *Procedia CIRP*, vol. 69, p. 517-522, 2018, doi: 10.1016/j.procir.2017.11.133.

[2] S. Koonaphapdeelert, J. Moran, P. Aggarangsi, et A. Bunkham, « Low pressure biomethane gas adsorption by activated carbon », *Energy for Sustainable Development*, vol. 43, p. 196-202, avr. 2018, doi: 10.1016/j.esd.2018.01.010.

[3] A. Baccioli, G. Caposciutti, A. Marchionni, L. Ferrari, et U. Desideri, « Poly-generation capability of a biogas plant with upgrading system », *Energy Procedia*, vol. 159, p. 280-285, févr. 2019, doi: 10.1016/j.egypro.2019.01.015.

[4] S. F. Ferreira, L. S. Buller, M. Berni, et T. Forster-Carneiro, « Environmental impact assessment of end-uses of biomethane », *Journal of Cleaner Production*, vol. 230, p. 613-621, sept. 2019, doi: 10.1016/j.jclepro.2019.05.034.

[5] Y. zhiyi et O. Xunmin, « Life Cycle Analysis on Liquefied Natural Gas and Compressed Natural Gas in Heavy-duty Trucks with Methane Leakage Emphasized », *Energy Procedia*, vol. 158, p. 3652-3657, févr. 2019, doi: 10.1016/j.egypro.2019.01.896.

[6] I. Ullah Khan *et al.*, « Biogas as a renewable energy fuel – A review of biogas upgrading, utilisation and storage », *Energy Conversion and Management*, vol. 150, p. 277-294, oct. 2017, doi: 10.1016/j.enconman.2017.08.035.

[7] J. Guilera *et al.*, « Synthetic natural gas production from biogas in a waste water treatment plant », *Renewable Energy*, vol. 146, p. 1301-1308, févr. 2020, doi: 10.1016/j.renene.2019.07.044.

[8] M. Torrijos, « State of Development of Biogas Production in Europe », *Procedia Environmental Sciences*, vol. 35, p. 881-889, 2016, doi: 10.1016/j.proenv.2016.07.043.

[9] F. Cucchiella, I. D'Adamo, et M. Gastaldi, « An economic analysis of biogas-biomethane chain from animal residues in Italy », *Journal of Cleaner Production*, vol. 230, p. 888-897, sept. 2019, doi: 10.1016/j.jclepro.2019.05.116.

[10] S. Khatun *et al.*, « Aerobic methane production by planktonic microbes in lakes », *Science of The Total Environment*, vol. 696, p. 133916, déc. 2019, doi: 10.1016/j.scitotenv.2019.133916.

[11] G. Myhre, D. Shindell, et J. Pongratz, « Anthropogenic and Natural Radiative Forcing », in *Climate change 2013 : the physical science basis; Working Group I contribution to the fifth assessment report of the Intergovernmental Panel on Climate Change*, T. Stocker, Éd. Cambridge: Ludwig-Maximilians-Universität München, 2014, p. 659-740. doi: https://doi.org/10.1017/CBO9781107415324.018.

[12] P. Balcombe, J. F. Speirs, N. P. Brandon, et A. D. Hawkes, « Methane emissions: choosing the right climate metric and time horizon », *Environ. Sci.: Processes Impacts*, vol. 20, n° 10, Art. n° 10, 2018, doi: 10.1039/C8EM00414E.

[13] O. Boucher et G. A. Folberth, « New Directions: Atmospheric methane removal as a way to mitigate climate change? », *Atmospheric Environment*, vol. 44, n° 27, p. 3343-3345, sept. 2010, doi: 10.1016/j.atmosenv.2010.04.032.

[14] E. Chan Gutiérrez, D. M. Wall, R. O'Shea, R. M. Novelo, M. M. Gómez, et J. D. Murphy, « An economic and carbon analysis of biomethane production from food waste to be used as a transport fuel in Mexico », *Journal of Cleaner Production*, vol. 196, p. 852-862, sept. 2018, doi: 10.1016/j.jclepro.2018.06.051.

[15] G. Pasini, A. Baccioli, L. Ferrari, M. Antonelli, S. Frigo, et U. Desideri, « Biomethane grid injection or biomethane liquefaction: A technical-economic analysis », *Biomass and Bioenergy*, vol. 127, p. 105264, août 2019, doi: 10.1016/j.biombioe.2019.105264.

[16] G. A. Von Wald, A. J. Stanion, D. Rajagopal, et A. R. Brandt, « Biomethane addition to California transmission pipelines: Regional simulation of the impact of regulations », *Applied Energy*, vol. 250, p. 292-301, sept. 2019, doi: 10.1016/j.apenergy.2019.05.031.
[17] F. Caputo, F. Cascetta, G. Lamanna, G. Rotondo, et A. Soprano, « Estimation of the damage in a natural gas flow line caused by the motion of methane hydrates », *Journal of Natural Gas Science and Engineering*, vol. 26, p. 1222-1231, sept. 2015, doi: 10.1016/j.jngse.2015.07.050.
[18] E. Ryckebosch, M. Drouillon, et H. Vervaeren, « Techniques for transformation of biogas to biomethane », *Biomass and Bioenergy*, vol. 35, n° 5, p. 1633-1645, mai 2011, doi: 10.1016/j.biombioe.2011.02.033.
[19] A. Bahadori, « Natural Gas Dehydration », in *Natural Gas Processing*, Elsevier, 2014, p. 441-481. doi: 10.1016/B978-0-08-099971-5.00009-X.
[20] F. Capra, F. Magli, et M. Gatti, « Biomethane liquefaction: A systematic comparative analysis of refrigeration technologies », *Applied Thermal Engineering*, vol. 158, p. 113815, juill. 2019, doi: 10.1016/j.applthermaleng.2019.113815.
[21] L. A. Pellegrini, G. De Guido, et S. Langé, « Biogas to liquefied biomethane via cryogenic upgrading technologies », *Renewable Energy*, vol. 124, p. 75-83, août 2018, doi: 10.1016/j.renene.2017.08.007.
[22] R. Chebbi, M. Qasim, et N. Abdel Jabbar, « Optimization of triethylene glycol dehydration of natural gas », *Energy Reports*, vol. 5, p. 723-732, nov. 2019, doi: 10.1016/j.egyr.2019.06.014.
[23] H. A. A. Farag, M. M. Ezzat, H. Amer, et A. W. Nashed, « Natural gas dehydration by desiccant materials », *Alexandria Engineering Journal*, vol. 50, n° 4, p. 431-439, déc. 2011, doi: 10.1016/j.aej.2011.01.020.
[24] M. Stewart et K. Arnold, « Dehydration Considerations », in *Gas Dehydration Field Manual*, Elsevier, 2011, p. 55-168. doi: 10.1016/B978-1-85617-980-5.00002-1.
[25] P. Gandhidasan, A. A. Al-Farayedhi, et A. A. Al-Mubarak, « Dehydration of natural gas using solid desiccants », p. 14, 2001.
[26] H. Lin *et al.*, « Dehydration of natural gas using membranes. Part I: Composite membranes », *Journal of Membrane Science*, vol. 413-414, p. 70-81, sept. 2012, doi: 10.1016/j.memsci.2012.04.009.
[27] H. Lin *et al.*, « Dehydration of natural gas using membranes. Part II: Sweep/countercurrent design and field test », *Journal of Membrane Science*, vol. 432, p. 106-114, avr. 2013, doi: 10.1016/j.memsci.2012.12.049.
[28] J. R. Du, L. Liu, A. Chakma, et X. Feng, « Using poly(N,N-dimethylaminoethyl methacrylate)/polyacrylonitrile composite membranes for gas dehydration and humidification », *Chemical Engineering Science*, vol. 65, n° 16, p. 4672-4681, août 2010, doi: 10.1016/j.ces.2010.05.005.
[29] K. Dalane, Z. Dai, G. Mogseth, M. Hillestad, et L. Deng, « Potential applications of membrane separation for subsea natural gas processing: A review », *Journal of Natural Gas Science and Engineering*, vol. 39, p. 101-117, mars 2017, doi: 10.1016/j.jngse.2017.01.023.
[30] K. Jevons et M. Awe, « Economic benefits of membrane technology vs. evaporator », *Desalination*, vol. 250, n° 3, p. 961-963, janv. 2010, doi: 10.1016/j.desal.2009.09.081.
[31] H.-B. Li, W.-Y. Shi, Y.-F. Zhang, D.-Q. Liu, et X.-F. Liu, « Effects of Additives on the Morphology and Performance of PPTA/PVDF in Situ Blend UF Membrane », *Polymers*, vol. 6, n° 6, p. 1846-1861, juin 2014, doi: 10.3390/polym6061846.
[32] S.-C. Chen, H.-H. Chang, T.-W. Cheng, Y.-L. Su, et L.-P. Cheng, « Strong effects of Tween 20 additive on the morphology and performance of poly(vinylidene fluoride) hollow-fiber membranes », *J. Appl. Polym. Sci.*, vol. 134, n° 11, mars 2017, doi: 10.1002/app.44600.
[33] H. Liu et X. Liao, « The effects of fluorocarbon special surfactant (FS-30) additive on the phase inversion, morphology and separation performance of poly(vinylidene fluoride) (PVDF) membranes », *Separation and Purification Technology*, vol. 212, p. 619-631, avr. 2019, doi: 10.1016/j.seppur.2018.11.060.

[34] D. Hou, G. Dai, H. Fan, J. Wang, C. Zhao, et H. Huang, « Effects of calcium carbonate nano-particles on the properties of PVDF/nonwoven fabric flat-sheet composite membranes for direct contact membrane distillation », *Desalination*, vol. 347, p. 25-33, août 2014, doi: 10.1016/j.desal.2014.05.028.
[35] S. Zhao, W. Yan, M. Shi, Z. Wang, J. Wang, et S. Wang, « Improving permeability and antifouling performance of polyethersulfone ultrafiltration membrane by incorporation of ZnO-DMF dispersion containing nano-ZnO and polyvinylpyrrolidone », *Journal of Membrane Science*, vol. 478, p. 105-116, mars 2015, doi: 10.1016/j.memsci.2014.12.050.
[36] Y. Ma, F. Shi, J. Ma, M. Wu, J. Zhang, et C. Gao, « Effect of PEG additive on the morphology and performance of polysulfone ultrafiltration membranes », *Desalination*, vol. 272, n° 1-3, p. 51-58, mai 2011, doi: 10.1016/j.desal.2010.12.054.
[37] Y. X. Ma, F. M. Shi, M. N. Wu, et J. Ma, « Effect of Additives in the Casting Solutions on the Morphology and Performance of PVDF Membranes », *AMR*, vol. 391-392, p. 1412-1416, déc. 2011, doi: 10.4028/www.scientific.net/AMR.391-392.1412.
[38] K. A. Gebru et C. Das, « Effects of solubility parameter differences among PEG, PVP and CA on the preparation of ultrafiltration membranes: Impacts of solvents and additives on morphology, permeability and fouling performances », *Chinese Journal of Chemical Engineering*, vol. 25, n° 7, p. 911-923, juill. 2017, doi: 10.1016/j.cjche.2016.11.017.
[39] Y. Ma, F. Shi, Z. Wang, M. Wu, J. Ma, et C. Gao, « Preparation and characterization of PSf/clay nanocomposite membranes with PEG 400 as a pore forming additive », *Desalination*, vol. 286, p. 131-137, févr. 2012, doi: 10.1016/j.desal.2011.10.040.
[40] W. Hu *et al.*, « PEG/PVDF membranes for separating organosulphur compounds from *n* -heptane: Effect of PEG molecular weight », *Can. J. Chem. Eng.*, vol. 95, n° 2, p. 364-371, févr. 2017, doi: 10.1002/cjce.22657.
[41] M. S. Chinnan et H. J. Park, « EFFECT of PLASTICIZER LEVEL and TEMPERATURE ON WATER VAPOR TRANSMISSION of CELLULOSE-BASED EDIBLE FILMS », *J Food Process Engineering*, vol. 18, n° 4, p. 417-429, déc. 1995, doi: 10.1111/j.1745-4530.1995.tb00375.x.
[42] C.-Y. Lin, K.-H. Liao, C.-F. Su, C.-H. Kuo, et K.-H. Hsieh, « Smart temperature-controlled water vapor permeable polyurethane film », *Journal of Membrane Science*, vol. 299, n° 1-2, p. 91-96, août 2007, doi: 10.1016/j.memsci.2007.04.028.
[43] A. M. Alakrach *et al.*, « Physical properties of plasticized PLA/HNTs bionanocomposites: effects of plasticizer type and content », *IOP Conf. Ser.: Mater. Sci. Eng.*, vol. 557, p. 012067, juin 2019, doi: 10.1088/1757-899X/557/1/012067.
[44] S. Jasmee, G. Omar, N. A. B. Masripan, A. A. Kamarolzaman, A. S. Ashikin, et F. Che Ani, « Hydrophobicity performance of polyethylene terephthalate (PET) and thermoplastic polyurethane (TPU) with thermal effect », *Mater. Res. Express*, vol. 5, n° 9, p. 096304, août 2018, doi: 10.1088/2053-1591/aad81e.
[45] Z. O. G. Schyns et M. P. Shaver, « Mechanical Recycling of Packaging Plastics: A Review », *Macromol. Rapid Commun.*, p. 2000415, sept. 2020, doi: 10.1002/marc.202000415.
[46] C. C. Lin, « Recycling technology of poly(ethylene terephthalate) materials », *Macromol. Symp.*, vol. 135, n° 1, p. 129-135, déc. 1998, doi: 10.1002/masy.19981350115.
[47] S. D. Mancini et M. Zanin, « Consecutive steps of PET recycling by injection: evaluation of the procedure and of the mechanical properties », p. 10.
[48] M. AL-Harbi, A. Alshaiban, M. F. Yassin, et A. Elmi, « Kinetic analysis and modelling of thermal degradation of perspex (PMMA) and perspex blend plastic waste », *Can. J. Chem. Eng.*, vol. 91, n° 7, p. 1281-1288, juill. 2013, doi: 10.1002/cjce.21741.
[49] O. Dada et C. Mbohwa, « Biogas Upgrade to Biomethane from Landfill Wastes: A Review », *Procedia Manufacturing*, vol. 7, p. 333-338, 2017, doi: 10.1016/j.promfg.2016.12.082.
[50] H. Afazeli, A. Jafari, S. Rafiee, et M. Nosrati, « An investigation of biogas production potential from livestock and slaughterhouse wastes », *Renewable and Sustainable Energy Reviews*, vol. 34, p. 380-386, juin 2014, doi: 10.1016/j.rser.2014.03.016.

[51] D. Díaz-Vázquez, S. C. Alvarado-Cummings, D. Meza-Rodríguez, C. Senés-Guerrero, J. de Anda, et M. S. Gradilla-Hernández, « Evaluation of Biogas Potential from Livestock Manures and Multicriteria Site Selection for Centralized Anaerobic Digester Systems: The Case of Jalisco, México », *Sustainability*, vol. 12, n° 9, p. 3527, avr. 2020, doi: 10.3390/su12093527.
[52] A. Berktay et B. Nas, « Biogas Production and Utilization Potential of Wastewater Treatment Sludge », *Energy Sources, Part A: Recovery, Utilization, and Environmental Effects*, vol. 30, n° 2, p. 179-188, nov. 2007, doi: 10.1080/00908310600712489.
[53] S. Harikishan, « Biogas Processing and Utilization as an Energy Source », in *Anaerobic Biotechnology for Bioenergy Production*, S. K. Khanal, Éd. Oxford, UK: Wiley-Blackwell, 2008, p. 267-291. doi: 10.1002/9780813804545.ch12.
[54] R. Murano, N. Maisano, R. Selvaggi, G. Pappalardo, et B. Pecorino, « Critical Issues and Opportunities for Producing Biomethane in Italy », p. 14, 2021.
[55] D. Pashchenko, R. Mustafin, et A. Mustafina, « Steam methane reforming in a microchannel reformer: Experiment, CFD-modelling and numerical study », *Energy*, vol. 237, p. 121624, déc. 2021, doi: 10.1016/j.energy.2021.121624.
[56] Y. Slotboom, S. Roosjen, A. Kronberg, M. Glushenkov, et S. R. A. Kersten, « Methane to ethylene by pulsed compression », *Chemical Engineering Journal*, vol. 414, p. 128821, juin 2021, doi: 10.1016/j.cej.2021.128821.
[57] X. Zhu, Z. Guo, W. Cen, et B. Mao, « Ethylene Polymerization Using Improved Polyethylene Catalyst », *Chinese Journal of Chemical Engineering*, vol. 19, n° 1, p. 52-56, févr. 2011, doi: 10.1016/S1004-9541(09)60176-2.
[58] A. Ray et A. Anumakonda, « Production of Green Liquid Hydrocarbon Fuels », in *Biofuels*, Elsevier, 2011, p. 587-608. doi: 10.1016/B978-0-12-385099-7.00027-9.
[59] N. O. Elbashir et F. T. Eljack, « A Method to Design an Advanced Gas-to-Liquid Technology Reactor for Fischer-Tropsch Synthesis », in *Proceedings of the 2nd Annual Gas Processing Symposium*, Elsevier, 2010, p. 369-377. doi: 10.1016/S1876-0147(10)02039-2.
[60] S.-K. Ryi, S.-W. Lee, J.-W. Park, D.-K. Oh, J.-S. Park, et S. S. Kim, « Combined steam and CO2 reforming of methane using catalytic nickel membrane for gas to liquid (GTL) process », *Catalysis Today*, vol. 236, p. 49-56, nov. 2014, doi: 10.1016/j.cattod.2013.11.001.
[61] A. Bahadori, « Natural Gas Dehydration », in *Natural Gas Processing*, Elsevier, 2014, p. 441-481. doi: 10.1016/B978-0-08-099971-5.00009-X.
[62] B. S. Kinigoma et G. O. Ani, « Comparison of gas dehydration methods based on energy consumption », *jasem*, vol. 20, n° 2, p. 253-258, juill. 2016, doi: 10.4314/jasem.v20i2.4.
[63] A. M. Braek, R. A. Almehaideb, N. Darwish, et R. Hughes, « OPTIMIZATION OF PROCESS PARAMETERS FOR GLYCOL UNIT TO MITIGATE THE EMISSION OF », *Part B*, vol. 79, p. 15, 2001.
[64] S. Ghanbari et C. H. Niu, « Characteristics of oat hull based biosorbent for natural gas dehydration in a PSA process », *Journal of Natural Gas Science and Engineering*, vol. 61, p. 320-332, janv. 2019, doi: 10.1016/j.jngse.2018.11.014.
[65] H. A. A. Farag, M. M. Ezzat, H. Amer, et A. W. Nashed, « Natural gas dehydration by desiccant materials », *Alexandria Engineering Journal*, vol. 50, n° 4, Art. n° 4, déc. 2011, doi: 10.1016/j.aej.2011.01.020.
[66] X. Y. Chen, H. Vinh-Thang, A. A. Ramirez, D. Rodrigue, et S. Kaliaguine, « Membrane gas separation technologies for biogas upgrading », *RSC Adv.*, vol. 5, n° 31, p. 24399-24448, 2015, doi: 10.1039/C5RA00666J.
[67] H. Lin *et al.*, « Dehydration of natural gas using membranes. Part I: Composite membranes », *Journal of Membrane Science*, vol. 413-414, p. 70-81, sept. 2012, doi: 10.1016/j.memsci.2012.04.009.
[68] « Chapter 1 - An Overview of Membrane Science and Technology », p. 23.
[69] M. Ulbricht, « Design and synthesis of organic polymers for molecular separation membranes », *Current Opinion in Chemical Engineering*, vol. 28, p. 60-65, juin 2020, doi: 10.1016/j.coche.2020.02.002.

[70] N. Abdullah, M. A. Rahman, M. H. Dzarfan Othman, J. Jaafar, et A. F. Ismail, « Membranes and Membrane Processes », in *Current Trends and Future Developments on (Bio-) Membranes*, Elsevier, 2018, p. 45-70. doi: 10.1016/B978-0-12-813549-5.00002-5.
[71] X. Ren, M. Kanezashi, H. Nagasawa, et T. Tsuru, « Plasma-assisted multi-layered coating towards improved gas permeation properties for organosilica membranes », *RSC Adv.*, vol. 5, n° 74, p. 59837-59844, 2015, doi: 10.1039/C5RA08052E.
[72] E. Lasseuguette et M.-C. Ferrari, « Polymer Membranes for Sustainable Gas Separation », in *Sustainable Nanoscale Engineering*, Elsevier, 2020, p. 265-296. doi: 10.1016/B978-0-12-814681-1.00010-2.
[73] A. Ghosh, E. A. Mistri, et S. Banerjee, « Fluorinated Polyimides », in *Handbook of Specialty Fluorinated Polymers*, Elsevier, 2015, p. 97-185. doi: 10.1016/B978-0-323-35792-0.00003-9.
[74] J. Wilcox, « Membrane Technology », in *Carbon Capture*, New York, NY: Springer New York, 2012, p. 177-218. doi: 10.1007/978-1-4614-2215-0_5.
[75] « Safety Data Sheet », p. 10.
[76] T. Phaechamud et S. Chitrattha, « Pore formation mechanism of porous poly(dl-lactic acid) matrix membrane », *Materials Science and Engineering: C*, vol. 61, p. 744-752, avr. 2016, doi: 10.1016/j.msec.2016.01.014.
[77] B. Yu *et al.*, « Fabrication of PLA/CNC/CNT conductive composites for high electromagnetic interference shielding based on Pickering emulsions method », *Composites Part A: Applied Science and Manufacturing*, vol. 125, p. 105558, oct. 2019, doi: 10.1016/j.compositesa.2019.105558.
[78] A. Celebioglu et T. Uyar, « Electrospun porous cellulose acetate fibers from volatile solvent mixture », *Materials Letters*, vol. 65, n° 14, p. 2291-2294, juill. 2011, doi: 10.1016/j.matlet.2011.04.039.
[79] H. Nguyen, M.-Y. Hsiao, K. Nagai, et H. Lin, « Suppressed crystallization and enhanced gas permeability in thin films of cellulose acetate blends », *Polymer*, vol. 205, p. 122790, sept. 2020, doi: 10.1016/j.polymer.2020.122790.
[80] « Safety Data Sheet », p. 12.
[81] « Safety Data Sheet », p. 9.
[82] I. V. Grishagin, « Automatic cell counting with ImageJ », *Analytical Biochemistry*, vol. 473, p. 63-65, mars 2015, doi: 10.1016/j.ab.2014.12.007.
[83] C. Williams, Y. Wu, et D. F. Bowers, « ImageJ analysis of dentin tubule distribution in human teeth », *Tissue and Cell*, vol. 47, n° 4, p. 343-348, août 2015, doi: 10.1016/j.tice.2015.05.004.
[84] A. Hattori, E. Ohta, M. Nagai, K. Iwabuchi, et H. Okano, « A new approach to analysis of intracellular proteins and subcellular localization using cellprofiler and imageJ in combination », *Methods*, p. S1046202321001110, avr. 2021, doi: 10.1016/j.ymeth.2021.04.019.
[85] N. Andrialovanirina, D. Ponton, F. Behivoke, J. Mahafina, et M. Léopold, « A powerful method for measuring fish size of small-scale fishery catches using ImageJ », *Fisheries Research*, vol. 223, p. 105425, mars 2020, doi: 10.1016/j.fishres.2019.105425.
[86] J. C. Peterson et M. C. DeRuiter, « Fluorescent Nuclei Measurements Macro (FNMM), a tool for automated cell quantification in ImageJ », *Software Impacts*, vol. 6, p. 100030, nov. 2020, doi: 10.1016/j.simpa.2020.100030.
[87] C. Udalagama, X. Chen, A. A. Bettiol, et F. Watt, « An ion beam analysis software based on ImageJ », *Nuclear Instruments and Methods in Physics Research Section B: Beam Interactions with Materials and Atoms*, vol. 306, p. 59-63, juill. 2013, doi: 10.1016/j.nimb.2012.12.026.
[88] M. Dufek, « Production Acknowledgments », p. 228.
[89] N. Inoue, Y. Takashima, M. Suga, T. Suzuki, Y. Nemoto, et O. Takai, « Observation of wet specimens sensitive to evaporation using scanning electron microscopy », *Microscopy*, vol. 67, n° 6, p. 356-366, déc. 2018, doi: 10.1093/jmicro/dfy041.
[90] W. Lee et K. C. Toussaint, « Quantitative analysis of the effect of environmental-scanning electron microscopy on collagenous tissues », *Sci Rep*, vol. 8, n° 1, p. 8491, déc. 2018, doi: 10.1038/s41598-018-26839-x.

[91] A. M. Donald, « The use of environmental scanning electron microscopy for imaging wet and insulating materials », *Nature Mater*, vol. 2, n° 8, p. 511-516, août 2003, doi: 10.1038/nmat898.
[92] S. Ebnesajjad, « Material Surface Preparation Techniques », in *Surface Treatment of Materials for Adhesive Bonding*, Elsevier, 2014, p. 95-138. doi: 10.1016/B978-0-323-26435-8.00006-X.
[93] « ImageJ ». https://imagej.net/Welcome (consulté le nov. 02, 2019).
[94] Y. Zhang, S. Jin, Y. Wang, et Y. Wang, « Characterization of the pore size distribution with SEM images processing for the tight rock », in *2015 IEEE International Conference on Information and Automation*, Lijiang, China, août 2015, p. 653-656. doi: 10.1109/ICInfA.2015.7279367.
[95] P. Gibson, C. Kendrick, D. Rivin, L. Sicuranza, et M. Charmchi, « An Automated Water Vapor Diffusion Test Method for Fabrics, Laminates, and Films », *Journal of Coated Fabrics*, vol. 24, n° 4, p. 322-345, avr. 1995, doi: 10.1177/152808379502400407.
[96] C16 Committee, « Test Methods for Water Vapor Transmission of Materials », ASTM International. doi: 10.1520/E0096_E0096M-10.
[97] F02 Committee, « Test Method for Determining Gas Permeability Characteristics of Plastic Film and Sheeting », ASTM International. doi: 10.1520/D1434-82R15E01.
[98] M. K. Purkait, M. K. Sinha, P. Mondal, et R. Singh, « Introduction to Membranes », in *Interface Science and Technology*, vol. 25, Elsevier, 2018, p. 1-37. doi: 10.1016/B978-0-12-813961-5.00001-2.
[99] J.-J. Shieh et T.-S. Chung, « Phase-Inversion Poly(ether imide) Membranes Prepared from Water-Miscible/Immiscible Mixture Solvents », *Ind. Eng. Chem. Res.*, vol. 38, n° 7, p. 2650-2658, juill. 1999, doi: 10.1021/ie9807912.
[100] W. H. Binder et M. Dunky, « Membrane Technology », in *Encyclopedia of Polymer Science and Technology, Concise*, H. F. Mark, Éd. John Wiley & Sons, 2013, p. 657-667.
[101] K. J. Roy, T. V. Anjali, et A. Sujith, « Poly(vinyl chloride) Asymmetric Membrane Modified with Poly (ethylene glycol): Effect of Additive Concentration on the Morphology and Performance », *Polymer-Plastics Technology and Engineering*, vol. 56, n° 9, p. 1017-1025, juin 2017, doi: 10.1080/03602559.2016.1253731.
[102] E. Saljoughi, M. Amirilargani, et T. Mohammadi, « Effect of PEG additive and coagulation bath temperature on the morphology, permeability and thermal/chemical stability of asymmetric CA membranes », *Desalination*, vol. 262, n° 1-3, p. 72-78, nov. 2010, doi: 10.1016/j.desal.2010.05.046.
[103] S. P. Kusumocahyo, S. K. Ambani, S. Kusumadewi, H. Sutanto, D. I. Widiputri, et I. S. Kartawiria, « Utilization of used polyethylene terephthalate (PET) bottles for the development of ultrafiltration membrane », *Journal of Environmental Chemical Engineering*, vol. 8, n° 6, p. 104381, déc. 2020, doi: 10.1016/j.jece.2020.104381.
[104] S. Zhao *et al.*, « Performance improvement of polysulfone ultrafiltration membrane using PANiEB as both pore forming agent and hydrophilic modifier », *Journal of Membrane Science*, vol. 385-386, p. 251-262, déc. 2011, doi: 10.1016/j.memsci.2011.10.006.
[105] M. O. Mavukkandy, M. R. Bilad, A. Giwa, S. W. Hasan, et H. A. Arafat, « Leaching of PVP from PVDF/PVP blend membranes: impacts on membrane structure and fouling in membrane bioreactors », *J Mater Sci*, vol. 51, n° 9, p. 4328-4341, mai 2016, doi: 10.1007/s10853-016-9744-7.
[106] N. I. Mat Nawi *et al.*, « Development of Hydrophilic PVDF Membrane Using Vapour Induced Phase Separation Method for Produced Water Treatment », *Membranes*, vol. 10, n° 6, p. 121, juin 2020, doi: 10.3390/membranes10060121.
[107] M. Z. Yunos, Z. Harun, H. Basri, et A. F. Ismail, « Studies on fouling by natural organic matter (NOM) on polysulfone membranes: Effect of polyethylene glycol (PEG) », *Desalination*, vol. 333, n° 1, p. 36-44, janv. 2014, doi: 10.1016/j.desal.2013.11.019.
[108] N. Stojilovic, « Why Can't We See Hydrogen in X-ray Photoelectron Spectroscopy? », *J. Chem. Educ.*, vol. 89, n° 10, p. 1331-1332, sept. 2012, doi: 10.1021/ed300057j.
[109] V.-D. Hodoroaba, « Energy-dispersive X-ray spectroscopy (EDS) », in *Characterization of Nanoparticles*, Elsevier, 2020, p. 397-417. doi: 10.1016/B978-0-12-814182-3.00021-3.

[110] T. Rönnhult, B. Brox, et G. Fritze, « The influence of surface topography on the x-ray intensity in electron microprobe analysis (EDS/WDS) », *Scanning*, vol. 9, n° 2, p. 81-87, 1987, doi: 10.1002/sca.4950090205.
[111] L. Liu, Y. Chen, S. Li, et M. Deng, « THE EFFECT OF A SUPPORT LAYER ON THE PERMEABILITY OF WATER VAPOR IN ASYMMETRIC COMPOSITE MEMBRANES », *Separation Science and Technology*, vol. 36, n° 16, p. 3701-3720, déc. 2001, doi: 10.1081/SS-100108357.
[112] E. Saljoughi et T. Mohammadi, « Cellulose acetate (CA)/polyvinylpyrrolidone (PVP) blend asymmetric membranes: Preparation, morphology and performance », *Desalination*, vol. 249, n° 2, p. 850-854, déc. 2009, doi: 10.1016/j.desal.2008.12.066.